ANATOMY OF SELECT FLUVIAL DEPOSITS IN THE MAUCH CHUNK GROUP, SOUTHERN WEST VIRGINIA, USA

By

Alan Frederick McCreary

A thesis submitted to the faculty of
The University of North Carolina at Charlotte
in partial fulfillment of the requirements
for the degree of Master of Science in
Earth Science

Charlotte

2017

Approved by:

_____
Dr. John Diemer

_____
Dr. Scott Hippensteel

_____
Dr. Andy Bobyarchick

ABSTRACT

ALAN FREDERICK MCCREARY. Anatomy of select fluvial deposits in the Mauch Chunk Group, Southern West Virginia, USA. (Under the direction of DR. JOHN DIEMER)

The Mauch Chunk Group has been interpreted as a product of multiple transgressions and regressions (Miller and Eriksson, 2000; Beuthin and Blake, 2004). An outcrop containing the upper Hinton Formation and Princeton Formation, the middle two formations of the Mauch Chunk Group, occurs along US-460 in Princeton, West Virginia, 2.6 kilometers east of the Interstate 77 Princeton exit. In order to understand the sedimentology and depositional history at those outcrops, sedimentologic logs were compiled, facies were identified and bundled into facies associations, photographic panoramas with line drawing overlays were constructed, and rock samples were taken. From the logged sections and facies architecture, a depositional history was interpreted. That history was supplemented with a provenance study where the samples were analyzed with a scanning electron microprobe to document oxide weight percentages. The upper Hinton Formation and the Princeton Formation were deposited through a combination of autocyclic and allocyclic processes. The mineralogy does not conclusively tie the sandstone deposits to the same source; however, mineral identifications did indicate the provenance to be an area with both igneous and metamorphic rocks. The presence of growth faulting indicates that the location of the cross-bedded sandstone that comprises the Princeton Formation at the US-460 outcrop may have been influenced by syn-depositional tectonism.

DEDICATION

I would like to thank my family: Bryan, Sonja, Lindsey, and Jennifer. Your love, support and encouragement over these past few years has driven me to work harder, aim higher, and challenge myself to a level that I did not think was possible. I hope that I have and will continue to make you proud.

I would also like to thank my wonderful girlfriend Madison for listening to me vent over the last two years as my project was changed, altered, switched, and every other setback. Every time I wanted to quit, you wouldn't let me, and I can't thank you enough for that.

ACKNOWLEDGMENTS

I would like to thank the following individuals, without whom this project would not have been possible:

- My adviser, Dr. John Diemer, who revised countless editions of every aspect of this report, and who challenged my thought process the whole way.
- My committee members, Dr. Andy Bobyarchick and Dr. Scott Hippensteel, who asked the tough questions throughout and making sure my evidence was solid.
- Dr. Stephen Kuehn of Concord University, who helped me through point counts, mineralogy assignment, and SEM imaging. Without your help, potential provenance would not have been discovered.
- Dr. Valerie Reynolds, who helped with mineral identifications.
- Stephen Rachide, who served as the one who would sit in my office for hours discussing every abstract concept until something solid formed. Thank you for believing in me and being a true friend.
- Jordan Smith, who served as my photographer from a distance whenever I needed new or better images of the outcrop. Your help was much appreciated.
- Professor Bill Garcia, who answered obscure questions and helped discuss varying mechanisms within the region of study.
- Friends who have helped with field research, including: Madison Chase, Jareth Wieland, Jimmy Lowe III, and Jacob Meadows.

TABLE OF CONTENTS

LIST OF TABLES

LIST OF FIGURES

CHAPTER 1: INTRODUCTION

1.1 INTRODUCTION

The Paleozoic geologic history of West Virginia is generally agreed upon when viewed from a regional perspective. During the Alleghanian Orogeny, a combination of tectonic uplift and oceanic transgressions and regressions resulted in the deposition of the Alleghanian clastic wedge, part of which can be seen in what is present-day West Virginia. Some of the formations comprising a portion of the clastic wedge are the focus of this study (Figure 1). These formations belong to the Mauch Chunk Group, although the basal Bluefield Formation is not included in this study nor is the upper part of the Bluestone Formation. Over the last 100 years, there have been five major evaluations of the Mauch Chunk Group (Krebs and Teets, 1916; Reger, 1926; Englund, 1986; Miller and Eriksson, 2000; Beuthin and Blake, 2004). In this study, the focus will be on part of the Mauch Chunk Group, which is the uppermost major group of the Mississippian in southern West Virginia.

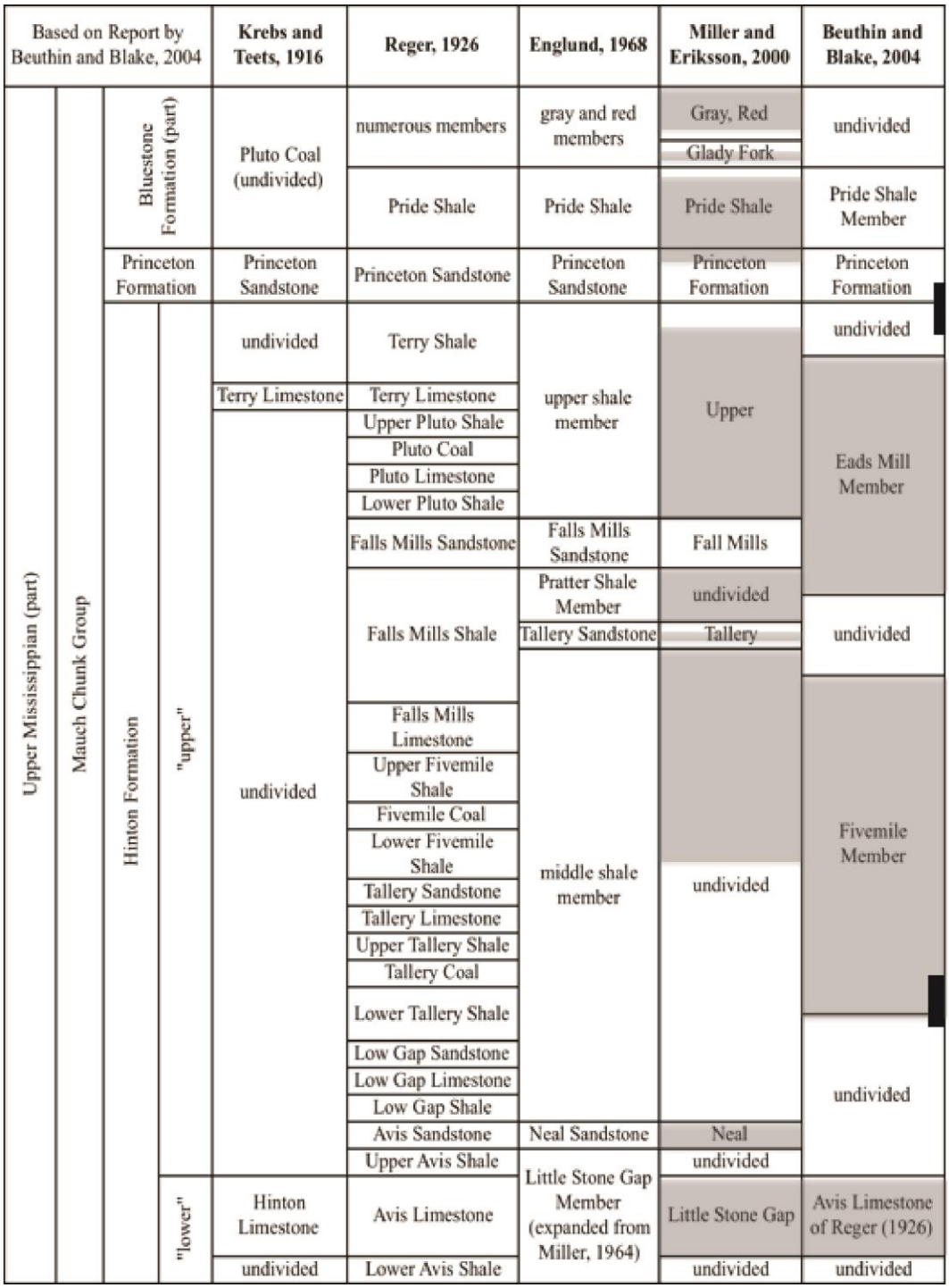

Figure 1: Comparative stratigraphic nomenclature for the Upper Mississippian Mauch Chunk Group by various authors. The occurrence of sea level transgressions (gray) and regressions (white) are based on the authors' interpretations. Authors without clear interpretations of transgressions or regressions (Krebs and Teets 1916; Reger 1926; Englund 1968) are left completely white. The underlying Bluefield Formation, which is overlain by the Hinton Formation, is not shown on this figure. Black vertical bars indicate (A) the study interval for this research (uppermost Hinton Fm and the Princeton Fm) and (B) the location of previous research done at Brush Creek Falls (in the lower Hinton Fm including the base of the Fivemile Member).

The Mauch Chunk Group is Late Mississippian in age (approximately 323.5 to 316.5 Ma) and was deposited in fluvial, deltaic, estuarine, near-shore shallow marine, and deep-water marine environments (Miller and Eriksson, 2000; Beuthin and Blake, 2004). According to Beuthin and Blake (2004), it encompasses the Bluefield, Hinton, Princeton, and Bluestone Formations (Figure 1). The basal Bluefield Formation (not shown on Figure 1) is thought to have been deposited in a deep-water marine environment (Beuthin and Blake, 2004). It has a carbonate-dominated lower section and grades up into a predominantly siliciclastic upper section and is overlain by the Hinton Formation (Maynard *et al.*, 2006). While the lower part of the Hinton Formation is not discussed much in the five major studies mentioned above, it is generally agreed that there is a limestone marker bed (the 'Avis Limestone' of Reger, 1926; Figure 1) separating the lower and upper siliciclastic parts of the Hinton Formation. According to Miller and Eriksson (2000) the Mauch Chunk Group contains 17 fourth order transgressive-regressive (T-R) sequences, each representing about 400 ka.

The upper Hinton Formation, which was the focus of the study by Beuthin and Blake (2004), is a series of shales, argillaceous limestones, mudstones, and a few sandstones. It is within this portion of the Mauch Chunk Group that debate occurs about the number of T-R sequences. In particular, Miller and Eriksson (2000) described five sequences, while Beuthin and Blake (2004) only described two such sequences within the upper Hinton Formation (Figure 1).

Overlying the Hinton Formation is the Princeton Formation, which is composed of lithic arenite sandstones and quartz-pebble conglomerates (Miller and Eriksson, 2000). This is the only stratigraphic unit that is unanimously agreed upon by the authors of the

five previously mentioned major studies. Also, the Princeton Sandstone serves as a good marker unit to determine stratigraphic position due to its relatively distinctive composition of lithic arenite sandstones interbedded with quartz-pebble conglomerates.

Present throughout the Mauch Chunk Group are thick (meters to 20 meters thick) sandstones. Some of the sandstones were deposited in incised valleys filled with fluvial or estuarine sediments. These valley fills are thought to have formed during T-R cycles where the valleys were cut during lowstands and filled during subsequent transgressions. During a lowstand, the increase in topographic relief would have resulted in an environment more conducive to incision by rivers. During the subsequent transgression, the incised valley would be a site where flooding first occurred and where deposition would take place as base level rose.

The Princeton Formation possibly formed part of the fill in one such incised valley according to Miller and Eriksson (2000). It is a ledge-forming conglomerate up to 20 meters thick that outcrops in an approximately 20-km-wide northeast-southwest trending belt (Miller and Eriksson 2000). According to Miller and Eriksson (2000, p. 215): "The nested channel fills and coarse nature of the conglomeratic deposits suggest deposition in a gravel-bed braided-fluvial system (cf. Miall, 1996) that served as a conduit for extrabasinal clasts from the orogenic belt". Miller and Eriksson (2000, their figure 22, p. 229) interpreted the Princeton Formation as an incised valley fill marking the sequence boundary at the base of one of their third-order cycles, separating a Highstand Systems Tract (HST) from the overlying Transgressive Systems Tract (TST).

1.2 SEQUENCE STRATIGRAPHY

The American Geological Institute defines a sequence as a "succession of geologic events, processes, or rocks, arranged in chronological order" (Bates and Jackson, 1984, p. 459), whereas Prothero and Schwab (2014, p. 397) summarized Mitchum (1977) and Van Wagoner *et al.* (1988) and defined a sequence as "a relatively conformable succession of genetically related strata bounded by unconformities and their correlative conformities". Sequence stratigraphy has been referred to as "the historical geology of stratified rocks" (Emery and Myers, 1996, p. 3), and "the study of rock relationships within a chronostratigraphic framework of repetitive, genetically related strata bounded by surfaces of erosion or non-deposition, or their correlative conformities" (Van Wagoner *et al.*, 1988, p. 39).

Sequence stratigraphy has its origins in the work done by Laurence L. Sloss in his analysis of the North American craton and its widespread stratigraphic sequences (Sloss, 1964). While it was difficult for Sloss to prove a detailed sequence or pattern, he was able to show a general trend of depositional and non-depositional events. When examining tectonics in relation to depositional and non-depositional events, Sloss was exploring the possibility of cyclic craton movement above and below base level as a driving factor of sequencing (Figure 2). After analysis of all available data, Sloss determined that the North American craton experienced fold complexes similar to those described as second-order units by Bogdanoff (1960), who was doing similar work in Europe. These units were described as "major tectonic subdivisions in time and space, each characterized by definable areas of occurrence, by typical orientation of fold and

fault systems, and by a particular structural habit or style" (Bogdanoff, 1960 (as quoted in Sloss, 1964, p. 458)).

Sequence stratigraphy is a relatively new concept, emerging to prominence in the 1980s due to seismic work done by Exxon (Prothero and Schwab, 2014). Instead of focusing the argument on whether tectonics or eustasy drove the T-R sequences, sequence stratigraphy looks explicitly at unconformities and the thickness of layers bounded by unconformities and the correlative conformities to determine chronologies of events. Both base level cycling and alternating subsidence and uplift combine to drive sequence stratigraphy (Boggs, 2001). Posamentier and James (1993) stated that the key attributes to the sequence-stratigraphic approach included both the cyclic nature and chronostratigraphic framework, which was in agreement with the findings of Van Wagoner *et al.* (1988).

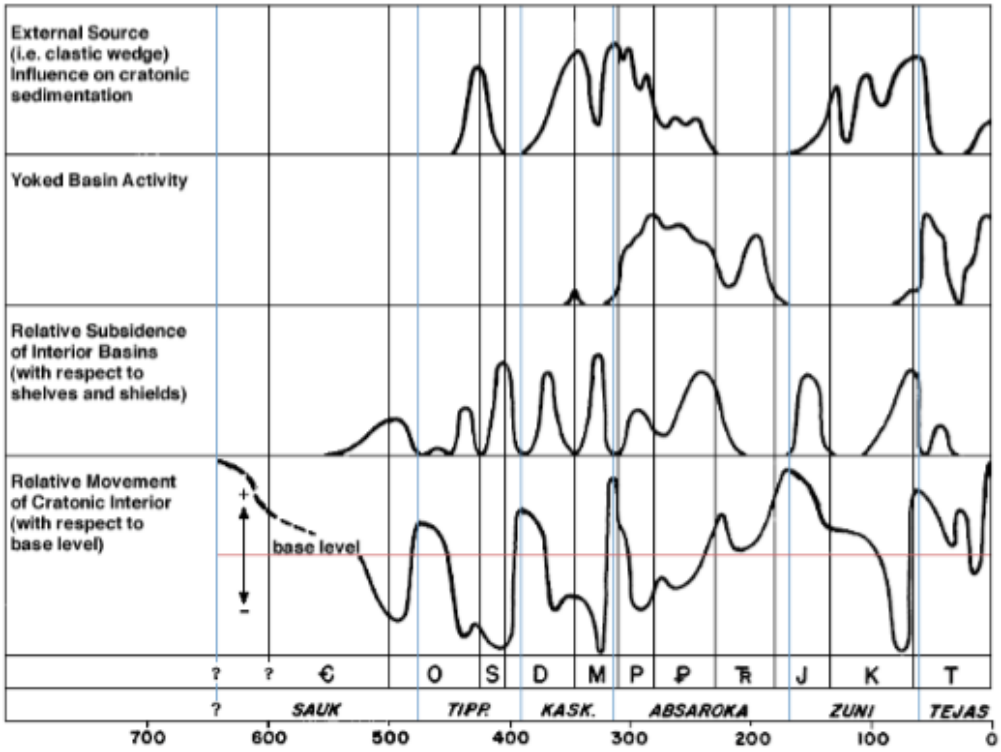

Figure 2: Tectonic activity of adjoining mobile belts (upper plot) as indicated by spread of clastic wedges to cratonic margins, and tectonic activity of interior of the North American craton (lower three plots) in terms of yoked basins, interior basins, and relative position with respect to base level (Sloss, 1964).

When using sequence stratigraphy, it is important to understand that there is no singular model that will explain every outcrop or core sample. Prior to the application of sequence stratigraphy as a tool, rather than a model, the factors at play in the area must be understood, such as sedimentation rates and tectonic activity (Posamentier and James, 1993). One of the major factors in sequence stratigraphy is a concept called accommodation, which refers to the available space for sediment accumulation relative to base level, or sea level (Boggs, 2001). If sea level remains static and sediment accumulation exceeds the available accommodation space, relative sea level will decrease as the sediment pushes the coast outward, resulting in a regressive phase. Conversely, if sediment accumulation does not continuously fill the available accommodation space, relative sea level will increase, and result in a transgressive phase.

There are two kinds of unconformities used in the application of sequence stratigraphy, Type 1 and Type 2 unconformities. Type 1 unconformities develop in response to relative sea-level fall, and can be characterized by basinward protruding clastic fans and potential incised valleys (Posamentier and James, 1993). This type of unconformity is easily identifiable in outcrops due to the cross-section containing potential incised valley fills overlying the unconformity, and a general trend of marine strata below the unconformity being overlain by fining upward fluvial sediment. Type 2 unconformities develop in response to steadily increasing relative sea-level rise, and are nearly impossible to identify in outcrops (Posamentier and James, 1993). As the relative sea level increases, the strata maintain a relatively consistent lithology, and appear as a thick, near-uniform layer.

1.3 FLUVIAL ARCHITECTURE

In this study, four types of stream systems will be considered when interpreting outcrop exposures: anastomosed, braided, meandering, and incised valley fills. Each stream system presents its own unique characteristics with implications for depositional setting, which can then be compared to Miller and Eriksson (2000) and Beuthin and Blake (2004) to either corroborate or reject their interpretations of the number of T-R sequences.

J.R.L. Allen (1966) coined the term 'fluvial architecture' in his keynote address at the First International Symposium on Fluvial Sedimentology to describe the geometry and internal structure of channels and overbank deposits (Miall, 1996). In 1966, Allen defined a hierarchy of flow fields, stating that they occurred in a series including small-scale ripples, large scale ripples, dunes, channels, and finally culminating in a combination of the four in an integrated system. This work was expanded upon by Friend (1983, p. 349), where channels were defined as "elongate depressions in the alluvial surface, with more or less clearly defined margins or banks between which the river flow is restricted for most of the year".

Anastomosing stream systems (Figure 3) derive their name from the medical term anastomosis, which was used to describe the connectedness between structures such as blood vessels. This term was first introduced by Smith and Smith (1980), and was interpreted in the fluvial setting as being

> An interconnected network of low-gradient, relatively deep and narrow, straight to sinuous channels with stable banks composed of fine-grained sediment (silt/clay) and vegetation…Separating the channels are floodplains consisting of vegetated islands, natural levees, and wetlands. Occasionally, crevasse channels and splay deposits occur in wetland areas. (Smith and Smith, 1980, p. 157).

Friend *et al.* (1979) and Friend (1983) noticed a 'ribbon structure' in addition to the channels of anastomosed systems. Ribbon structures are 'wings' of sandstone that extend laterally from the top of the channel margin with a width to depth ratio under 15 (Miall, 1996). These features fine distally and are likely the levee deposits that form adjacent to the fixed channels, which are typical of anastomosed rivers (Miall, 1996). Miall also stated that since these rivers are so complex and changing, it is unwise to assume that fluvial style will remain constant throughout a given stratigraphic unit.

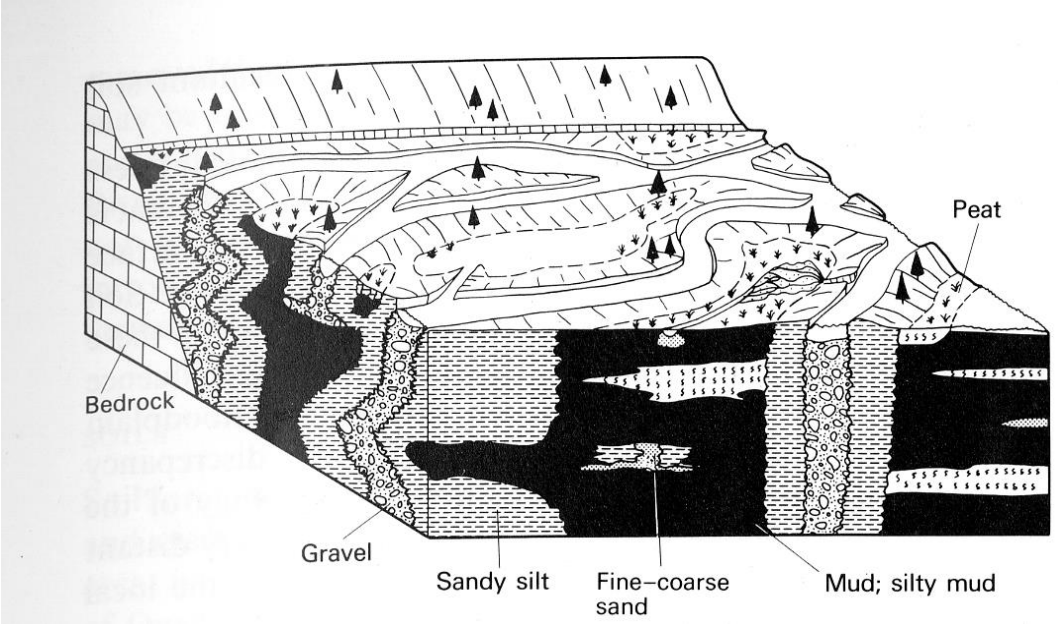

Figure 3: Block diagram of an anastomosing channel system (after Smith and Smith, 1980) (image from Reading, 1986).

Braided stream systems (Figure 4) differ from anastomosed systems due to the presence of more coarse-grained sediment load (Miall, 1996). Braided systems have limited vegetation along their banks. This allows braided channels to shift positions frequently resulting in abundant bar remnants and cut and fill channel structures. An analysis of limited case studies in the Appalachian Basin by Cotter (1978) confirmed that pre-Devonian fluvial deposits were generally formed in braided fluvial settings, while

those in the Devonian and Carboniferous were mostly meandering. These findings were later confirmed by Long (1978). These findings were thought to be due to the increase in vegetation, such as the emergence of seed ferns and scale trees in the Carboniferous, which helped stabilize banks due to extensive root systems (Smith and Smith, 1980).

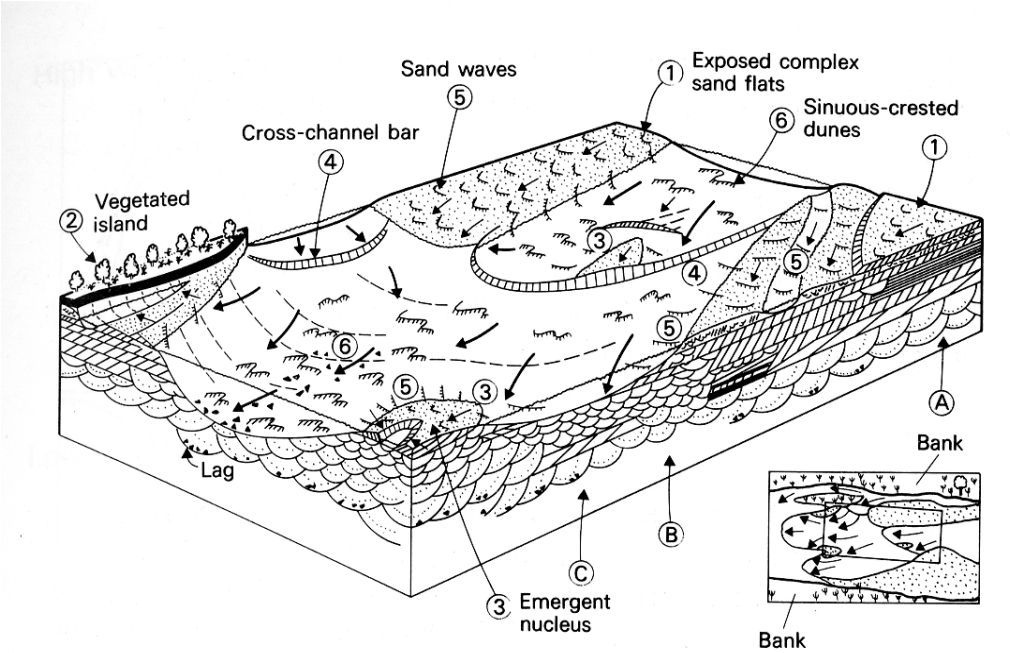

Figure 4: Block diagram of a braided stream system. Inset shows alteration in flow direction (image from Reading, 1986).

Meandering stream systems (Figure 5) typically have well-vegetated banks that resist lateral erosion. As a consequence, they contain a distinct cut bank and point bar deposits in cross-section. This geometry differs from braided systems as the cut bank and point bar are clearly defined in meandering streams due to the longevity of the central channel, which allows for lateral migration of the point bar. This migration forms lateral accretion surfaces that scale in height and width to the size of the overall channel. Meandering stream systems also have the ability to develop meander belts (Figure 6), which are due to the accumulation of channel sands, commonly in multiple storeys

composed of superimposed point bar deposits, bounded on either side by natural levee structures. As sediment accumulates, the system aggrades vertically, increasing its potential to break through its own levees and find a new path during an avulsion.

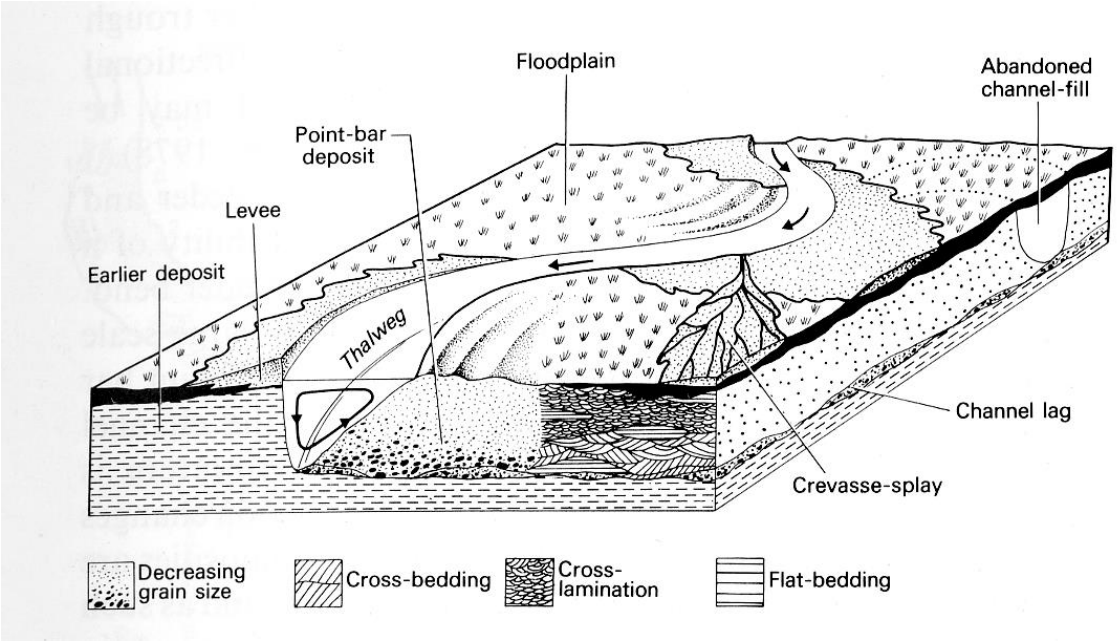

Figure 5: Block diagram for a meandering stream (image from Reading, 1986).

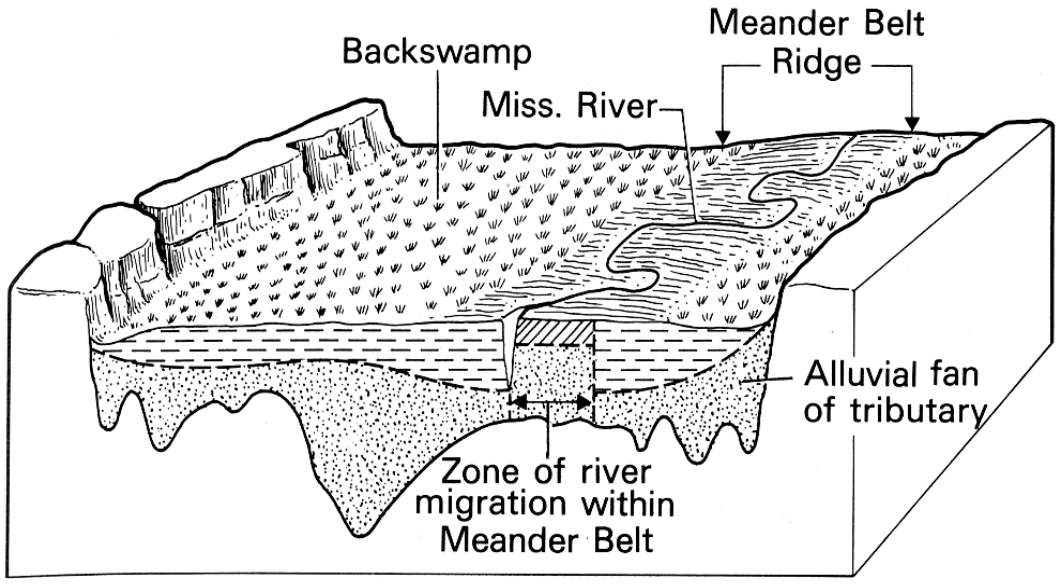

Figure 6: Block diagram of the Mississippi River meander belt system (image from Reading, 1986).

Incised valleys are the result of tectonic uplift, base level drop, or a combination of the two. This change in topographic relief leads to incision by the channel system, cutting through pre-existing layers. With the subsequent rise in relative base level, the incised valley becomes a site for deposition. The deposited material can fill the valley resulting in an incised valley fill (see examples in Figure 7). The presence of ravinement surfaces indicate periods of base level fluctuation where sediment that initially filled a valley was removed by an incising river during a base level drop. As base level dropped, the channel cut through some of the backfilled sediment producing a ravinement surface (Figure 7). With a subsequent rise in base level, the ravinement surface is covered by additional valley fill sediments. In a detailed example of this process illustrated in Figure 7a, Allen and Posamentier (1994) presented a model where base level first dropped to form the incised valley. Base level then rose and the valley filled for an interval represented by the two bottom layers in Figure 7a. Then base level dropped again, resulting in partial removal of those bottom two layers and the formation of a ravinement surface. With a subsequent rise in base level, the third layer was deposited. Two additional fluctuations in base level resulted in the top two layers in Figure 7a, each deposited on top of its own ravinement surface. In another example of the complex history of incised valley fills, Ashley and Sheridan (1997) presented a model where initial incision was followed by a rise in base level and the deposition of the bottom two layers, which filled most of the valley (Figure 7b). Then a base level drop caused erosion of much of the upper of those two layers and formation of ravinement surface 1. That incision was followed by a rise in base level which produced the thick layer composed of a channel fill with possible lateral accretion surfaces. A subsequent drop in base level has

resulted in the erosion of the top of the deposit as indicated by ravinement surface 3. Weber and others (2004) present a highly complicated system of multiple base level alterations and backfilling, with ravinement surfaces and cross-bedding present in all but the very bottom left layer (Figure 7c).

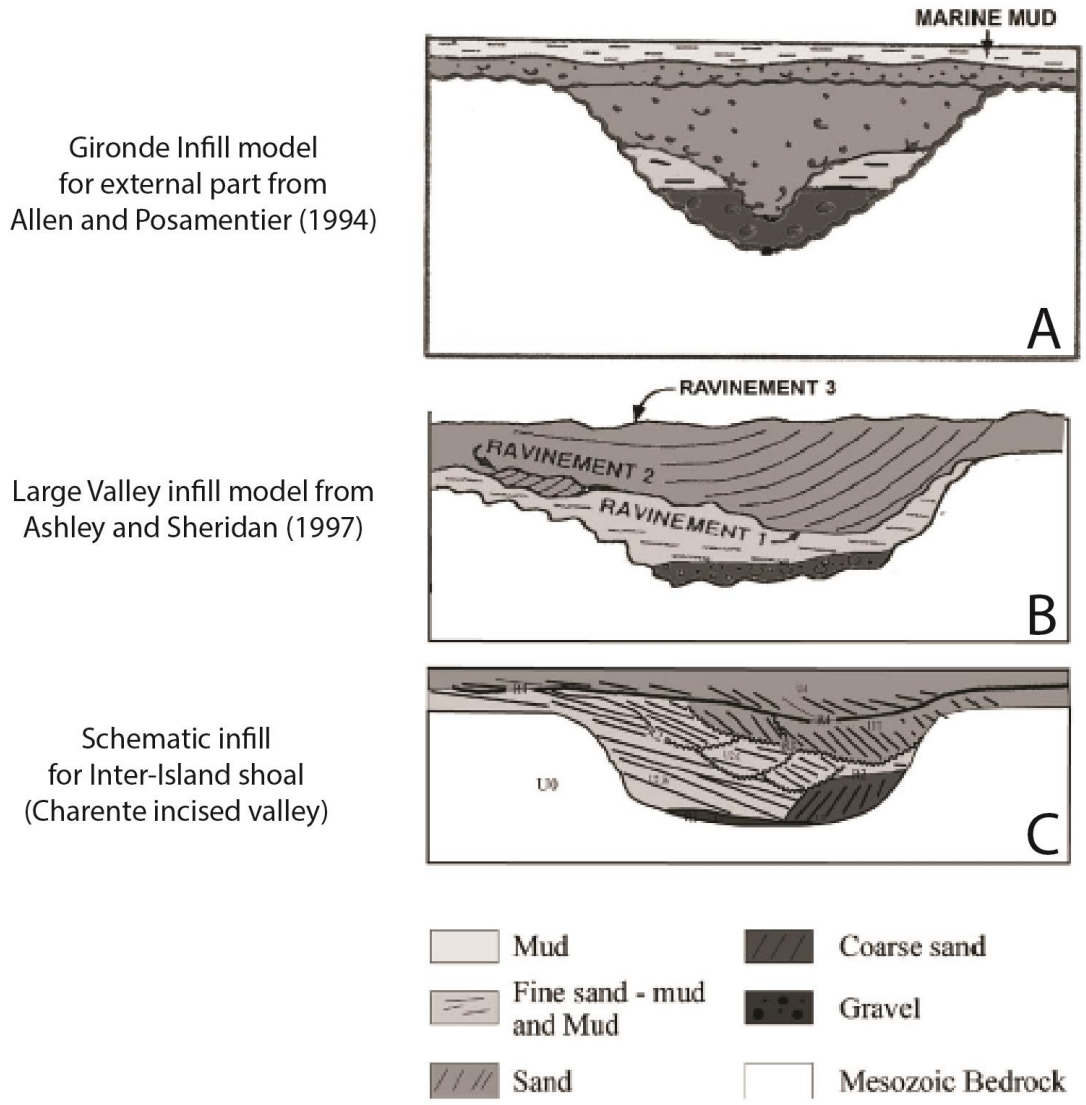

Figure 7: Comparisons of incised valley fills in models proposed by (A) Allen and Posamentier (1994), (B) Ashley and Sheridan (1997), and (C) Weber et al. (2004) (image from Weber et al., 2004, p. 35). The presence of multiple ravinement surfaces separating packages of sediments shows generations of systematic backfilling and downcutting caused by fluctuations in base level.

1.4 DISTRIBUTIVE FLUVIAL SYSTEMS AND MEGAFANS

While often used interchangeably in the literature, distributive fluvial systems (DFS) and megafans have been clearly differentiated (Weissmann *et al.*, 2010; Owen *et al.*, 2015). With the initial definition of DFSs, Weissmann and others (2010, p. 39) "use the term DFS to describe a pattern of channel and floodplain deposits that radiate outward from an apex that is located where the river enters the sedimentary basin". This classification, however, is only relevant for continental sedimentary basins, as Weissmann and others (2010, p. 39) "include only purely continental sedimentary basins, excluding review of fluvial systems in marine marginal basins". Weissmann and others (2010) go on to show that there is significant range in DFS length, ranging from less than 1 kilometer to over 700 kilometers, and state that:

> Significant differences exist between DFS depositional patterns and degradational rivers, including (1) radial pattern of channels from the DFS apex, (2) common down-DFS channel size decrease, (3) down-DFS grain size decrease, and (4) lack of lateral channel confinement on the DFS. (Weissmann et al. 2010, p. 42).

The narrow definition of the DFS term by Weissmann et al. (2010) was later critiqued by Sambrook Smith and others (2010), who cited lack of definitions for both continental sedimentary basins and marginal marine basins as a counter-argument to Weissmann and others' (2010) conclusions which implied that the DFS term could be applied to all river basins. Sambrook Smith and others (2010) further stated that

> of the criteria listed, only the first – 'radial pattern of channels from the DFS apex' – (p. 42) would appear to be truly diagnostic of DFS, and indeed what all previous studies have called simply an alluvial fan. (Sambrook Smith et al. 2010, p. e230).

In an effort to develop a usable differentiation, Owen and others (2015), including multiple authors from the Weissmann and others (2010) publication, selected the Salt Wash DFS in the Morrison Formation of the southwestern United States as a case study. Here, they further refined their criteria for a DFS by saying:

> Distributive fluvial systems are defined by: 1) channel patterns that radiate away from an apex; 2) a decrease in channel size and abundance downstream; 3) an increase in preservation of floodplain deposits relative to channel deposits downstream; 4) a decrease in grain size downstream; and 5) a change from amalgamated channel deposits in proximal areas to smaller fixed channels in distal areas. (Owen et al. 2015, p. 546).

This elaboration of the characteristics first proposed by Weissmann *et al.,* (2010), coupled with the conclusion from Davidson and Hartley (2014, p. 1010) that a minimum of "30 km is the appropriate measured length from apex to toe as a criterion to distinguish DFSs from alluvial fans", resulted in a refinement of the definition of DFSs in terms of their lateral extent and internal geometry. Owen and others (2015) broke from the practice of characterizing deposits in a lithostratigraphic manner, and suggested that a genetic classification technique more accurately represents the entire system as opposed to defining discrete individual systems contained within a DFS. In this manner, they suggested that DFSs formed through a series of depositional events across a span of time.

In discussing source provenance, Davidson and Hartley (2014) pointed out the relative difficulties due to rare preservation of the original source. However, it is possible to infer provenance through an understanding of regional tectonic activity and mapped extent of contributing fluvial systems. Similarly, Davidson and Hartley (2014) stated that precisely locating the distal termination point is difficult where the DFS terminates in a wetland environment.

When looking at DFS geomorphic features, Davidson and others (2013) cited previous studies (Hartley *et al.*, 2010; Weissmann *et al.,* 2010, 2011) when they stated that DFSs "have been referred to as megafans, alluvial fans and fluvial fans … although their distinction is perhaps arbitrary along a continuum of DFS scales" (Davidson et al. 2013, p. 82). This statement conflicted with the definitions of other authors' (Weissmann *et al.*, 2010; Owen *et al.*, 2015), since some of these fan systems can terminate in

marginal marine basins, whereas the DFSs interpreted both previously and in the study by Davidson and others (2013), explicitly focus on continental sedimentary basins. However, Davidson and his co-authors summarized their description of the geomorphology by stating:

> …dominant channel planform type was used to identify six different DFS types: (I) a single braided channel that bifurcates downstream into low sinuosity channels, (II) a single dominant braided channel, (III) a single braided channel that increases in sinuosity downstream, (IV) a dominant single sinuous channel system, (V) a single sinuous channel that bifurcates into smaller sinuous channels downstream, and (VI) multiple sinuous channels with no dominant single channel (Davidson *et al.*, 2013, p. 83).

They proposed that these six geomorphic types vary based upon factors such as discharge, sediment load, velocity, and channel size (Figure 8).

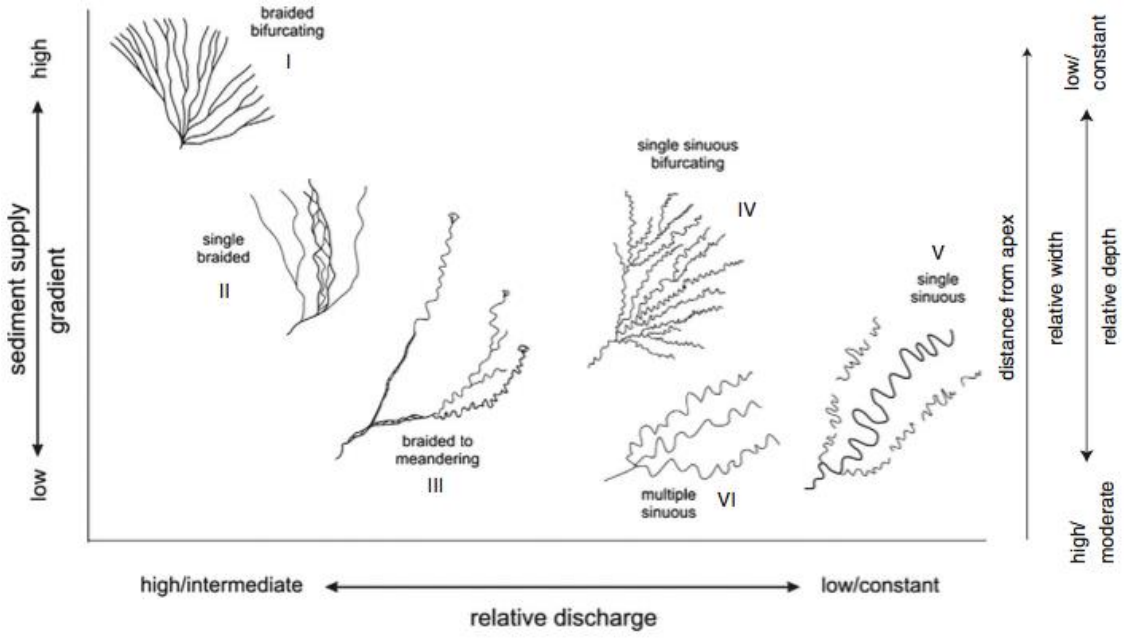

Figure 8: Proposed continuum of DFS types (from Davidson *et al.,* 2013, p. 84).

Fluvial megafans, as opposed to distributive fluvial systems, are not confined explicitly to continental sedimentary basins. Leier and others (2005, p. 289) cited previous research in explaining that fluvial megafans "form as rivers exit the topographic front of a mountain belt, migrate laterally in the adjacent basin, and deposit large fan-

shaped bodies of sediment". They go on further, again citing other authors, to explain the geomorphological differences between megafans and alluvial fans as

> … their unusually large area (areas of $10^3 – 10^5$ km^2 for fluvial megafans vs. generally <100 km^2 for alluvial fans), [and] low gradient (fluvial megafans, generally ~$0.1^o – 0.01^o$; alluvial fans ~$1^o – 4^o$) (Leier et al. 2005, p. 289)

and their lithologic differences, such as

> … sedimentary textures (sediments in fluvial megafans vary from boulders at the apex to predominantly silt and mud at their toes), and depositional processes (fluvial megafans are devoid of sediment gravity flows) (Leier et al. 2005, p. 289).

Whereas the literature on DFSs (Sambrook Smith *et al.*, 2010; Weissmann *et al.*, 2010; and others) discusses variance in length of overall systems and minimum standards for length from apex to toe, their constraints on fan area aren't as well defined as in Leier and others (2005). Further, where Davidson and others (2013) show the six types of DFS (Figure 8), work by Plink-Bjorklund and others (2014) showed that radial patterns are driven by river avulsions, and not bifurcations. A preferential migration due to avulsion showed seasonal discharge maximums and annual flooding, which Leier and others (2010) correlated to the monsoonal seasons of tropical climates, and they used the modern analogue of the megafan on the Kosi River as an example. In the buildup of formations, Horton and DeCelles (2001, p. 43) showed that "fluvial megafans may only develop once a drainage network has reached a particular size, roughly 10^4 km^2", which was based on their study of contemporaneous megafans.

1.5 PROBLEM STATEMENT

Sequence stratigraphy is a powerful tool for interpreting the depositional history of sedimentary basins. In particular, it is useful in shallow marine deposits when reconstructing the occurrence of transgressions and regressions driven by changes in

relative sea level. Important drivers for relative sea level change are tectonics and eustasy. One mechanism for eustatic sea level change is glaciation, where base levels fall during the onset of glacial periods and then climb again during deglaciation. Miller and Eriksson (2000) identified glacio-eustasy as the main driver for the fourth-order (400 ka) T-R cycles in the Mauch Chunk Group.

Changes in relative sea level can also affect fluvial systems. However, the evidence for relative sea level changes can be less obvious in fluvial systems compared to shallow marine deposits. Notable features that can record intervals of relative sea level lowstand in fluvial systems are horizons marked by incised valleys, accompanied by well-developed paleosols on adjacent interfluves. Multi-storey, laterally restricted channel fill deposits capped by laterally extensive sheet sands can record the subsequent transgressions.

The influence of an external mechanism (such as eustasy) affecting the depositional history of a basin can be referred to as an 'allocyclic' control on sedimentation. In contrast, there can be 'autocyclic' controls on sedimentation. For example, on aggrading fluvial plains, the process of lateral migration of channels within belts demarcated by levees can result in multi-storey sandstone bodies (channel belts) encased within fine-grained overbank deposits. Active channel belts can relocate on an alluvial plain by avulsion events, which can occur independently of base level changes. Thus, interbedded sandstones and mudstones can be produced by either allocyclic or autocyclic processes.

In this research project, well-exposed mudstones, cross-bedded sandstones and conglomerates in the Mauch Chunk Group of southern West Virginia were investigated

to determine if allocyclic processes, autocyclic processes, or a combination of the two, controlled their alluvial architecture. One outcrop is of immediate interest: the US Highway 460 outcrop east of the Interstate 77 Princeton exit. This outcrop was compared to other outcrops in the region, most notably the cross-bedded sandstone and conglomerate type section of the Princeton Formation in the town of Princeton, West Virginia. Furthermore, the results of this study were used to support or refute the sequence stratigraphy interpretations for the Mauch Chunk Group made by previous authors.

1.6 FIELD SITE LOCATIONS

The main field study site comprises a pair of outcrops, one on either side of US-460 east of the I-77 Princeton exit in West Virginia (Figure 9). UTM coordinates for the outcrops are 17S 498398.50mE, 4134156.70mN, with latitude and longitude measurements being 37°21'14.81"N, 81° 1'5.10"W. These two outcrops are located 2.8 km (1.7 miles) east of the I-77 Princeton exit, and measure approximately 300 meters and 200 meters for the northern and southern exposures, respectively. The northern exposure has two benches, although the upper bench is not accessible for traversing, while the southern exposure has one bench. This location was selected because of its accessibility, the presence of multiple channel fills, and the overall representative nature for the upper Hinton Formation lithostratigraphy which can be used to interpret its depositional history. The furthest lateral extents of these outcrops are obscured by vegetation along both northern and southern exposures, and the outcrops pinch out laterally due to topographic variability and excavation during road construction.

A second study site is located at 37°21'42.48"N and 81°7'34.19"W, which is the location for the type section of the Princeton Formation (Figure 10). This outcrop was visible from the parking lot of the Memorial Church of Christ in Princeton, West Virginia.

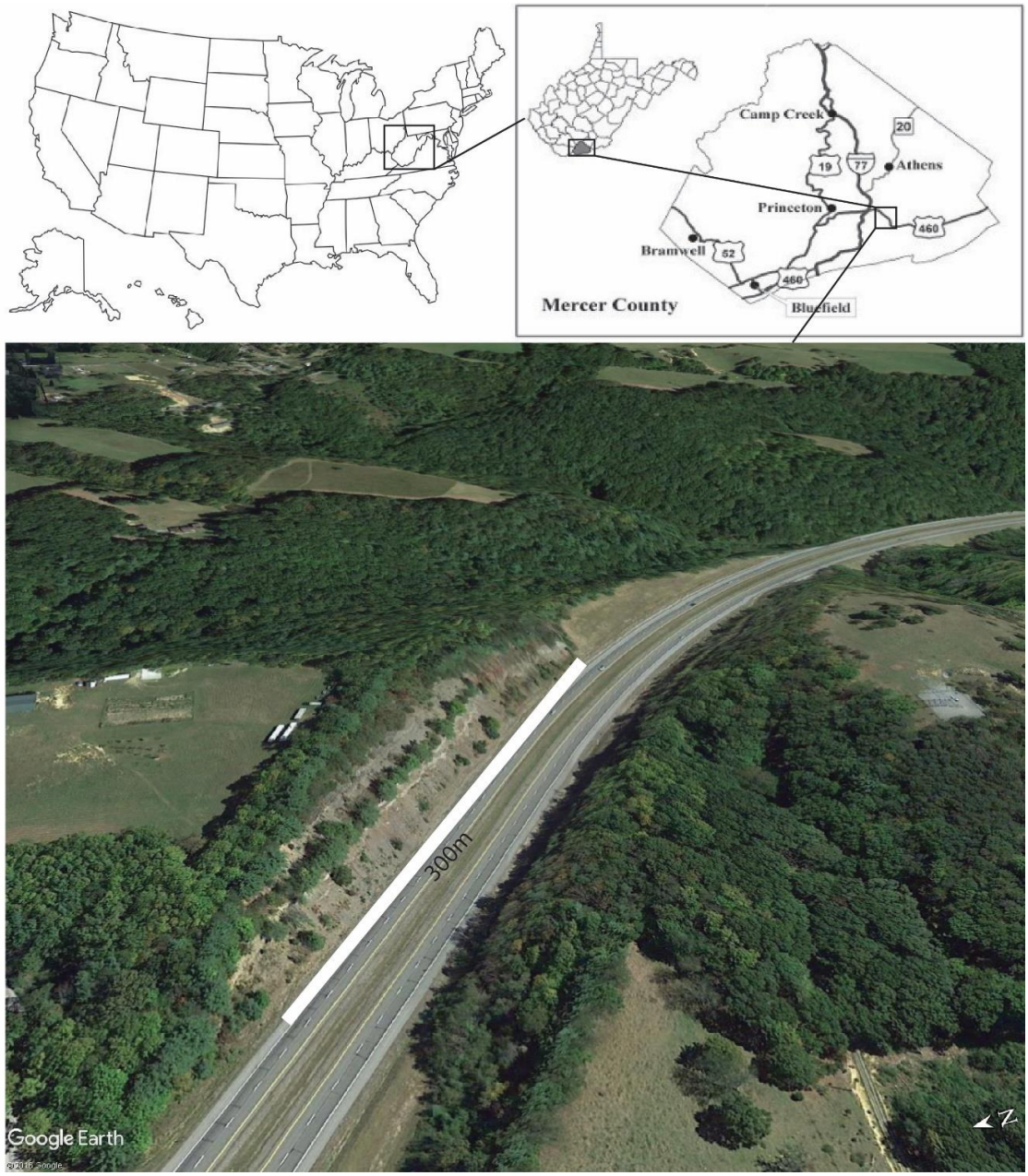

Figure 9: Main field site location as shown on the maps at country, state, and county scales, and in an oblique Google Earth image for the US-460 outcrops. North arrow in bottom-right of Google Earth image, with north to the left of image. The northern roadcut is in sunlight, whereas the southern exposure is in shadow in this image. (State map and Mercer County map images from www.visitedstatesmap.com and www.campcreekstatepark.com, respectively).

Figure 10: Outcrop for the Princeton Formation type section in the town of Princeton, West Virginia. Note the presence of well-rounded quartz pebbles and large-scale trough cross-stratification in this medium to coarse-grained sandstone (photo courtesy of Jordan Smith).

1.7 HYPOTHESES

1) If the cross-bedded sandstone bodies are the product of allocyclic processes (such as eustatic base level fall), then their alluvial architecture should contain recognizable features consistent with incision during drop in base level (such as erosion surfaces at the bases of incised valleys and well-developed paleosols on interfluves) followed by infilling (in the form of laterally confined multi-storey sandstones) during the subsequent transgression.
2) If the cross-bedded sandstone bodies are the product of autocyclic processes, then their alluvial architecture should contain features consistent with channel belt aggradation such as sub-horizontal basal erosion surfaces, fining upward point bar

deposits, levee deposits, crevasse splay deposits and moderately developed paleosols.

3) If the US Highway 460 outcrop is autocyclic in nature, then it could be assigned to the 'Coastal Plain-Dominated Sequence' of Miller and Eriksson (2000, p. 226). This could assist in assigning this outcrop to one of the T-R sequences proposed by Miller and Eriksson (2000, their figure 6, p. 216).
4) If it is possible to distinguish between allocyclic and autocyclic controls on the stratigraphy of the Mauch Chunk Group, then it may be possible to evaluate the relative merits of various sequence stratigraphy interpretations made by previous authors.
5) If mineralogy can be determined for the sandstones present within the US Highway 460 outcrop and at the type section outcrop in Princeton, WV, source provenance can be interpreted. Further, if the sandstones show highly consistent mineralogy, they can be tied to one system and were likely formed during a short interval of time.

CHAPTER 2: PREVIOUS WORK

2.1 LITERATURE REVIEW

Analysis of the Mauch Chunk Group in southern West Virginia and Virginia can be traced back to work done in 1916 by Krebs and Teets, where they first attempted to construct a stratigraphic column based on sparse outcrops. While this work proved to be a valuable foundation for studies in this area, it was very limited in terms of named units and lithologic analysis. It included only four named units and left most of the upper Hinton Formation as 'undivided' (Figure 1).

In 1926, Reger continued the work done by Krebs and Teets. However, as noted by Beuthin and Blake (2004), Reger made the mistake of over-subdividing the stratigraphy into layers that did not exhibit lateral continuity throughout large portions of the field area (Figure 1). Instead, Reger classified layers based on individual outcrops and then attempted to construct a complete stratigraphic column, which led to 27 separate named units (Figure 1). He did this even though some of those units were only localized deposits and not representative of the overall stratigraphic makeup (Beuthin and Blake, 2004). While Reger's 1926 interpretation attempted to apply stratigraphic nomenclature to the previously undivided upper Hinton Formation of Krebs and Teets (1916), it led to confusion in future field analysis.

Recognizing some of the errors of Reger, Englund (1968) took Reger's column and refined the nomenclature to present a more representative and continuous stratigraphic sequence throughout this section of the Mauch Chunk Group (Figure 1). In his attempt to consolidate nomenclature, Englund (1968) subdivided a majority of the upper Hinton Formation into two main groups, his 'upper shale member' and 'middle shale member'. This ultimately misrepresented the units that were present in the upper Hinton Formation, as there are bands of sandstone, mudstone, and limestones present within these 'shale' members (Beuthin and Blake, 2004).

Working with the stratigraphy established by Englund (1968), Miller and Eriksson (2000) revised that nomenclature by removing most of the lithologic terms from the unit names with the exception of the Pride Shale (Figure 1). By doing this, they recognized that their named units could contain a variety of lithologies including thinly interbedded layers that comprised minimal percentages of the defined units. In their interpretation of T-R sequences, Miller and Eriksson (2000) utilized deep-well gamma log data (Figure 11) to correlate their T-R sequences. Miller and Eriksson identified five T-R sequences in the upper Hinton Formation, nine T-R sequences in the portion of the Mauch Chunk Group that is used in this study, and twelve T-R sequences total in their study, which spans from the middle of the underlying Bluefield Formation to the middle of the overlying Bluestone Formation (Figure 11). However, the viability of five sequences in the study area over the relatively short time frame (~7 million years) is suspect due to the time required for either glacioeustasy or tectonic activity to alter sea level that drastically. It is the author's opinion that some of the T-R sequences by Miller and Eriksson (2000) were not due to allocyclic processes such as eustasy, but rather could

be localized phenomena driven by autocyclic processes such as peat swamp progradation followed by abandonment and compaction in a deltaic or coastal plain environment.

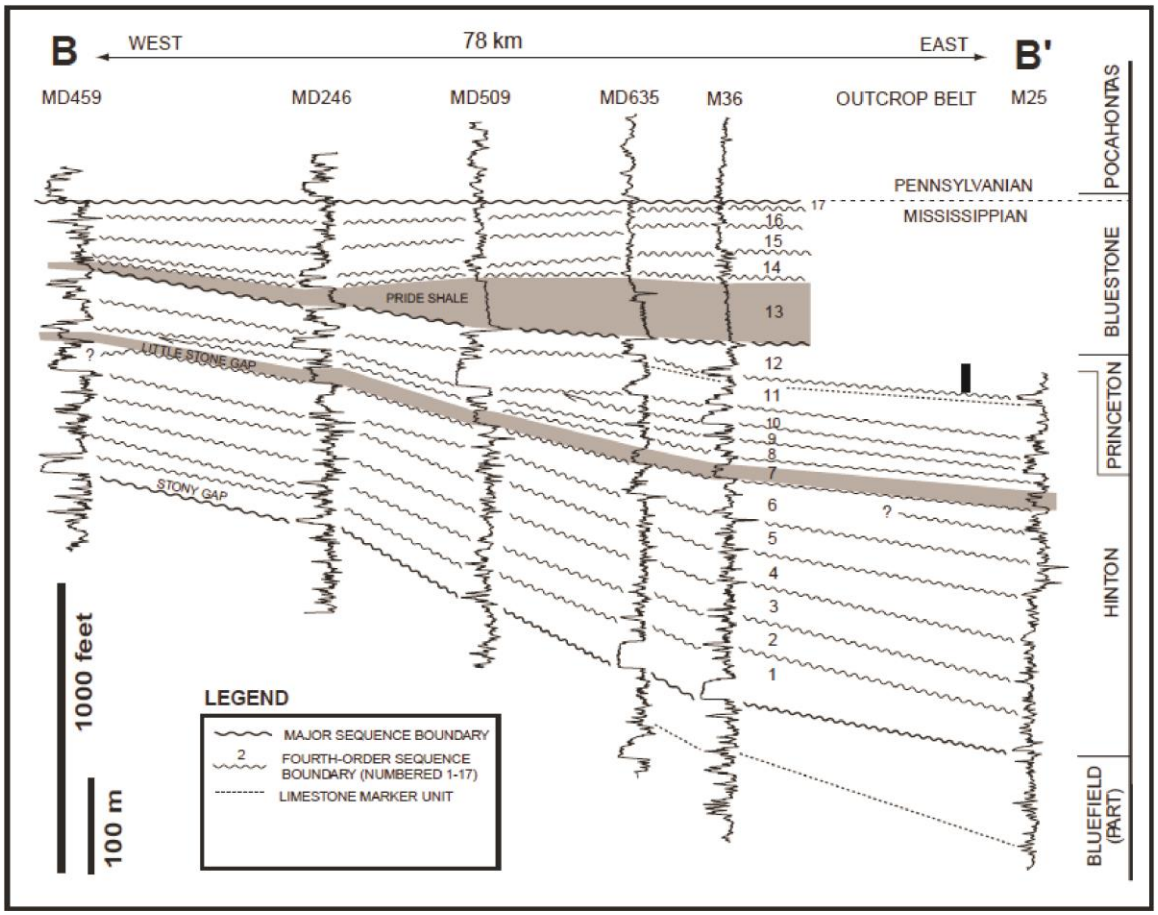

Figure 11: Stratigraphic cross-section of the study area by Miller and Eriksson (2000) utilizing gamma log data to correlate units. Low gamma readings are interpreted as argillaceous limestones, medium readings are sandstones, and higher readings indicate shales. Numbered layers are high frequency, 400 ka events, showing T-R sequencing of any magnitude. Estimated location of the US-460 outcrop is labeled by a vertical black bar between locations M36 and M25, which extends from sequence 12 into the base of sequence 13.

Beuthin and Blake (2004, p. 165), in reviewing the history of stratigraphic interpretations containing the variations in nomenclature, attempted to reconcile the previously differentiated units into a more definitive set of five units "in accordance with the North American Stratigraphic Code" (North American Commission on Stratigraphic Nomenclature, 1983) (Figure 1). Through the renaming of units, Beuthin and Blake (2004) differentiated the Fivemile Member and Eads Mill Member of the upper Hinton

Formation, citing both as ‘marine zones’. They later clarified the term ‘marine zones’ by saying “these beds were integrated into genetically related packages of facies that record regional transgressions” (Beuthin and Blake, 2004, p. 166). With this explanation for the Fivemile and Eads Mill Members, as well as their previous interpretation that the Avis Limestone was exclusively deep marine, Beuthin and Blake (2004) identified two T-R sequences in the upper Hinton Formation, and three T-R sequences within the study area of the Mauch Chunk Group (Figure 1). Interspersed between the named units in the upper Hinton Formation are undivided units, which are lithologically described as a combination of sandstones, mudstones, and paleosols. These undivided sections contain evidence for the regressive portions of the T-R sequences that Beuthin and Blake proposed, although not explicitly stated in their interpretation.

Bedrock geologic maps for the study area (Beuthin and Blake 2001, 2002; Matchen *et al*. 2011; Peck *et al*. 2013) show that most of the Hinton Formation is left as undifferentiated, citing a lack of outcrops as the reason for not differentiating the Fivemile and Eads Mill Members. This interpretation, while understandable, makes future work in the field area difficult, as the Fivemile and Eads Mill Members regionally vary in thickness between 3 – 27 m and 28 – 42 m, respectively (Beuthin and Blake, 2004).

Starting in 2012, students and faculty at Concord University in Athens, West Virginia, began fieldwork in the Brush Creek Falls area near Eads Mill, West Virginia (Figure 1). Through this work, a conglomeratic channel fill was discovered that had pyrite-coated limestone grains (Matchen *et al.*, 2013). This channel fill became an area of interest due to the complexity of deposition and flow conditions that would have been

required to deposit rounded limestone clasts, which required high energy flow systems, and the disseminated pyrite to be precipitated out, which required anoxic and limited flow environments. This site was studied in more detail, during which time another channel filled with conglomerate was discovered (McCreary and Matchen, 2014). At this newly discovered conglomeratic channel fill, the presence of rounded and angular coal clasts, nodular pyrite and marcasite, and microscopic fossils were noted in addition to the pyrite-coated limestone clasts. After examining the surrounding stratigraphy, combined with analysis of chemical and mass-percentage composition of the conglomeratic fill, it was hypothesized that this channel sandstone was the result of episodic storm rip-up events followed by rapid burial in an anoxic environment (McCreary and Matchen, 2014). This preliminary research, while stratigraphically below the upper Hinton Formation and Princeton Formation of the current study, offered insight into the morphology of high-energy channel systems associated with base level drop.

In 2014, Ron Blakey published a series of paleogeographic reconstructions for the North American continent. Of interest for this study are the four maps from the Early Mississippian through the Late Pennsylvanian (Figure 12), from which the Late Mississippian was enlarged to see more detail around the time of deposition for the upper Hinton Formation and Princeton Formation (Figure 13). These maps were selected to show the presence of an epicontinental sea attached to the Rheic Ocean during most of the deposition of the Mauch Chunk Group, followed by the subsequent regression path during the Late Mississippian and Pennsylvanian. These maps also show the progression of the Alleghanian Orogeny, which is believed to have caused a tectonically driven relative sea level change (Miller and Eriksson, 2000). However, since these maps are

only snapshots in time and spaced millions of years apart, an accurate understanding of the T-R sequences cannot be discerned from these maps alone. These maps also are not sufficiently detailed to confirm or deny the interpretation that glacioeustasy was the driver of sea level changes (Miller and Eriksson, 2000; Vance, 2007; Cawthern, 2007). They can, though, help to show the construction of the westward-thinning clastic wedge associated with the Alleghanian Orogeny, resulting in a major overall regression in the field area (Miller and Eriksson, 2000; Beuthin and Blake, 2004).

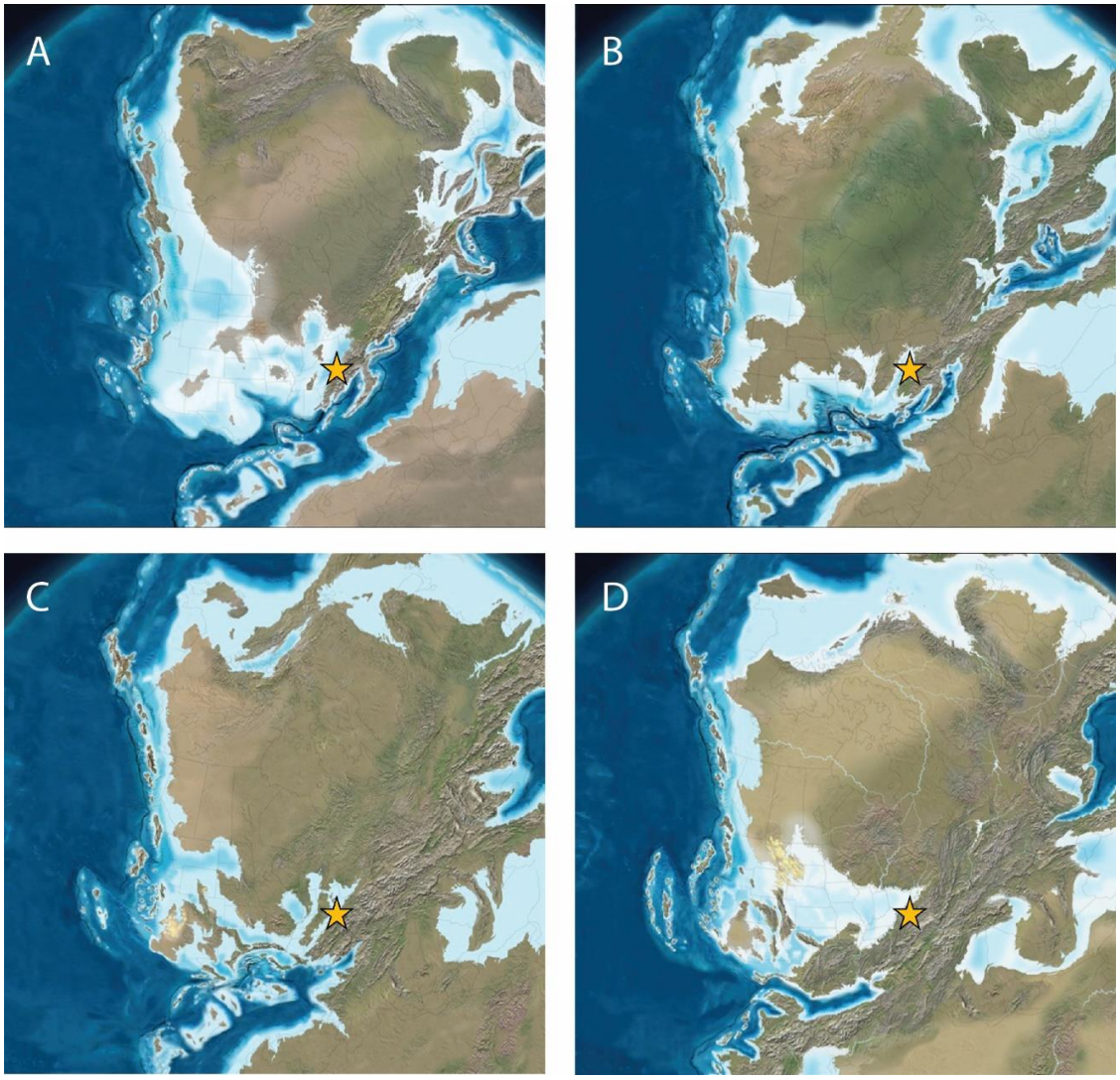

Figure 12: Paleogeographic maps constructed by Ron Blakey (2014) showing the Laurentia and Gondwana super-continent positions and the evolution of orogenic belts in the (A) Early Mississippian, (B) Late Mississippian, (C) Early Pennsylvanian, and (D) Late Pennsylvanian. Field location is marked by the yellow star.

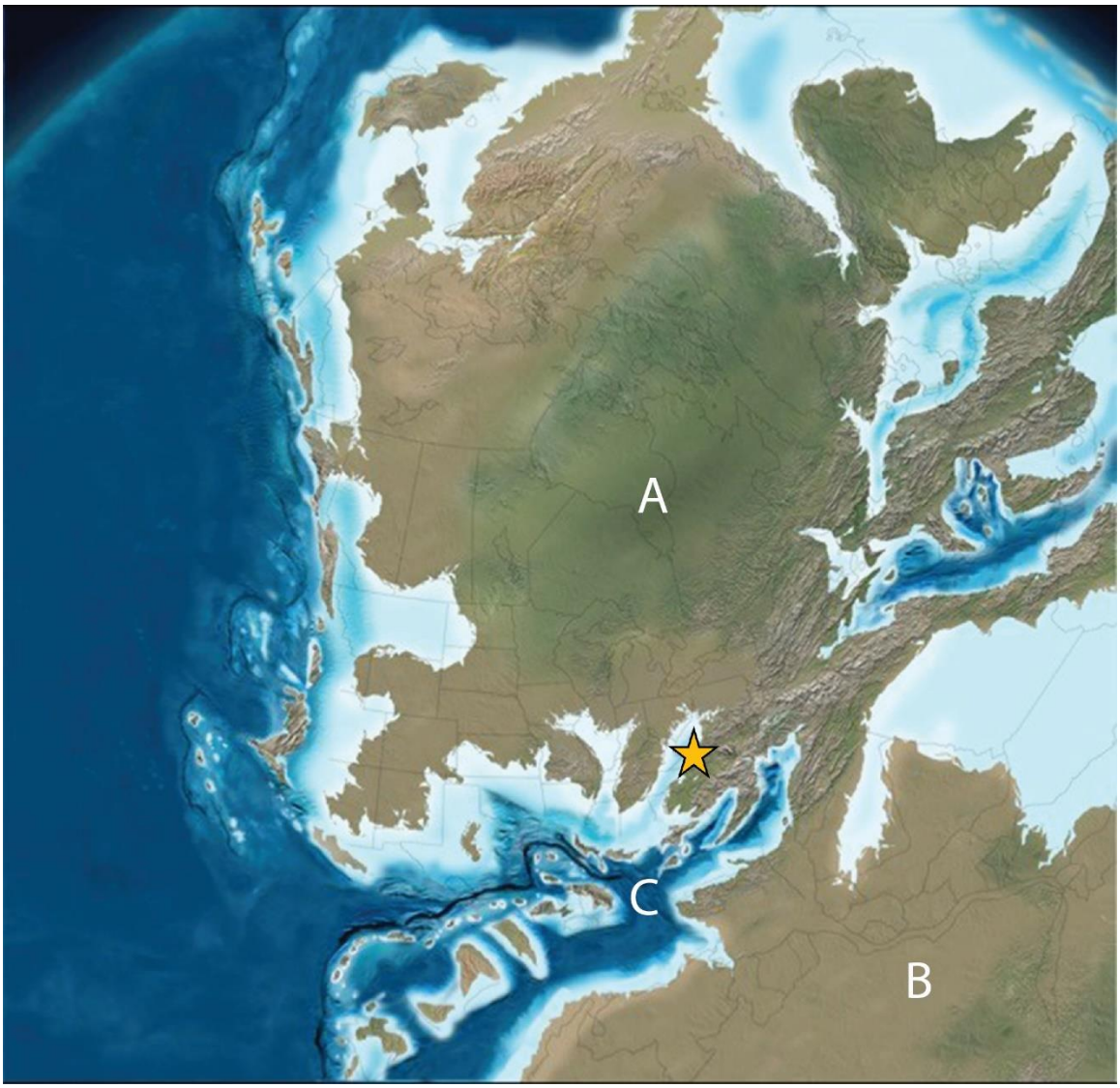

Figure 13: Enhanced view of the collision between (A) Laurentia and (B) Gondwana, leading to the regression of the epicontinental sea attached to the (C) Rheic Ocean during the Late Mississippian (Blakey, 2014). Field location is marked by the yellow star.

2.2 PREVIOUS FIELDWORK

In the Brush Creek Falls area near Eads Mill, West Virginia, a conglomeratic channel fill deposit was examined in the fall of 2012 (Matchen *et al.*, 2013). This channel fill is located stratigraphically within the lower Fivemile Member of the Hinton Formation (Figure 1). Further studies combined field analysis with point counts (Figures 14-15), mass percentage analyses (Figure 16), and chemical composition mapping

(Figure 17) on a scanning electron microprobe (Matchen *et al.*, 2013; McCreary and Matchen, 2014). These investigations, incorporating 114 points (Figure 14) and 60 points (Figure 15), showed that the channel fill contained rounded limestone clasts, rounded and angular coal clasts, nodular and disseminated pyrite and marcasite, microscopic marine fossils, and a mudstone/quartz matrix. This channel fill is oriented in a NE-SW direction, although lateral continuity could not be confirmed due to dense vegetation and soil cover. Limestone clasts present in this sandstone body are imbricated indicating provenance from the N-NE of the field area. The imbrication data factor into the current research, as they corroborate findings by previous authors (Pinnix, 1993; Miller and Eriksson, 2000) of paleoflow direction for much of the Hinton Formation to the S-SW. The conglomeratic channel fill exhibits morphology that is also seen in the upper Hinton Formation and Princeton Formation. The similar morphologies are likely due to similar processes, which is regression due to a drop in base level followed by incision.

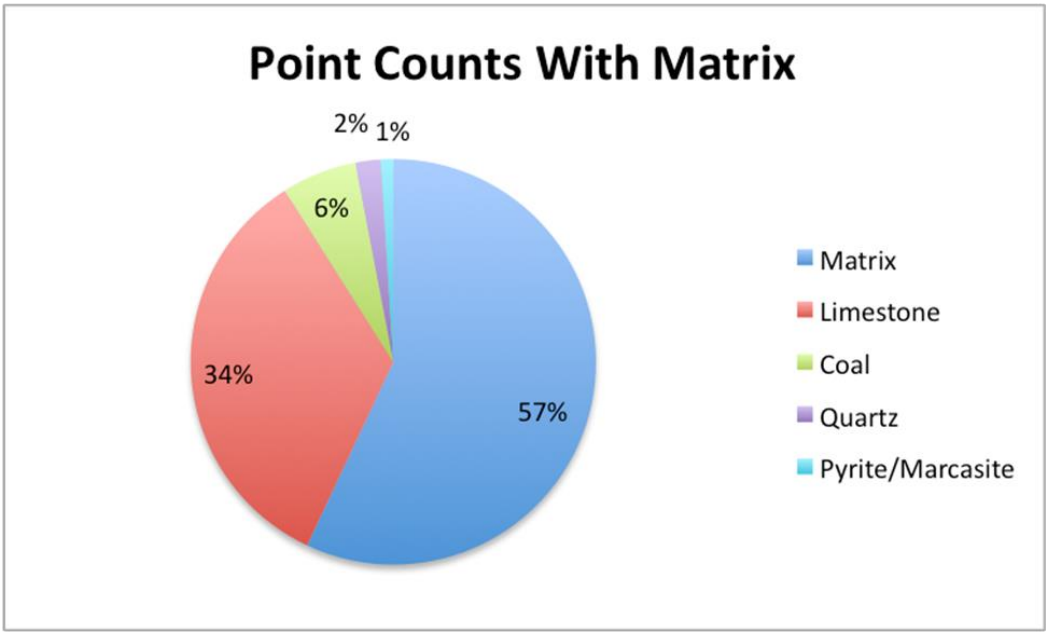

Figure 14: Point counts of fill composition for the valley fill in the lower Fivemile Member including matrix (McCreary and Matchen, 2014).

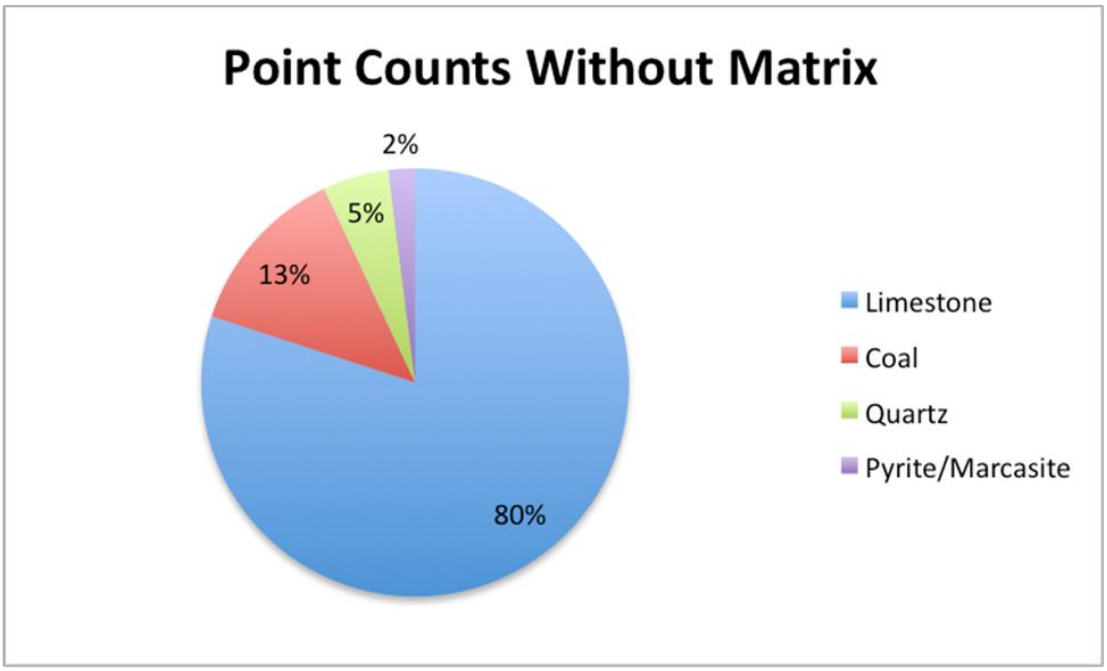

Figure 15: Point counts of fill composition for the valley fill in the lower Fivemile Member not including the matrix (McCreary and Matchen, 2014).

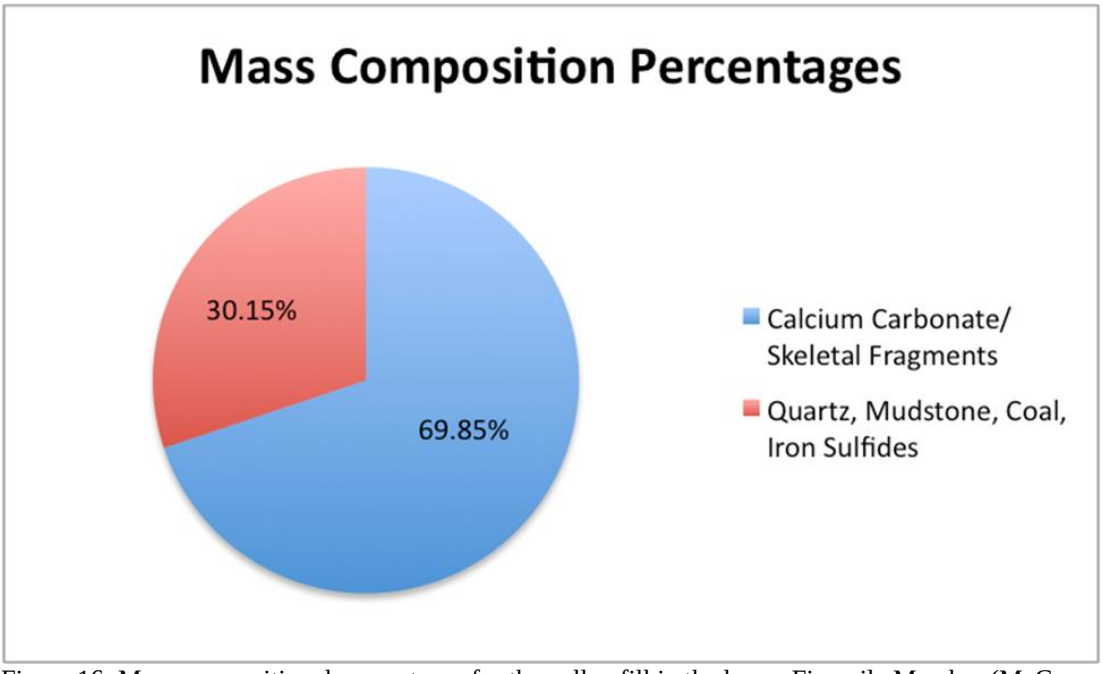

Figure 16: Mass compositional percentages for the valley fill in the lower Fivemile Member (McCreary and Matchen, 2014).

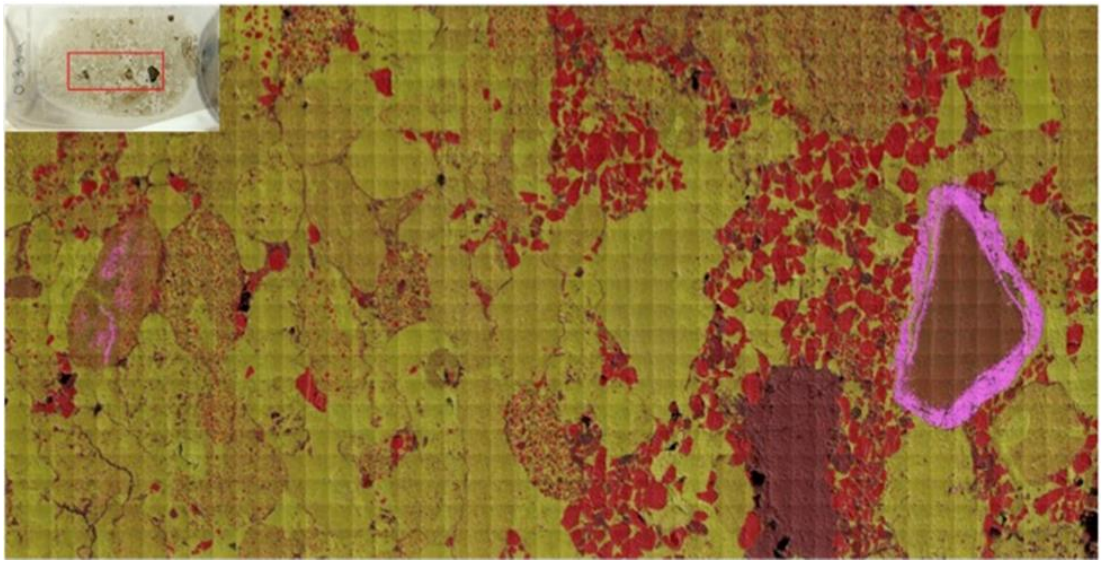

Figure 17: ARL-SEMQ chemical mapping of a thin section from the lower Fivemile Member valley fill (Matchen et al., 2013). Elements that are present include calcium (yellow-tan), silica (red), and sulfur (pink). The calcium (yellow-tan) represents limestone clasts, the silica (red) represents quartz, and the sulfur (pink) represents pyrite.

CHAPTER 3: METHODOLOGY

3.1 FIELD WORK

The main field study location comprises two outcrops, one on either side of US-460, approximately 2.8 kilometers (1.7 miles) east of the Interstate 77 Princeton exit in West Virginia (Figure 9). UTM coordinates for the outcrops are centered on 17S 498398.50m E 4134156.70m N, with latitude and longitude measurements being 37°21'14.81" N and 81°1'5.10" W. A secondary study location was also examined, with latitude and longitude measuring 37°21'42.48" N and 81°7'34.19" W (Figure 10). The secondary location is the type section for the Princeton Formation, and is located in the town of Princeton, West Virginia.

A photomosaic was constructed for the outcrops along both the north and south sides of US-460. Also, thirteen sections were sedimentologically logged at those two outcrops. The sedimentologic logs document the lithofacies and lithofacies architecture present in both outcrops. At each logged section, individual layers were characterized by lithology, color, grain size, sedimentary structures, outcrop geometry, and body and trace fossils. From these descriptions, lithofacies were identified and lithofacies assemblages were constructed in order to accurately interpret the conditions that prevailed at the time of deposition.

Samples were also taken at several locations along the outcrop and tied to the sedimentologic logs. Of these samples, 12 of the sandstone samples were sent to the National Petrographic Services, Inc. (NPS) laboratory in Houston, Texas, to make thin sections. These thin sections were then examined under a petrographic microscope and analyzed with an ARL-SEMQ scanning electron microprobe to obtain point counts of mineralogy and to construct chemical maps showing the distribution of major, minor, and trace elements.

3.2 THIN SECTION PETROGRAPHY

Thin sections were analyzed with an ARL – SEMQ (Applied Research Labs – Scanning Electron Microprobe Quantometer) scanning electron microprobe, housed at Concord University in Athens, West Virginia, under the direction of Dr. Stephen Kuehn. To analyze mineralogy, point counts were done for each thin section to obtain both quantitative and qualitative EDS (energy dispersive spectroscopy) data. Scanning electron microprobes (also referred to as electron probe micro-analyzers) operate as described by AMETEK, Inc. on their website (Electron Probe Micro-Analysis, 2016),

> EPMA works by bombarding a micro-volume of a sample with a focused electron beam (typical energy = 5-30 keV) and collecting the X-ray photons thereby emitted by the various elemental species. Because the wavelengths of these X-rays are characteristic of the emitting species, the sample composition can be easily identified by recording WDS spectra (Wavelength Dispersive Spectroscopy). WDS spectrometers are based on the Bragg's law and use various moveable, shaped monocrystals as monochromators.

Through this technique, specific chemical compositions can be analyzed per point, and then in combination with optical petrographic microscope examination, mineralogy can be determined. High resolution plane-polarized and cross-polarized scans of each slide were taken, which were then analyzed in comparison with the point counts to ensure

accuracy. On the thin section for a sample from the Princeton Formation type section (AMPSS-TL), an EDS chemical map was done due to metamorphic rock fragments being present, which will be discussed in the data section.

In order for the thin sections to be useable on the ARL-SEMQ, they had to be polished down further than the degree of polishing provided by NPS. To do this, a Buehler MetaServ 250 grinder-polisher (Figure 18) was utilized. They were first polished using 3-micron, 1-micron and 0.3-micron grit, each for five minutes (Figure 19). During the polishing process, the 1-micron grit ran out before it could be used on three of the thin sections, so these three thin sections were polished for ten minutes with the 0.3-micron grit.

Figure 18: Buehler MetaServ 250 grinder-polisher used to prepare thin sections for ARL-SEMQ.

Figure 19: 3-micron grit (left), as well as 1-micron and 0.3-micron grits (right).

After polishing was completed, the thin sections were scanned in both plane-polarized and cross-polarized light using an Epson Perfection V850 Pro Dual Lens System – High Pass Optics scanner and cross-polarizing film. They were then carbon-coated using a Denton Vacuum DV-502. Once coated, they were loaded into the ARL-SEMQ two at a time and calibrated using a modified tephra glass technique designed by Dr. Stephen Kuehn. Finally, they were each assigned a polygon grid, with point-count spacing adjusted so that close to 200 points per slide were examined. During this last step, each corner point was selected and chemically analyzed if unusual grains were present, and each of the points used for the count was manually inspected to ensure that the analysis was done on a grain as opposed to matrix material. There may have been a slight bias towards selecting grains with higher backscatter energy readings, but probably not enough to influence mineralogical trends.

Once the ARL-SEMQ analysis was finished analyzing the points on both slides, the elemental data were analyzed for ‘unusual’ grains. These ‘unusual’ grains were then chemically mapped using the EDS. After all point counts were completed, a detailed EDS chemical map of one thin section, AMPSS-TL, was conducted. This thin section was selected due to the conglomeratic nature of the sample, which varied from the eleven other relatively homogenous thin sections, and the presence of potential metamorphic rock fragments when examined under a petrographic microscope.

3.3 LOG SECTIONS

Representative locations were identified at intervals along the road cuts and were sedimentologically logged. Each log recorded the lithology, grain size, sedimentary structures, color, bedding thickness, and bioturbation in a vertical section. The field data were then recorded in a digital logging package known as SedLog, available for free through Royal Holloway at the University of London. Those digital logs appear later in the data section. From those logs, lithofacies were identified and recurring packages of lithofacies were grouped into three lithofacies associations.

3.4 FACIES

Individual facies were identified that correlate across both outcrops. These facies were selected based upon characteristics such as grain size, color, sedimentary structures, bedding thickness, and lithology.

3.5 FACIES ASSOCIATIONS

Facies associations are a collection of one or more lithofacies. If discrete lithofacies typically occur together, they were assigned to the same lithofacies association.

3.6 PHOTOMOSAICS

Pictures were taken facing both the northern and southern outcrops, and then stitched together into photomosaics for each exposure. At each exposure, the photographs were taken from a distance of about 20-25 meters between the outcrop and camera. This allowed for a compilation of images that showed the entire vertical section of the exposure within each photograph, but with enough overlap between photographs to limit distortion. The photomosaics were started at one end of the outcrop and were compiled laterally, with between five and ten meters of lateral movement between photographs. This resulted in about one-third overlap between the photographs, thereby minimizing distortion of the images. Each picture incorporated a field assistant (Stephen Rachide, who is about 1.75 meters tall) for scale. Construction of a photomosaic in this fashion, as opposed to a panoramic photograph taken from one location by swiveling the camera, allowed for minimal vertical and horizontal distortion of the photographic record of the outcrop. Once the photographs were stitched into a final composite photomosaic, facies associations were correlated, and recorded with line drawing overlays showing the contacts between facies associations. A color-coded panorama was then constructed that documented the lithofacies architecture of the exposure recorded in those images. The architecture of the facies associations could then be analyzed across the entire outcrop.

Due to the lengths of the southern and northern outcrops, the complete panorama reproduced in the text is at a small scale. In order to better see details, portions of the outcrop were enlarged and coupled with their respective logged sections. This was done to show a higher level of detail and make it easier to analyze the facies architecture.

CHAPTER 4: DATA

4.1 FACIES

The siltstone facies is a red to red-brown siltstone and rare mudstone (Figure 20). Grain size ranges from clay-silt to silt-very fine sand. The beds are centimeters up to a meter thick, with common blocky structures ranging from millimeters to centimeters in scale. These blocky structures were present in nearly every layer, although a platy fabric was observed where blocky structures were absent. The blocks have polished surfaces and locally exhibit clay films. The upper portions of the siltstones exhibit sub-vertical tubules that are lighter in color, and are decimeters in length and centimeters in width. Some of the tubules taper downward, indicative of root casts.

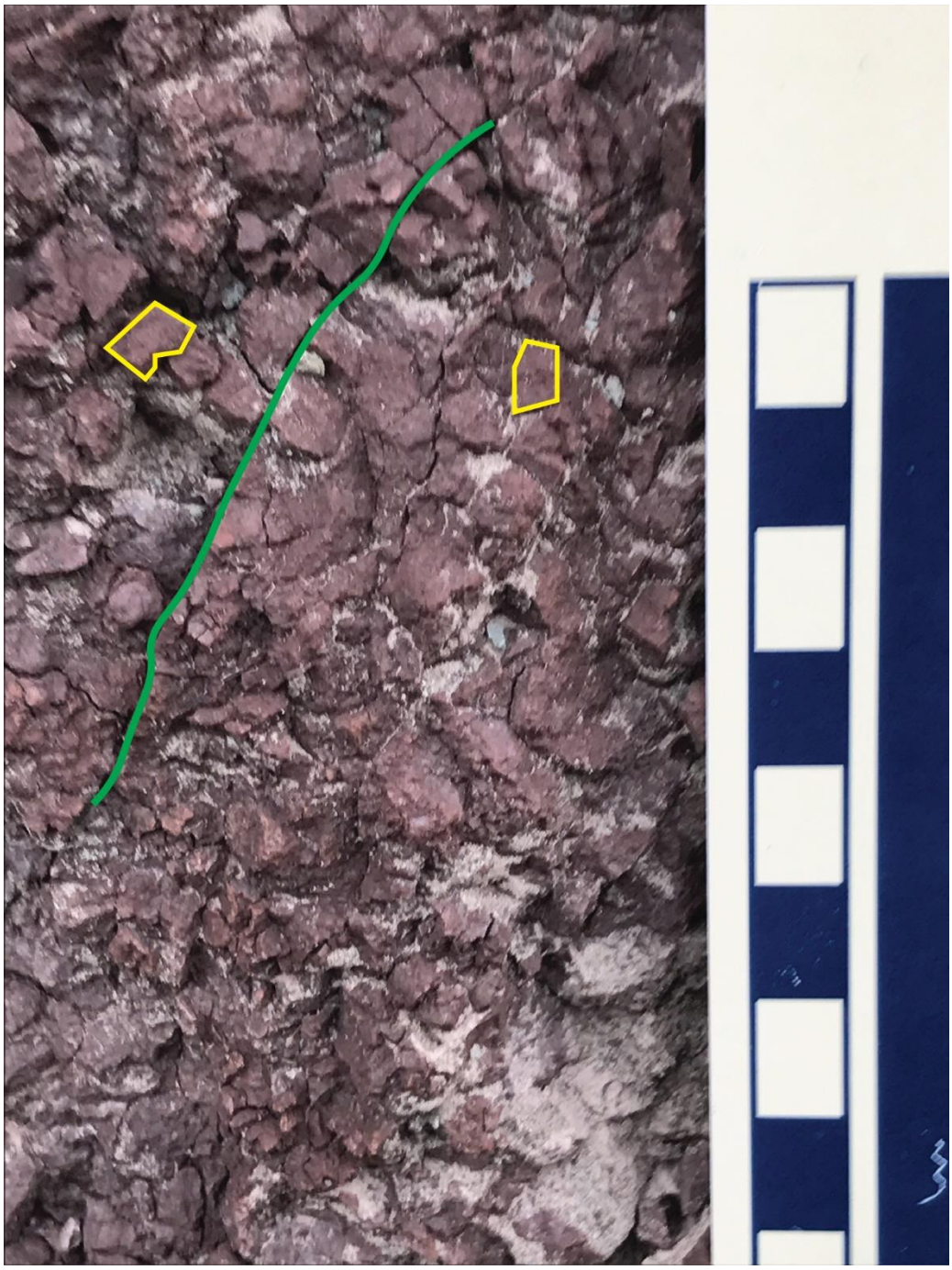

Figure 20: Siltstone facies with a through-going fracture (green line) and blocky structures (two of the cm-scale blocks are outlined in yellow). Scale is in centimeters.

The thin-bedded sandstone facies is a light to medium gray, with occasional dark gray colors, and composed of quartz wacke and quartz litharenite. Grain sizes of this facies ranges from very fine to fine sand, and the sandstones typically fine upward. The beds are centimeters to a decimeter thick, with occasional beds more than ten centimeters

thick. The thin-bedded sandstone facies is massive to cross-laminated. The bases of the thin sandstone beds are generally sharp and erosional (Figure 21).

Figure 21: The thin-bedded sandstone facies (units marked by arrows) are centimeters to decimeters thick and are light to medium gray in color. The interbedded units not labeled with arrows and exhibiting blocky fabric belong to the siltstone facies.

The medium-bedded sandstone facies occurs as both cross-stratified and planar stratified sandstones with subordinated cross-laminations (Figures 22 and 23). The medium-bedded sandstone facies is medium to dark gray in color, with local off-white to light gray colors. It is dominantly composed of quartz litharenite. Grain sizes range from fine to coarse, and this facies generally fines upward within a bedset. The beds range from ten centimeters to one meter in thickness. The medium-bedded sandstone facies can be traced laterally over tens of meters and locally tapers gradually, thereby exhibiting a lenticular morphology. The cross-bedding and cross-lamination orientations indicate that paleoflow was oriented generally toward the south-southwest. Most of the outcrop faces are also aligned in a southwest orientation, thus if lateral accretion surfaces are present, they are difficult to observe (Figure 22).

Figure 22: Medium-bedded sandstones (noted by the arrows) exhibiting lenticular morphology in the center of the photograph. Planar-stratified medium-bedded sandstone (left extent of larger medium-bedded sandstone deposit noted with arrow) also occurs. The remainder of this outcrop consists of the siltstone facies (red in color), and the thin sandstone facies (gray in color with thin beds).

Figure 23: Planar-stratified medium-bedded sandstone deposit (arrow) extending tens of meters before pinching off. Other sandstones present, which are gray in color, belong to the thin-bedded sandstone facies. Red layers belong to the siltstone facies.

The thick, cross-bedded well-cemented sandstone facies is a tan to light gray to medium gray quartz litharenite (Figure 24). Grain sizes range from fine to coarse sand, with the basal section containing pebbles, making it locally a conglomerate. There are multiple generations of cross-bedding present with cross-bed sets ranging from decimeters to a meter in thickness. The beds range from twenty centimeters to two meters thick, with the amalgamation of beds reaching up to four meters. This lithofacies is laterally extensive for hundreds of meters along the southern outcrop, but does not occur in the northern outcrop. The basal contact is erosive, the top contact is planar, and this well-cemented facies forms overhangs in the road cut (Figure 24).

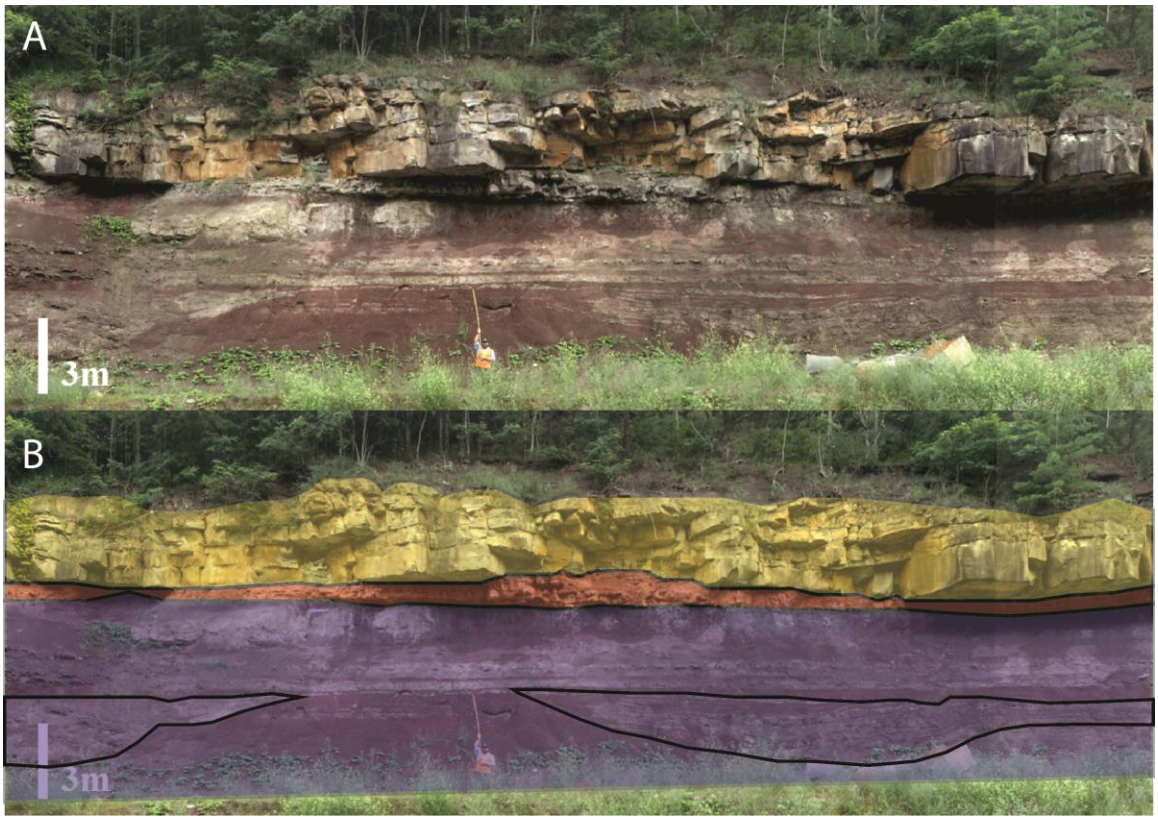

Figure 24: (A) Thick-bedded sandstone facies at the top of the outcrop extends hundreds of meters with variable bedding thicknesses. This well-cemented lithofacies forms an overhanging ledge immediately above a planar stratified medium-bedded sandstone. Red units at the base of the outcrop (at the interval indicated by the geologist with the extended stadia rod) belong to the siltstone facies. Thin gray layers to the right of the geologist filling a broad symmetrical channel belong to the thin sandstone facies. (B) Color overlay shows the thick-bedded sandstone facies (yellow), planar-stratified medium-bedded sandstone facies (red), and a combination of siltstone facies and thin-bedded sandstone facies (purple). Channel forms are outlined in the purple portion of the overlay.

4.2 FACIES ASSOCIATIONS

Facies Association 1: Interbedded siltstones and thin-bedded sandstones.

Facies Association 1is dominated by decimeter to meter-thick siltstones that range in color from red to brown to, rarely, gray. The siltstones are interbedded with centimeter to decimeter thick cross-laminated fine sandstones that are light gray in color. The siltstones and fine-grained sandstones are quartz wackes to quartz litharenites. Facies association 1 is laterally extensive for tens of meters and the ratio of the sandstones to siltstones varies, as does the thickness. The siltstones within this facies association

contain centimeter-scale blocky fabric with clay films, and, in its upper portions, sub-vertical tubules that are centimeters in diameter and decimeters in length. The sub-vertical tubules are light gray to tan in color in contrast to the dominantly red siltstone matrix (Figure 25).

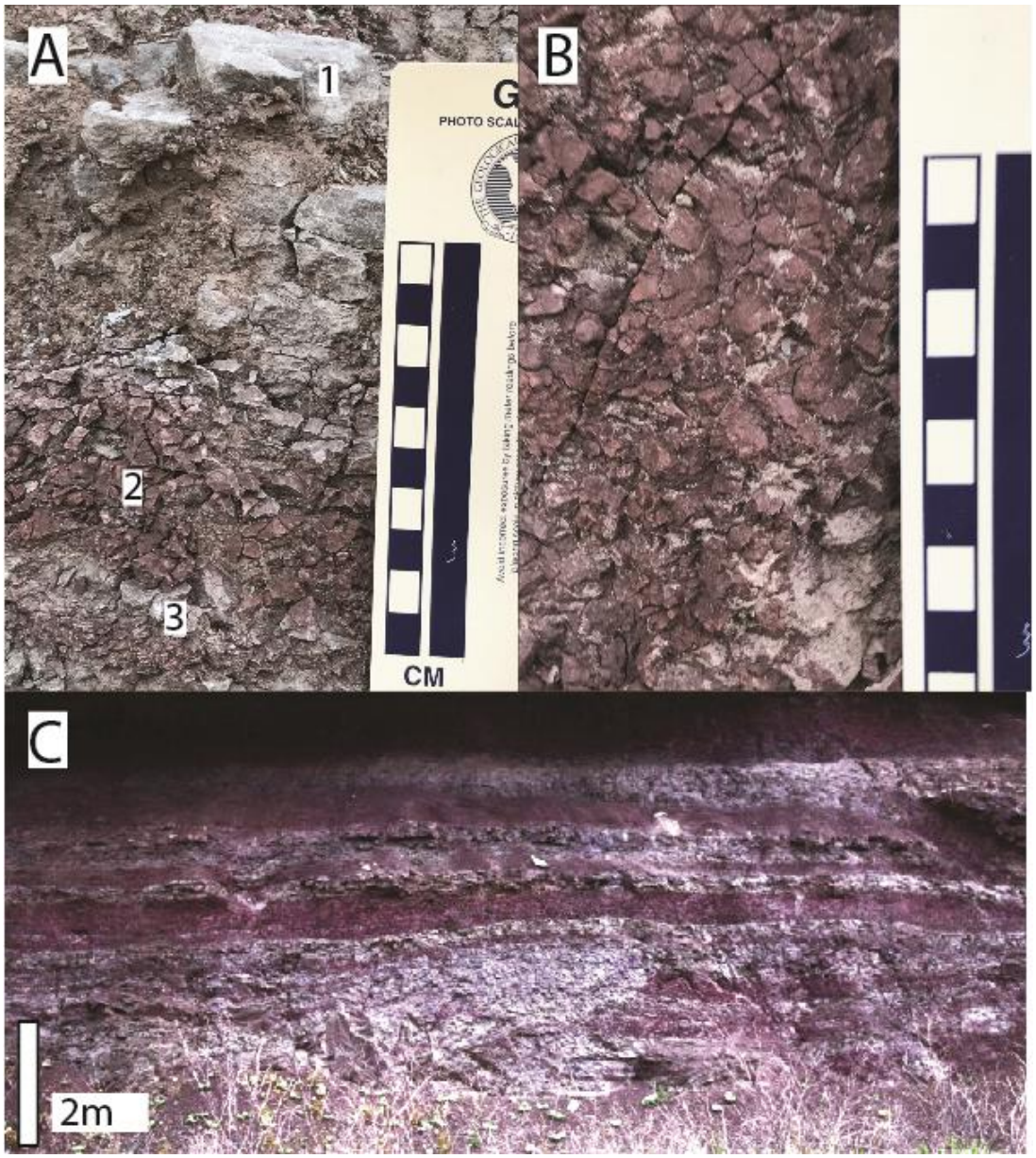

Figure 25: Facies association 1. (A) Thin sandstones (1 and 3) and siltstone (2) are interbedded. (B) Siltstone containing cm scale blocky structure interpreted as peds. (C) View from a distance of the southern outcrop illustrating the frequent alteration between thin sandstones (gray) and siltstones (red-purple) with lateral variability. Note the presence of a portion of a channel fill composed of this facies association in the lower left part of the image. Image C is a close-up of Figure 24 where the entire channel fill can be seen and it has been color-adjusted to highlight the alternating pattern of the siltstone and thin-bedded sandstone facies.

Facies Association 2: Lenticular, erosively-based, medium-bedded sandstones

Facies Association 2 comprises off-white, light to medium to dark gray, very fine to medium grained, massive to locally cross-laminated and cross-bedded quartz litharenite sandstones that occur in beds about10 centimeters to one meter thick. Beds have erosive basal contacts beneath small (1-2 meters deep) channel fills and gradational basal contacts beneath decimeter thick, tabular deposits with planar tops. This facies association comprises tabular to lenticular units that can be traced laterally for meters to tens of meters before pinching out (Figure 26).

Figure 26: Facies association 2. (A) A 2-meter thick channel form appears to migrate laterally to the right, and features consistent with lateral accretion surfaces can be seen. (B) Outline of a channel deposit in facies association 2 from an oblique view. Channel size variability is common, with some exhibiting a greater depth to width ratio (A) while others are broader (B). In both images, facies association 2 is outlined with a black line. All other strata present belong to facies association 1.

Facies Association 3: Erosively-based, thick-bedded, cross-stratified sandstones

Facies Association 3 comprises off-white, tan to light-gray, fine to medium to coarse-grained, massive to trough cross-stratified, quartz litharenites. The beds in this facies association are decimeters to meters in thickness, and have erosive basal contacts with decimeters of relief. The facies association extends laterally for tens to hundreds of meters forming distinctive cliffs in outcrops. Its thickness varies laterally from 1 to 4 meters (Figure 27).

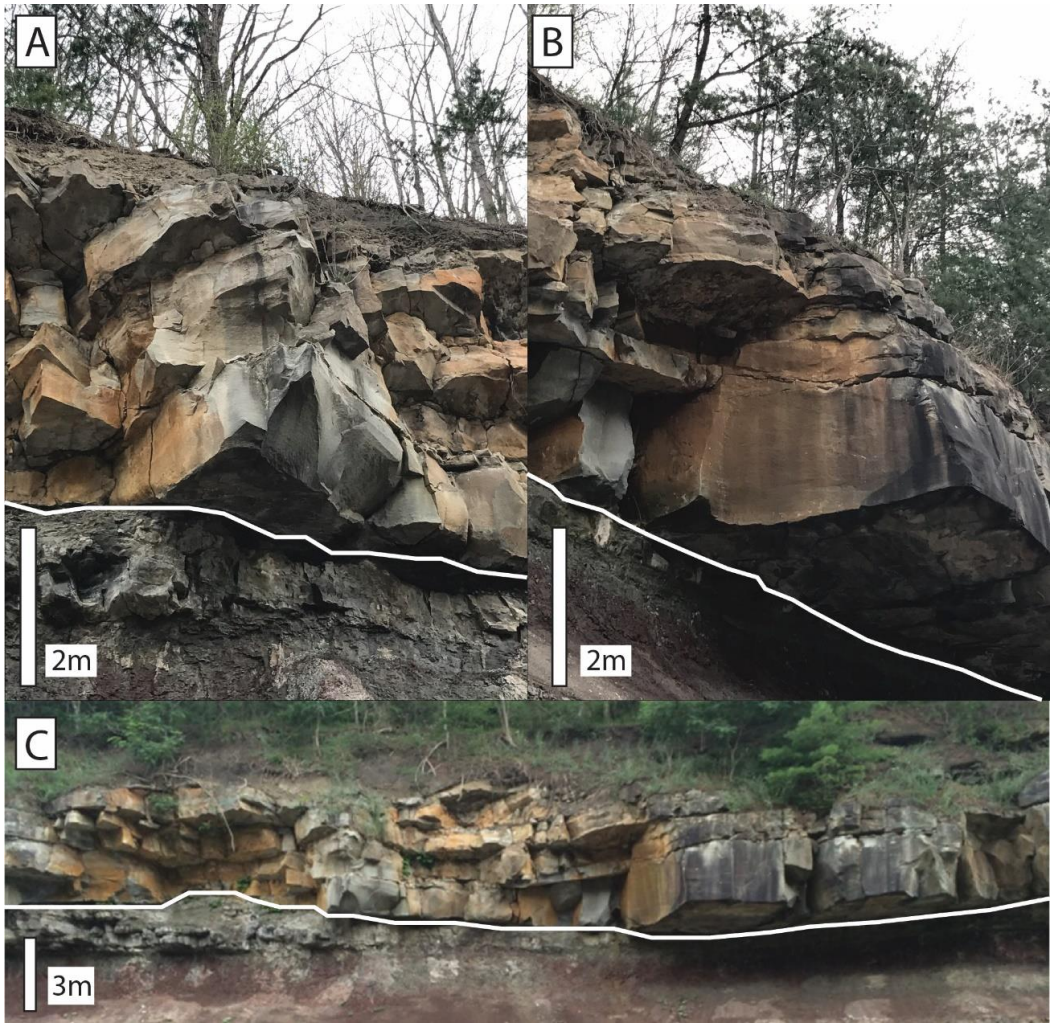

Figure 27: Facies association 3. (A and B) The distinctive cliff-forming nature of this facies association in the southern outcrop creates fifty centimeter to two meter overhangs. (C) Looking south from across US-460, the laterally variable thickness and sections with overhangs can be seen. Possible lateral accretion surfaces dipping to the left (east) are also visible. In all images, basal erosion surfaces are marked by white lines, which separate facies association 3 (above line) from facies associations 1 and 2 (below line). Above facies association 3, the outcrop is obscured by dense vegetation and soils.

4.3 SEDIMENTOLOGIC LOGS

Sedimentologic logs were taken at thirteen locations to better understand the lithology and to examine potential patterns of deposition. In the field, observations were recorded based on grain size, color, unit thickness, sedimentary features, lithology, fossils, and paleoflow directions. Once field observations were completed, SedLog was utilized to construct digitized logs (Figures 28-39). On the left side of each log, numbers for each **logged unit** are displayed which correlate to sample numbers, while the right side has numbers that correlate to **depositional units** which can be composed of one or more logged units. It is the depositional units (made of one or more logged units) that are portrayed on the photomosaics later in this report. Asterisks next to logged unit numbers show where thin section samples were taken. A facies association column is furthest right, which will be used to interpret depositional environments. Sedimentologic log five is not included, as its thickness could not be determined and it overlays the Princeton Formation, and therefore was stratigraphically above the study interval.

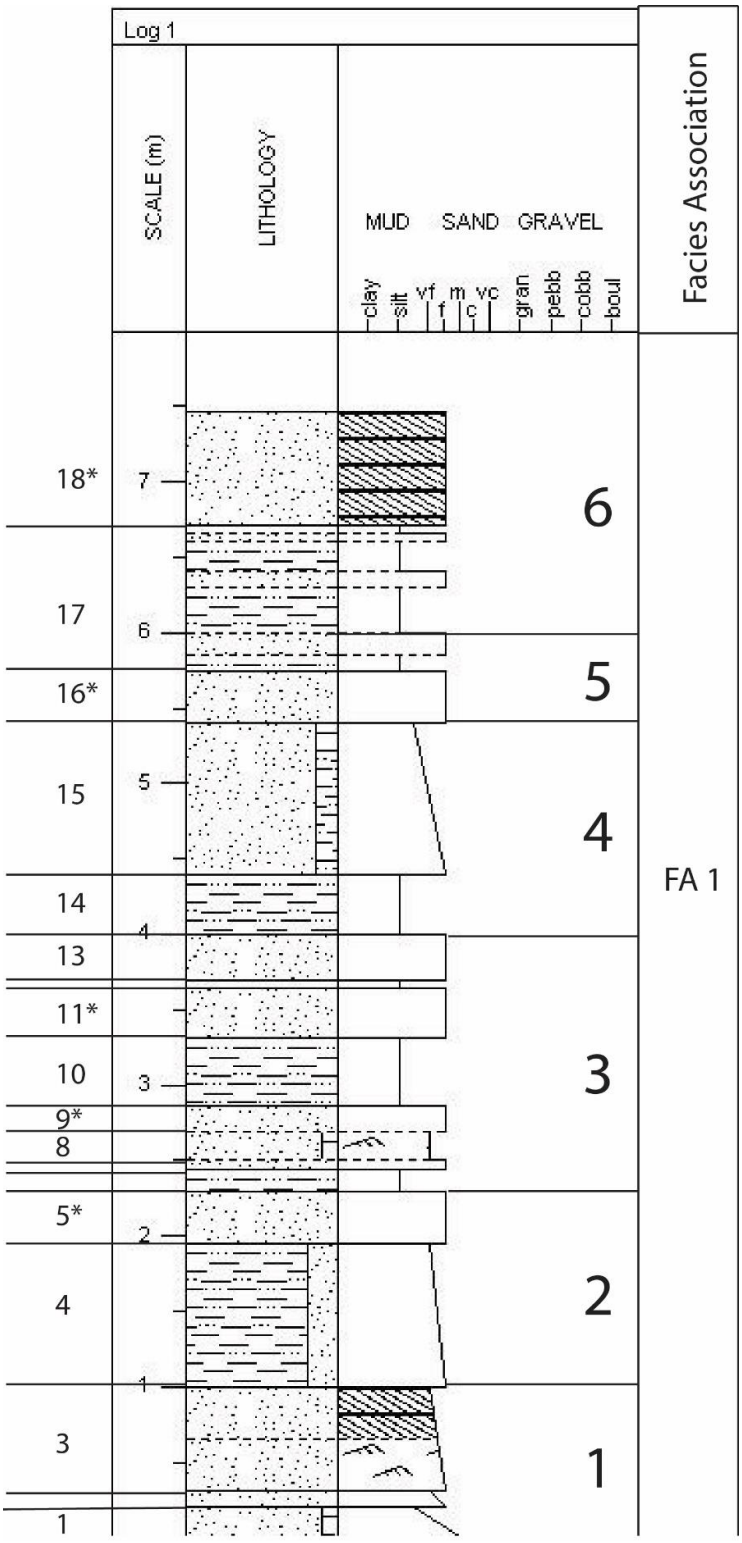

Figure 28: Log 1. Cross-lamination is present in the bottom of the third and eighth logged units, with cross-bedding present in the top of the third and eighteenth logged units. The numbers on the left of the log refer to the 'logged units', whereas the numbers on the right are 'depositional units' composed of one or more logged units. The facies association designation appears in the right column.

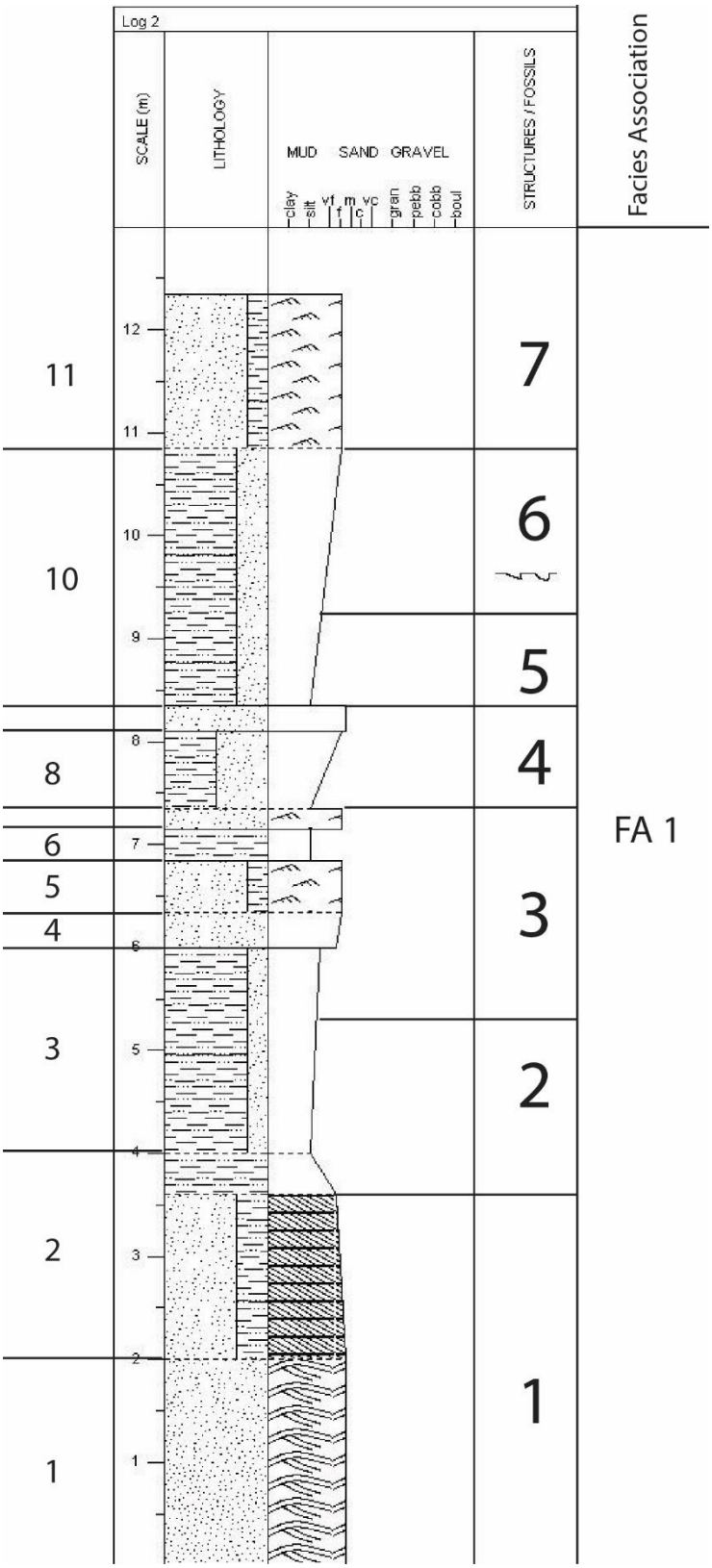

Figure 29: Log 2. Cross-stratification is present in the bottom two logged units. Cross-lamination is present in the sixth, eighth, and eleventh logged units. Scour marks were present in the tenth logged unit.

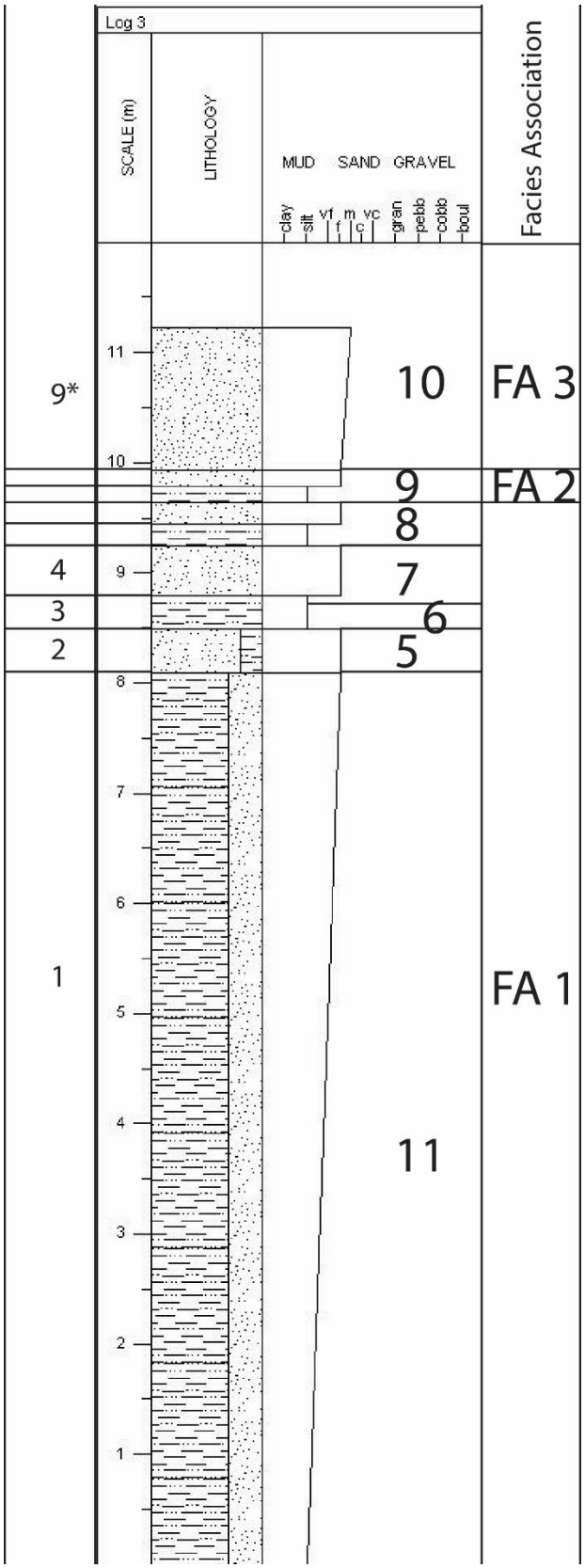

Figure 30: Log 3.

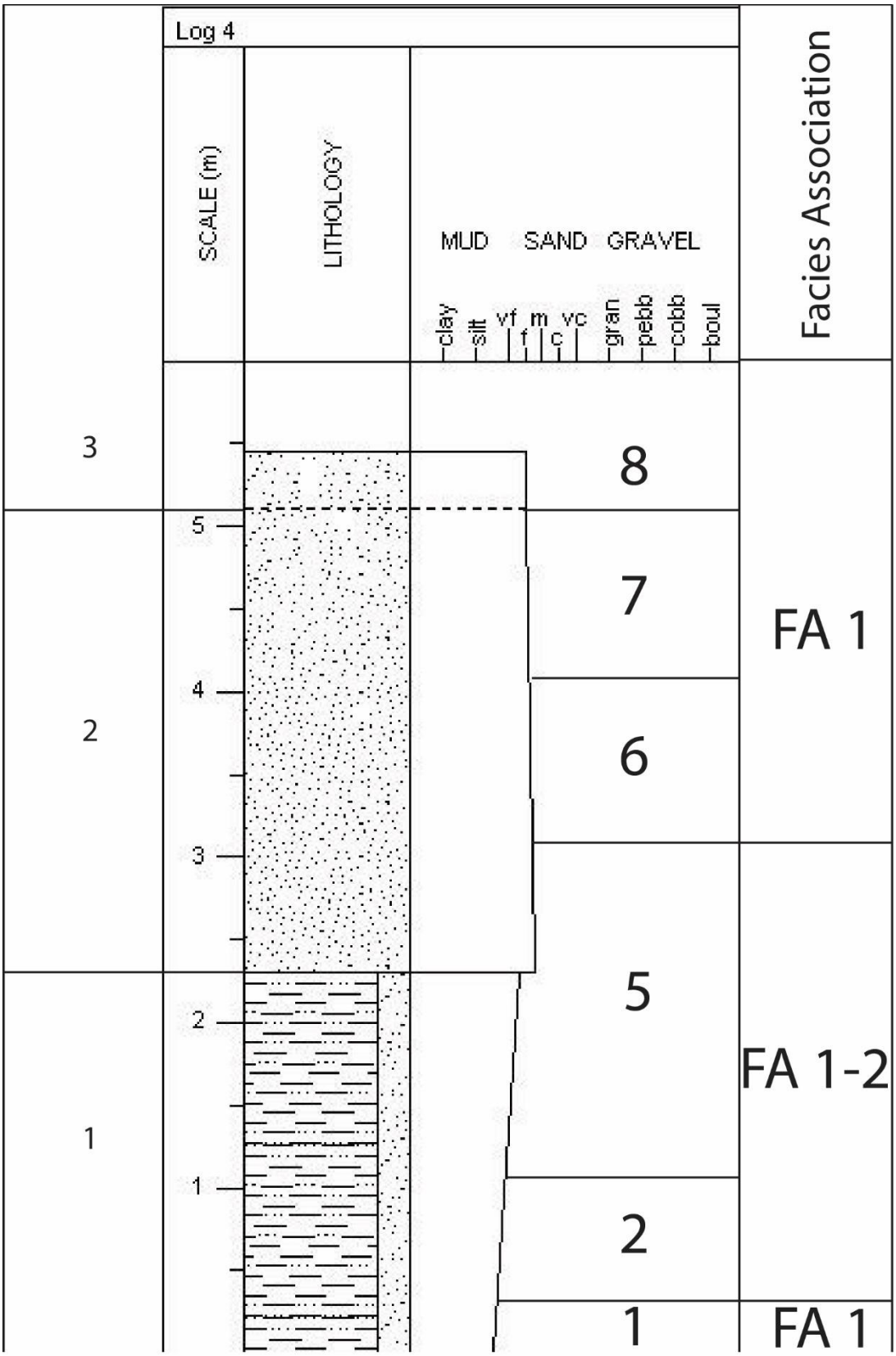

Figure 31: Log 4. Depositional units 2 and 5 are characterized as FA 1-2 due to the lithologic similarities to FA 1, while having a geometry similar to a channel form of FA 2.

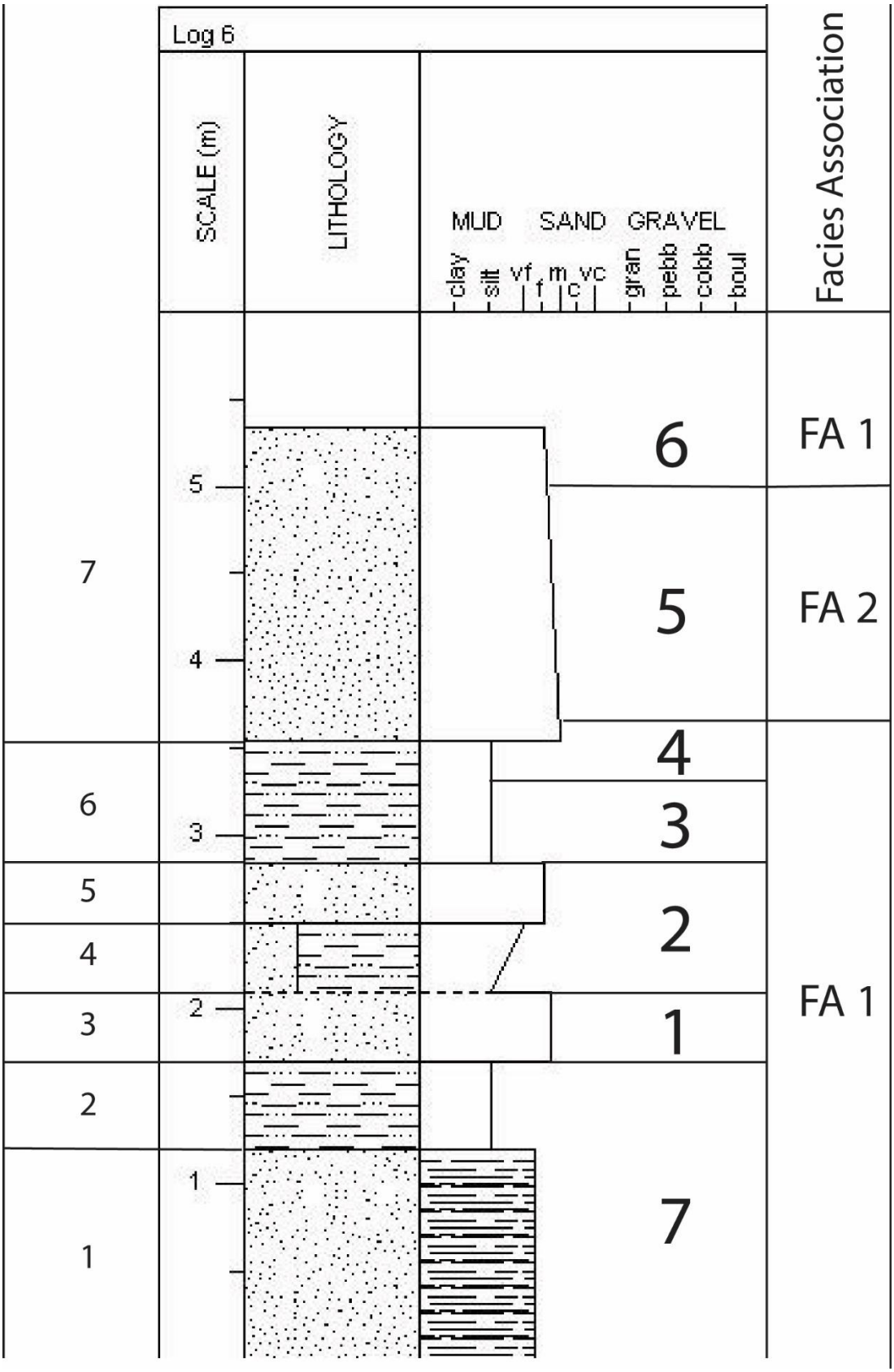

Figure 32: Log 6. Horizontal planar laminations are present in the bottom unit.

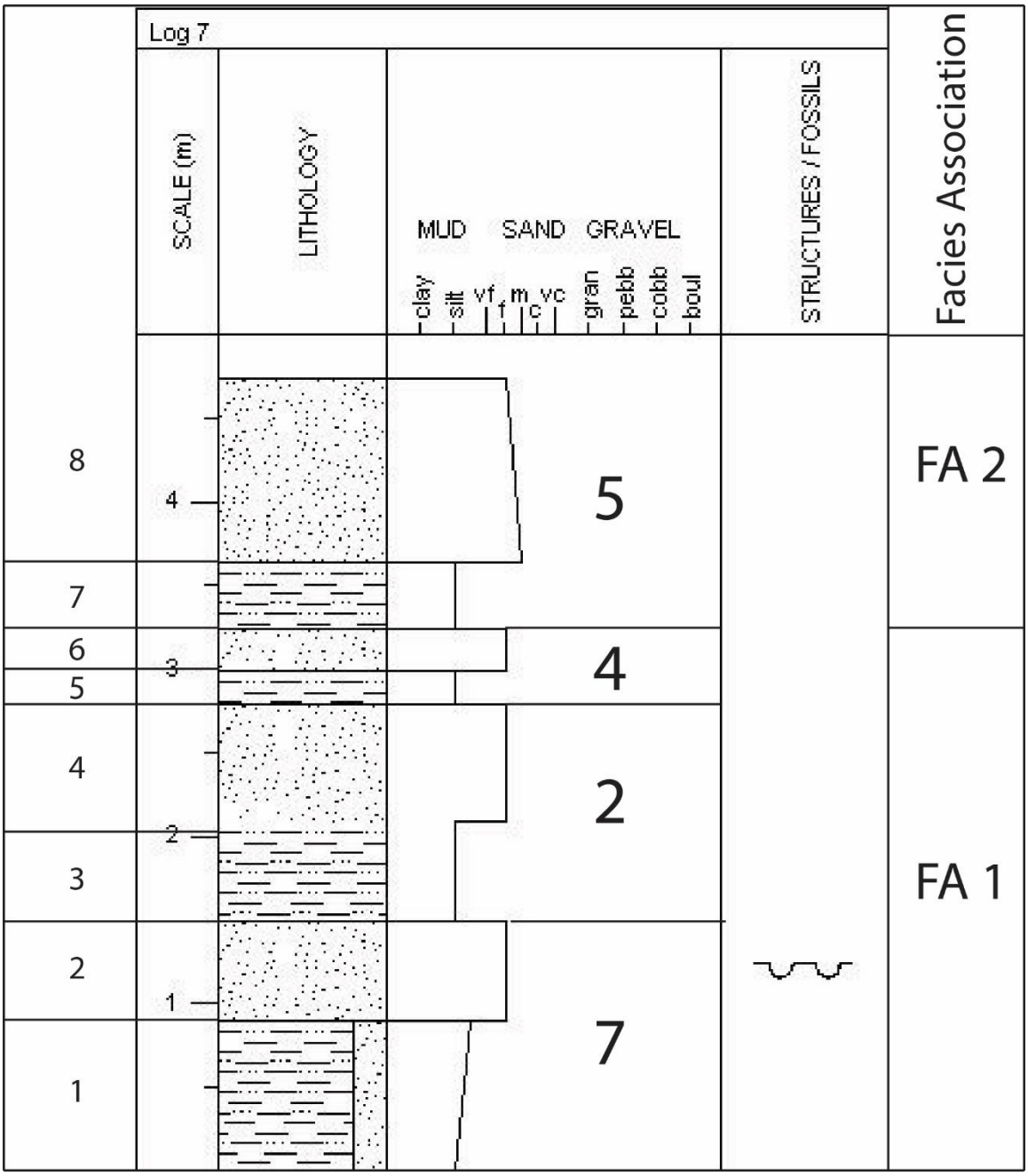

Figure 33: Log 7. Load casts were present in the second logged unit.

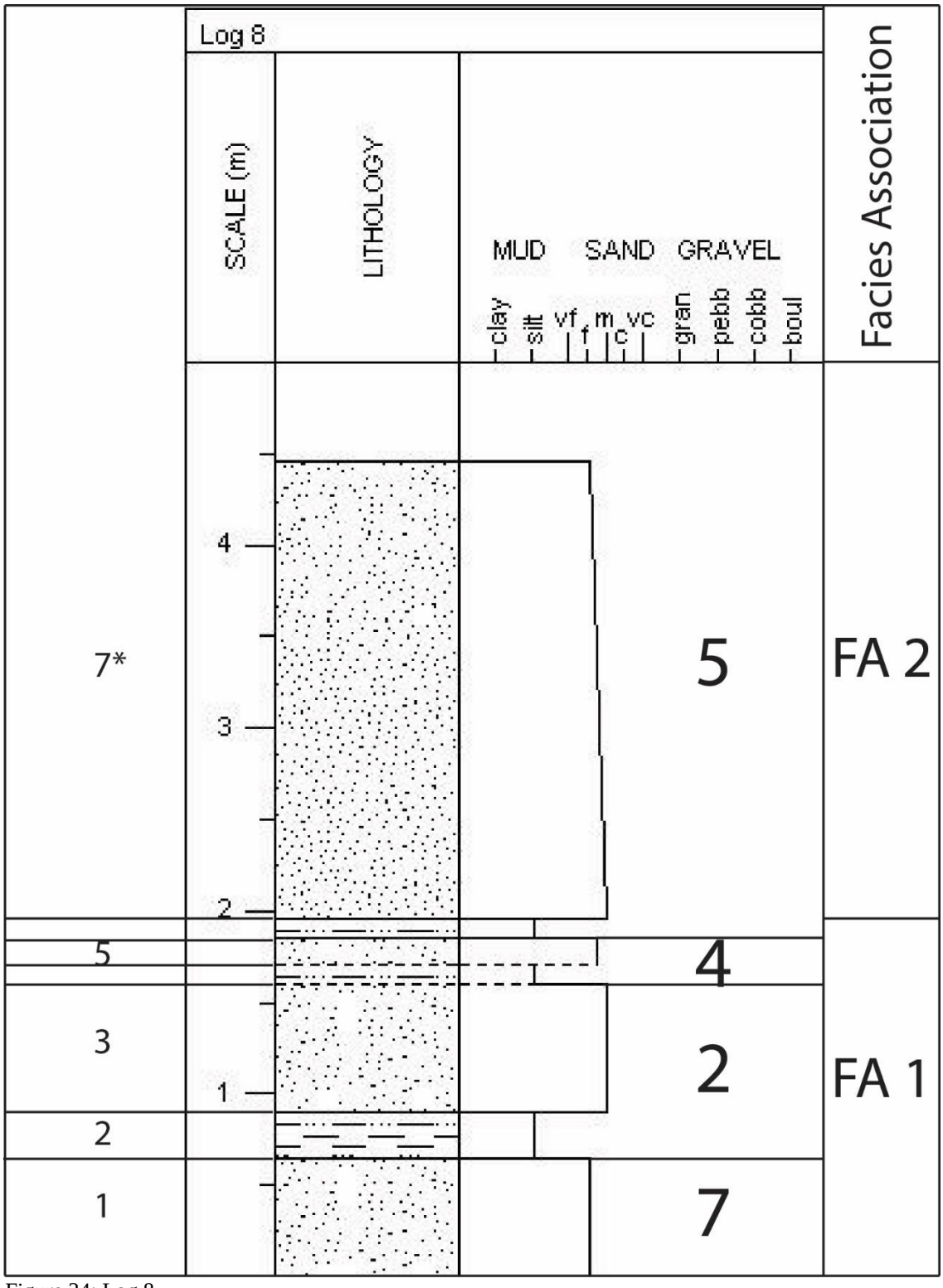

Figure 34: Log 8.

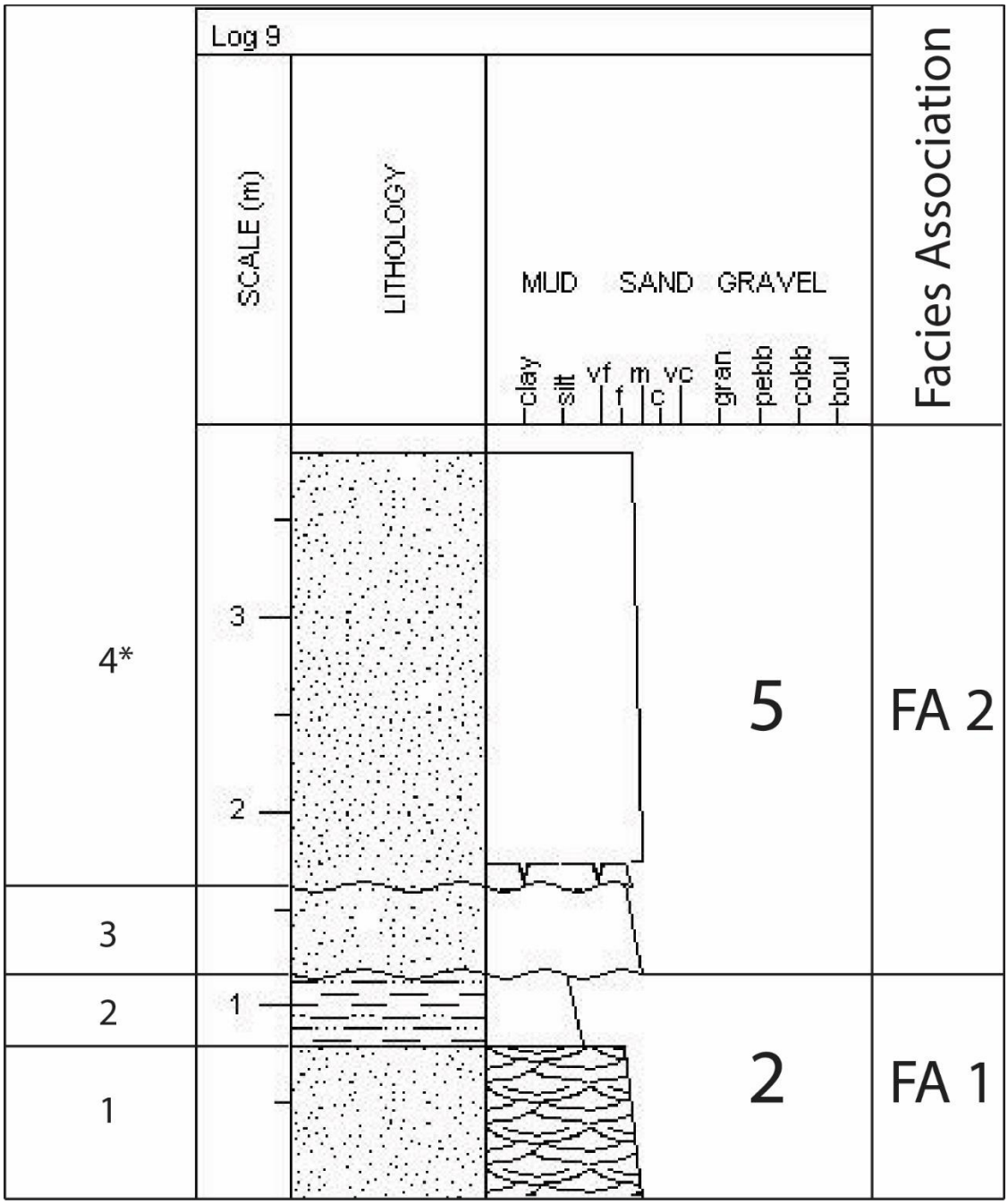

Figure 35: Log 9. Cross-bedding is present in logged unit 1. Mud cracks are present at the bottom of logged unit 4.

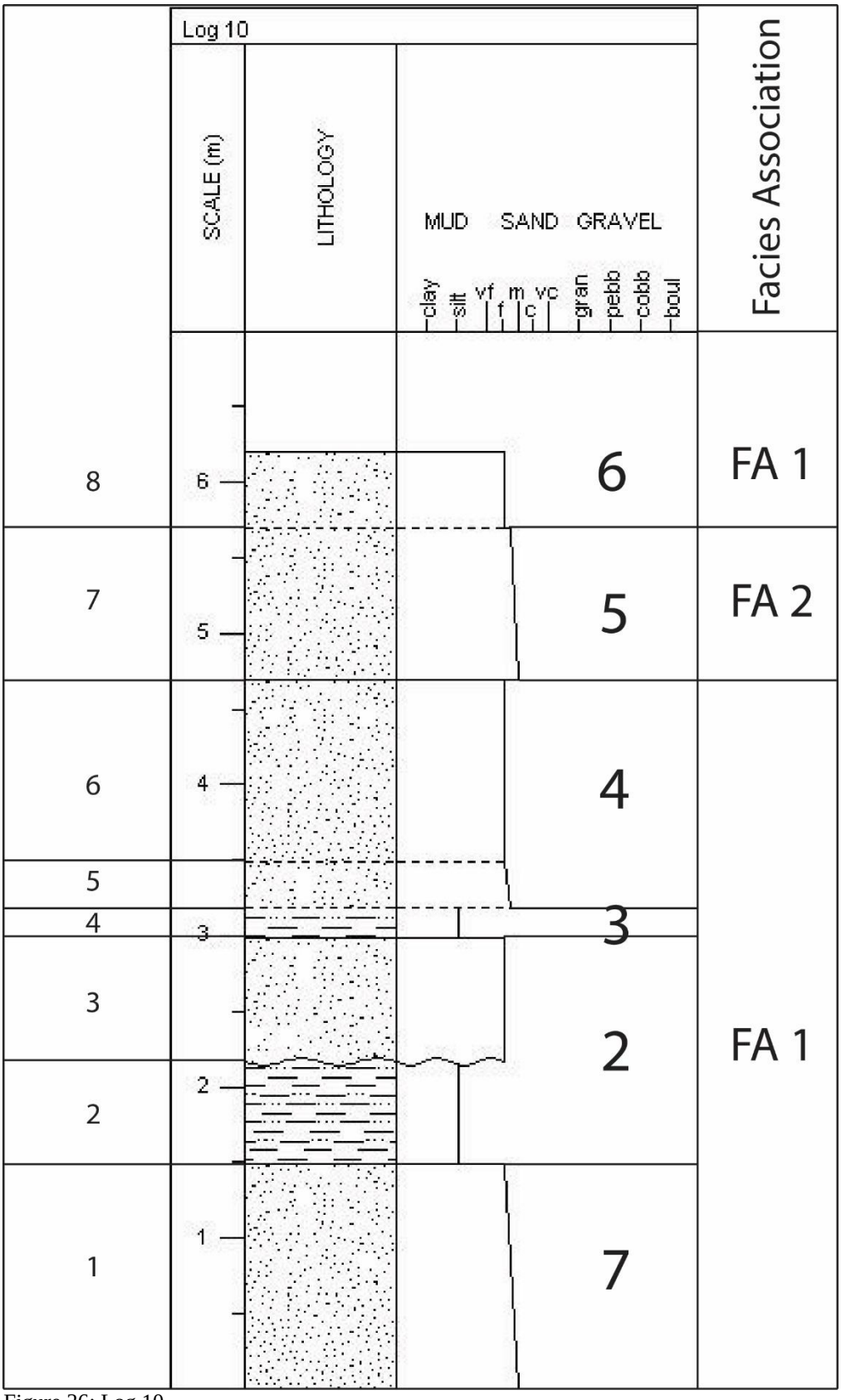

Figure 36: Log 10.

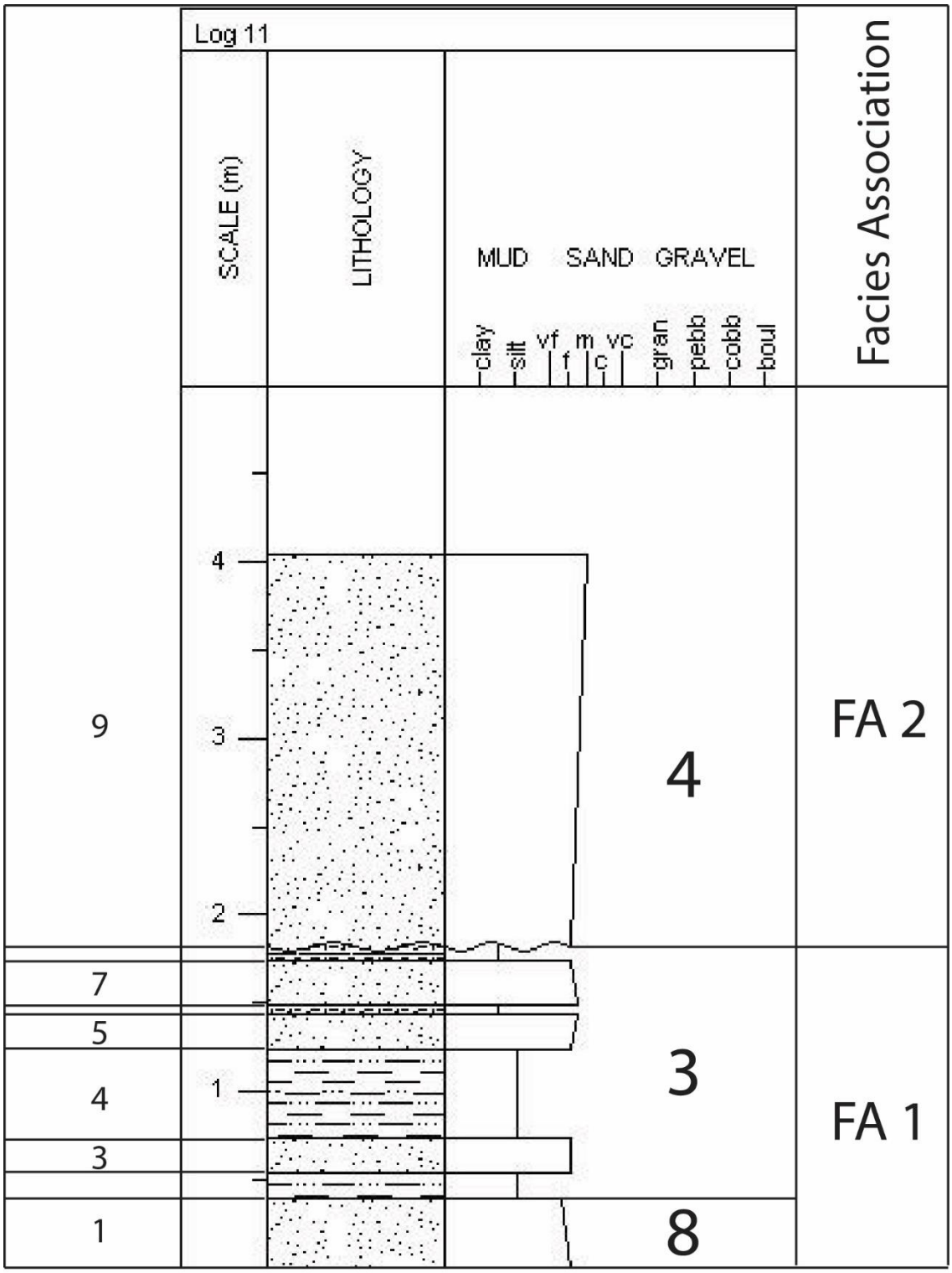

Figure 37: Log 11.

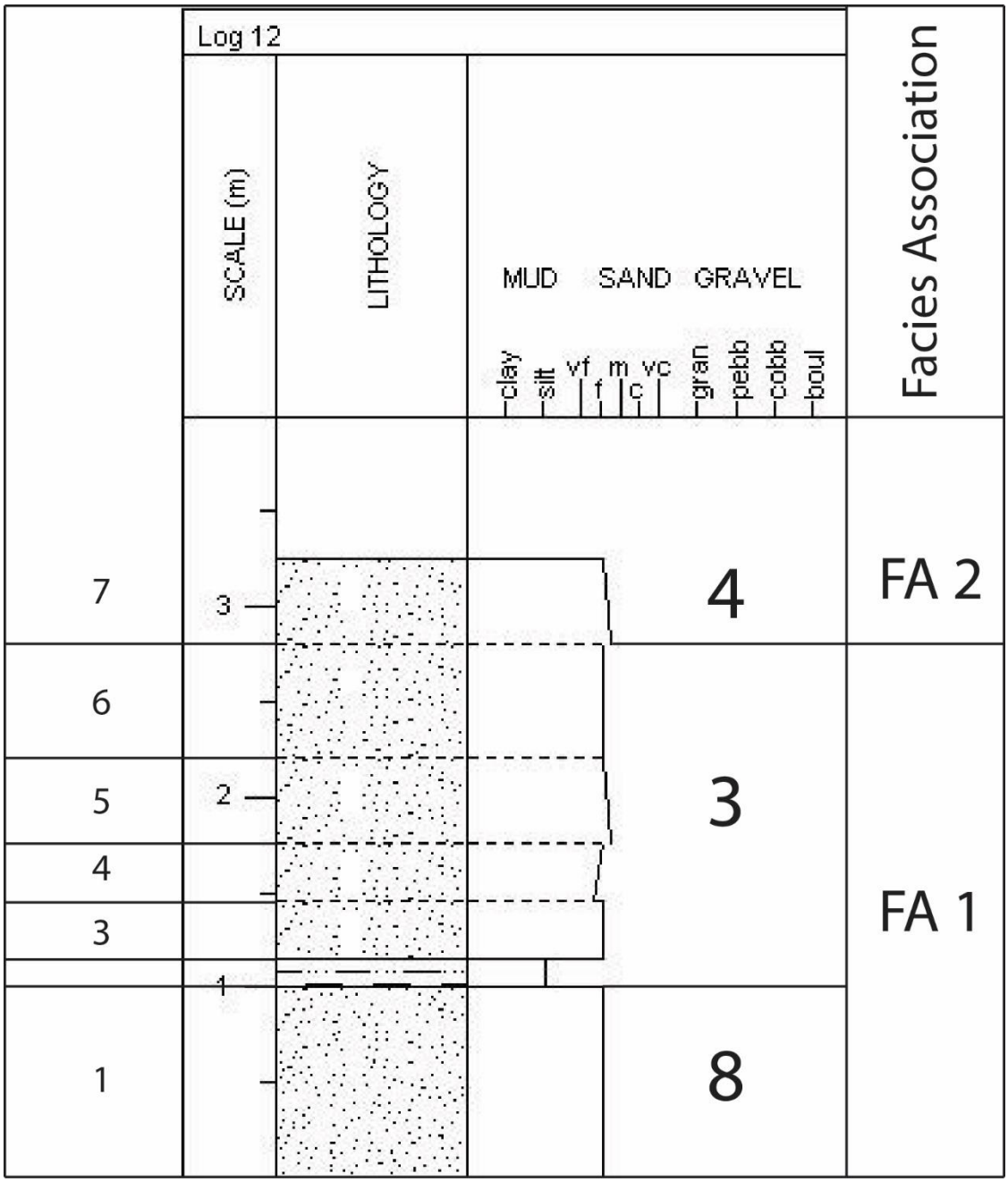

Figure 38: Log 12.

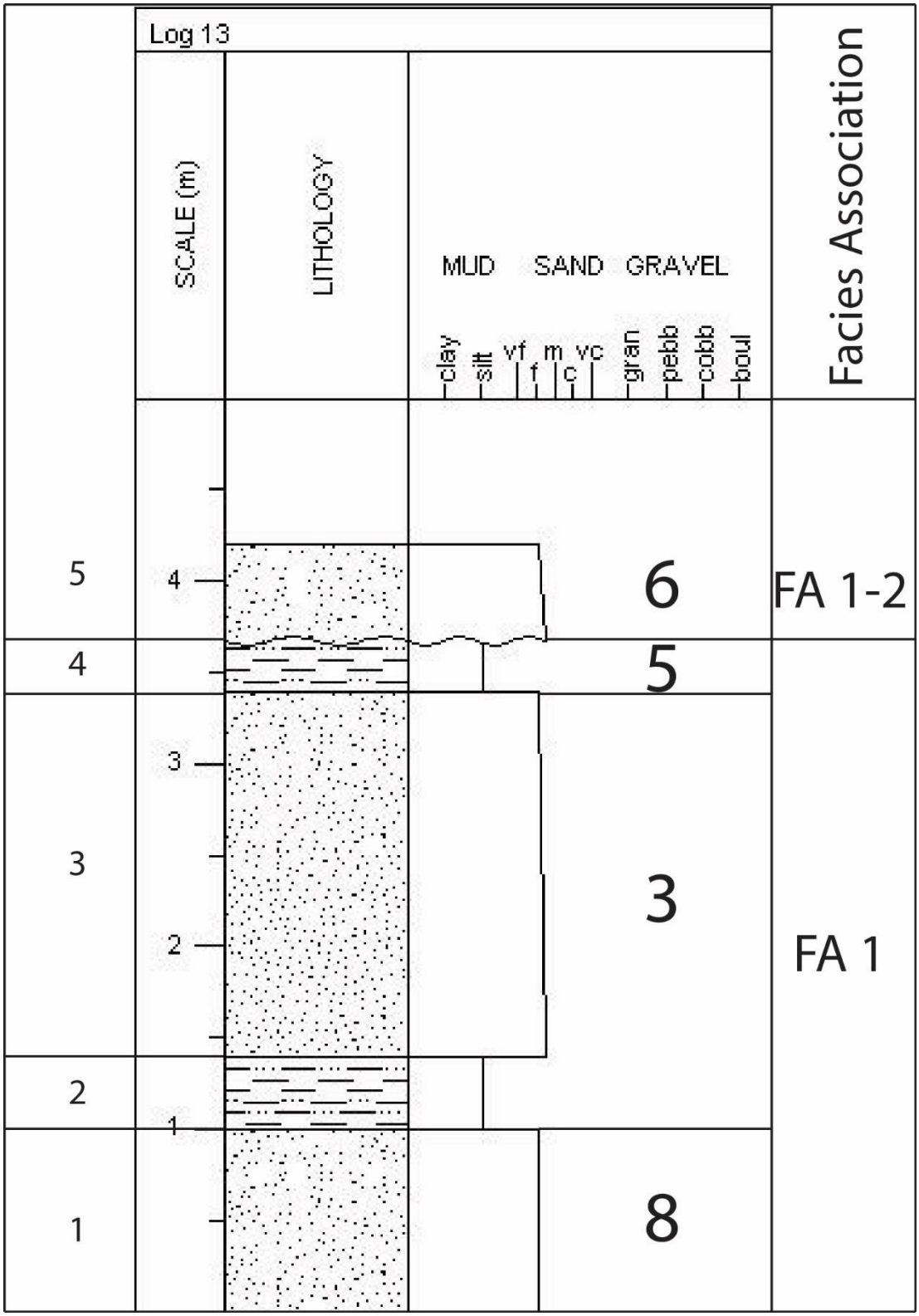

Figure 39: Log 13. Depositional unit 6 is characterized as FA 1-2 due to the lithologic similarities to FA 1, while having a geometry similar to a channel form of FA 2.

4.4 PHOTOMOSAICS

Due to the size of the outcrops, a single photomosaic portraying the entire outcrop was not included in-text due to the amount of detail lost at that reduced scale. To circumvent this issue, photomosaics for each of the outcrops were split into three sections (Figures 40-41) and boxes were added to denote sections that were further enlarged to show more detail where the logs were taken (Figures 42-45). Complete photomosaics are available as supplementary files.

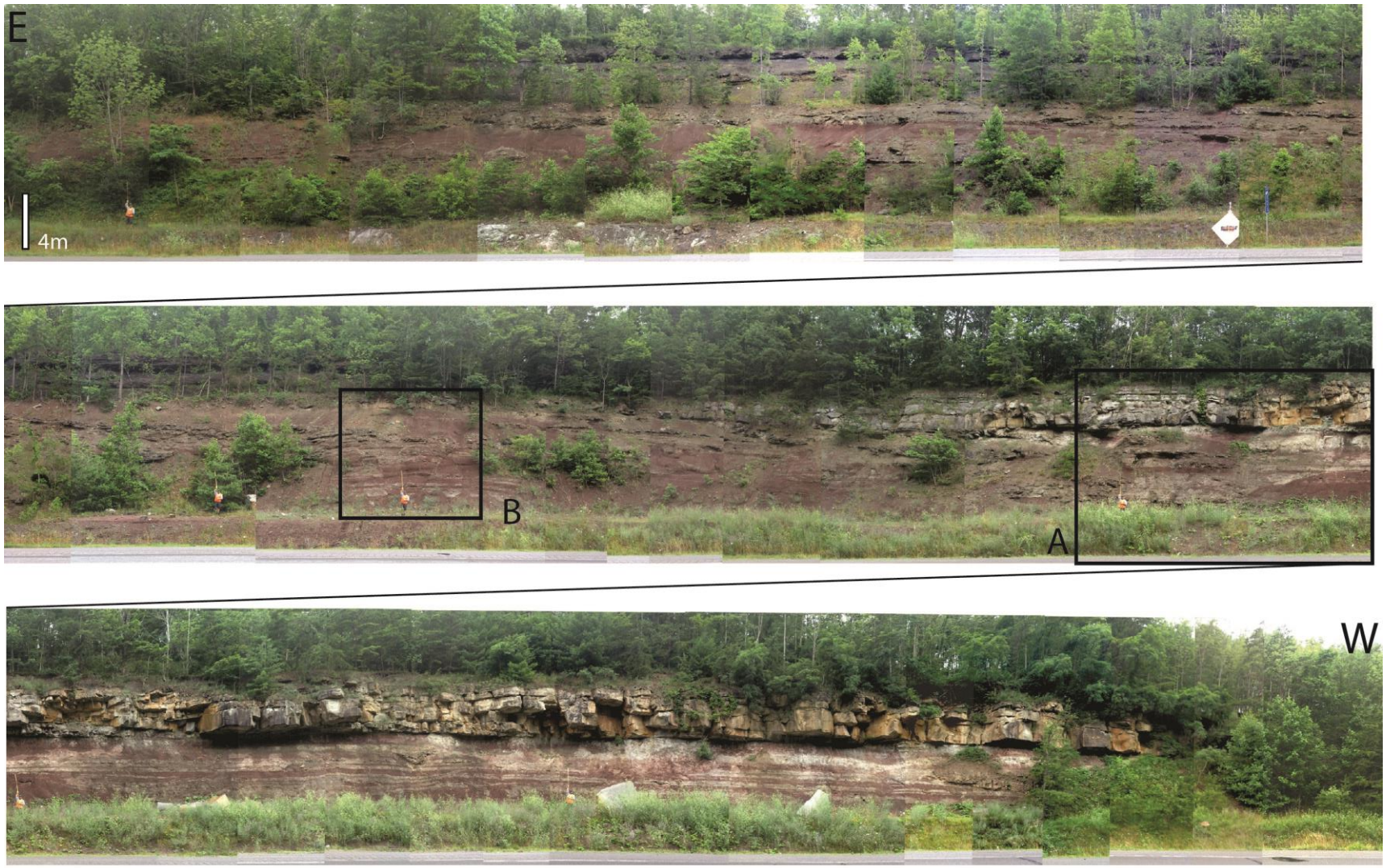

Figure 40: Photomosaic of southern outcrop spanning from the eastern-most side at the top-left to the western-most side at the bottom-right. Boxed sections provided to show the location for enlarged view of logs 3-4 (A) and the horst and graben location (B).

Figure 41: Photomosaic of northern outcrop spanning from the western-most side at the top-left to the eastern-most side at the bottom-right. Boxed sections provided to show the location for enlarged view of logs 1-2 (A), logs 6-10 (B), and logs 11-13 (C). There is a normal fault located in boxed section A.

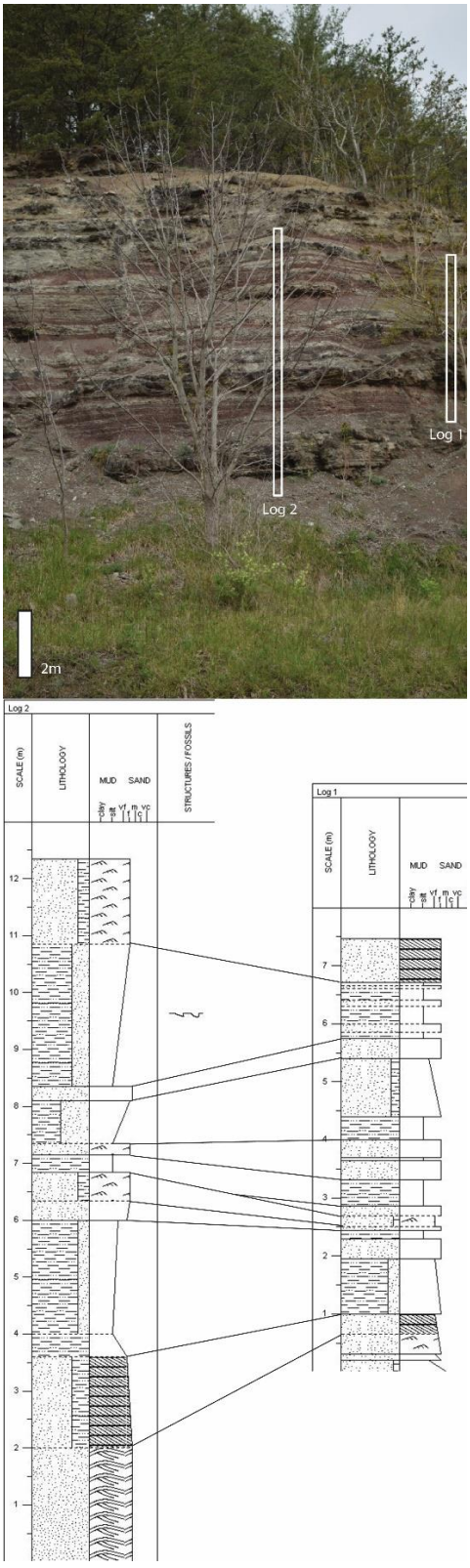

Figure 42: Enlarged view of a portion of the northern outcrop (area outlined in Box A in Figure 41). The stratigraphy within Box A is recorded by logs 1 and 2. All units belong to facies association 1.

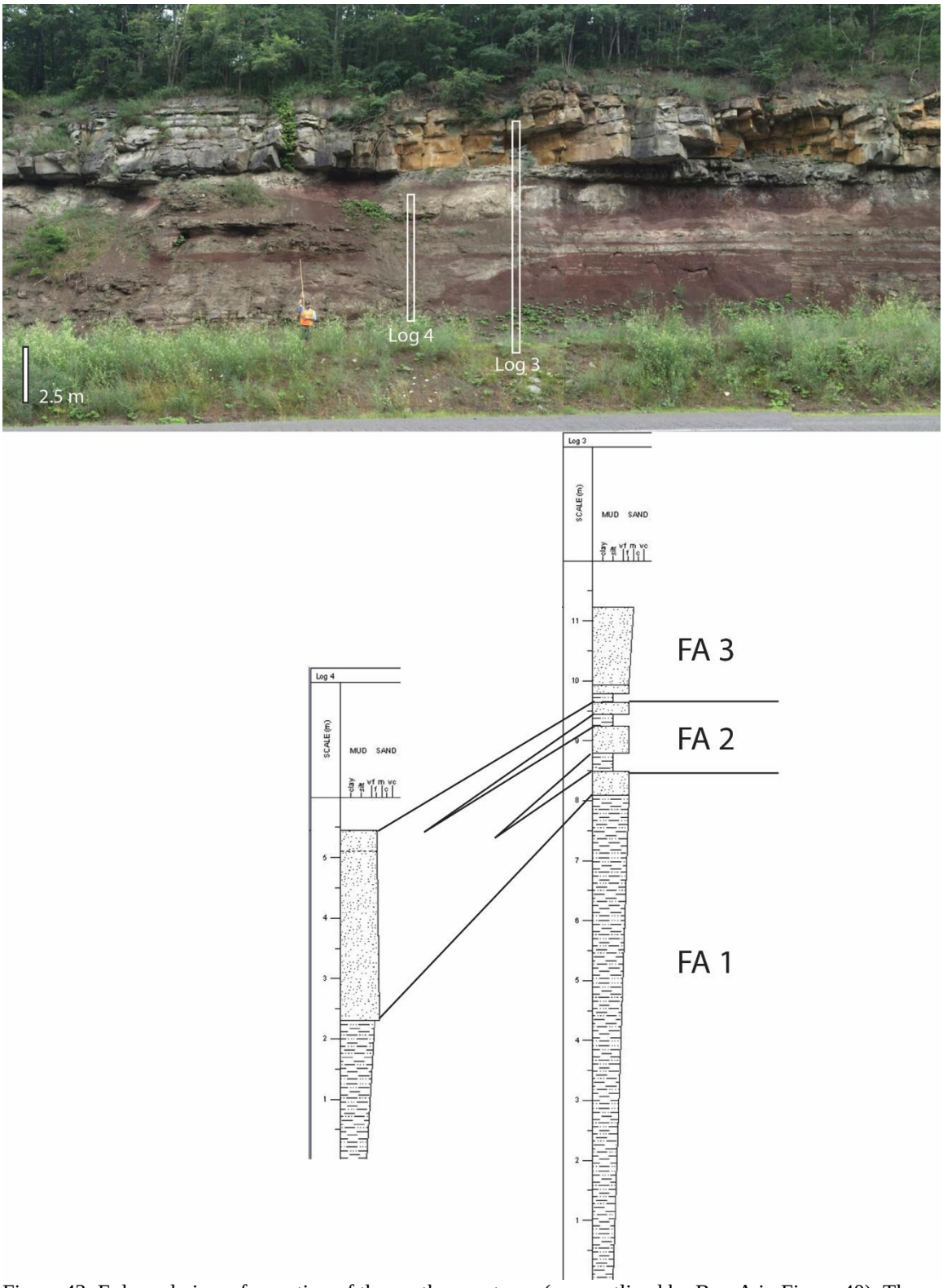

Figure 43: Enlarged view of a portion of the southern outcrop (area outlined by Box A in Figure 40). The stratigraphy within Box A is recorded by logs 3 and 4.

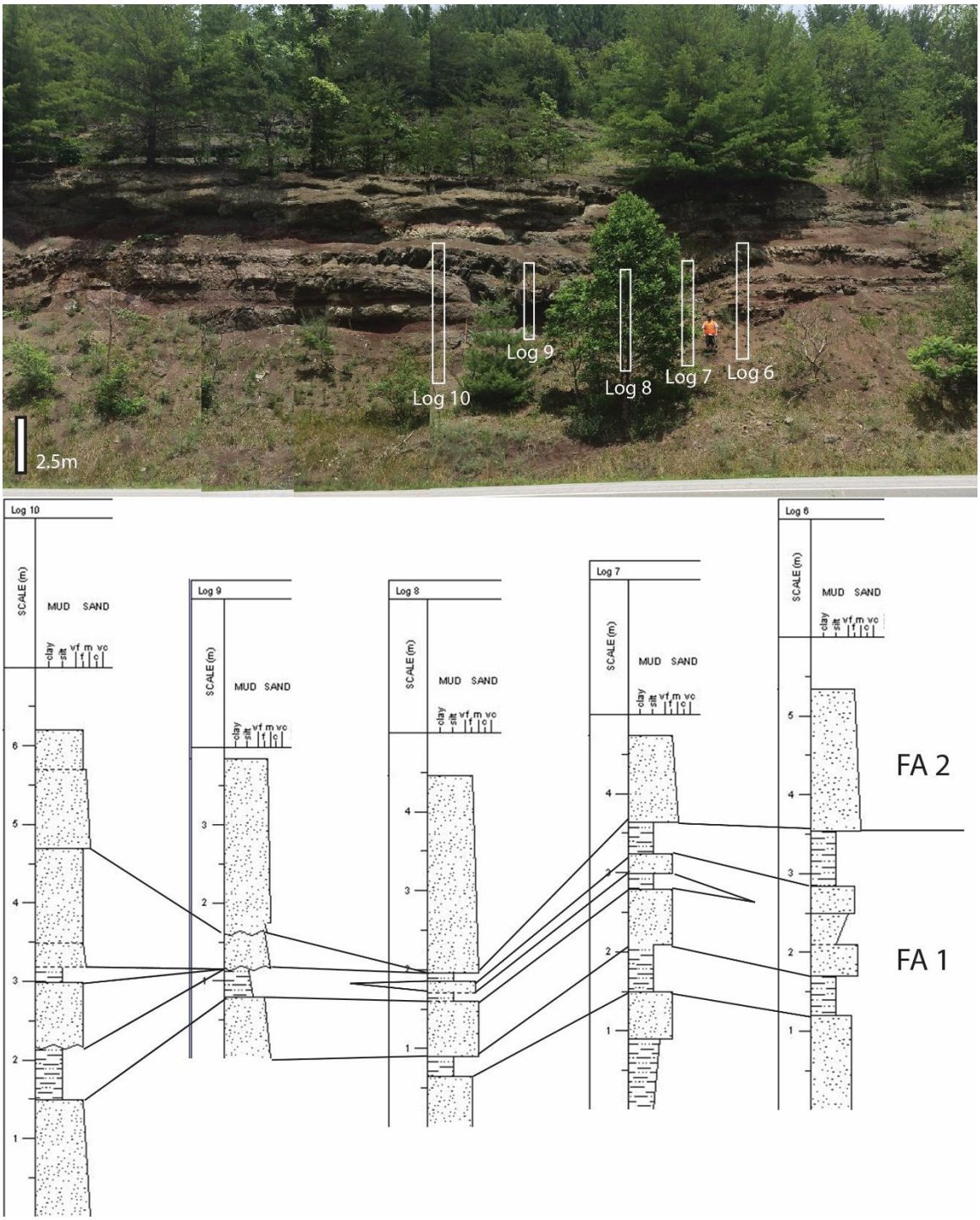

Figure 44: Enlarged section of northern photomosaic (area outlined by Box B in Figure 41). Logs 6-10 document the stratigraphy within Box B of Figure 41.

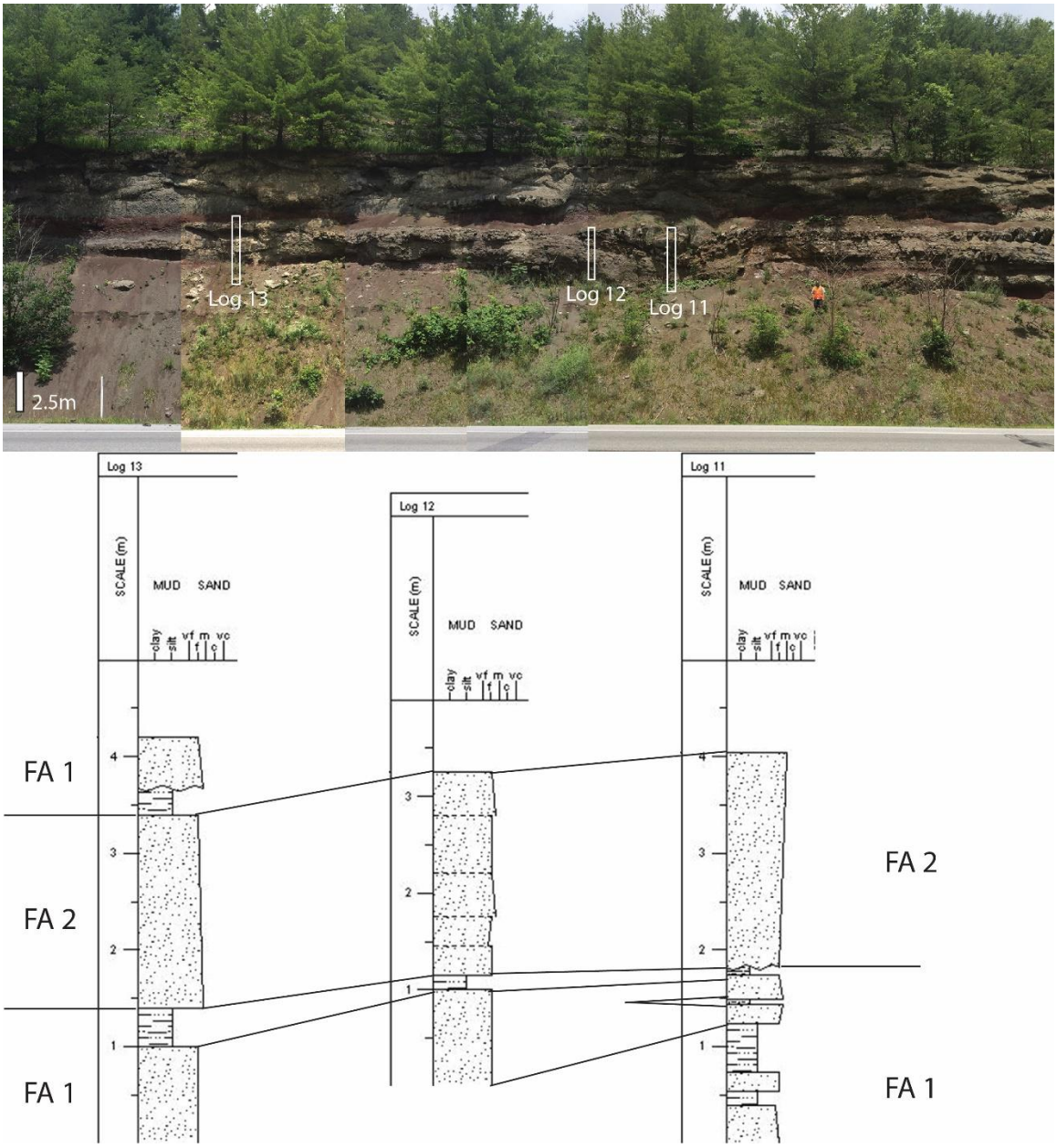

Figure 45: Enlarged section of northern photomosaic (area outlined by Box C in Figure 41). Logs 11-13 document the stratigraphy within Box C.

4.5 OVERLAYS OF CLOSE-UP VIEWS OF CROSS-SECTIONS

For each of the locations where logged sections were taken, a composite figure was constructed to show (A) the unaltered outcrop, (B) the outcrop with line drawings of the contacts separating the numbered depositional units, and (C) the outcrop with the numbered depositional units highlighted by color washes (Figures 46-49). This was done to better understand the architecture of the depositional units. Locations of logs are indicated by white outlines to show their relationship to depositional unit boundaries.

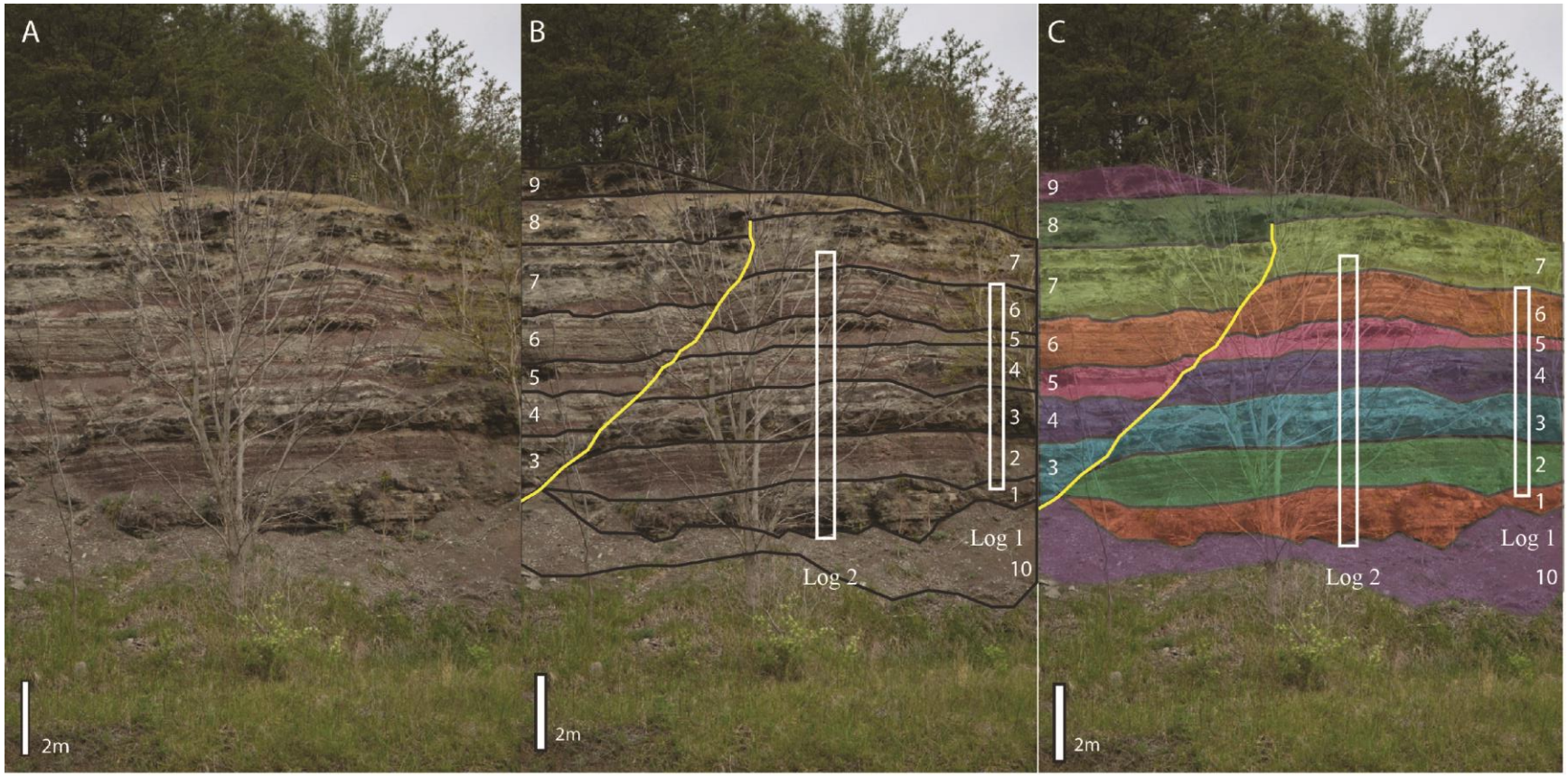

Figure 46: Close-up view of photomosaics where logged sections 1 and 2 were measured (see Box A on Figure 41). (A) Photograph of the site. (B) Line drawing ovelay showing the locations of logged sections and contacts between depositional units (see logs 1 and 2, Figures 28 and 29). (C) Color wash overlay depicting the extent of each depositional unit. Depositional units 1-9 are all assigned to facies association 1. Note that unit 10 is float and there is a normal fault (yellow line) with the downthrown block on the left (west).

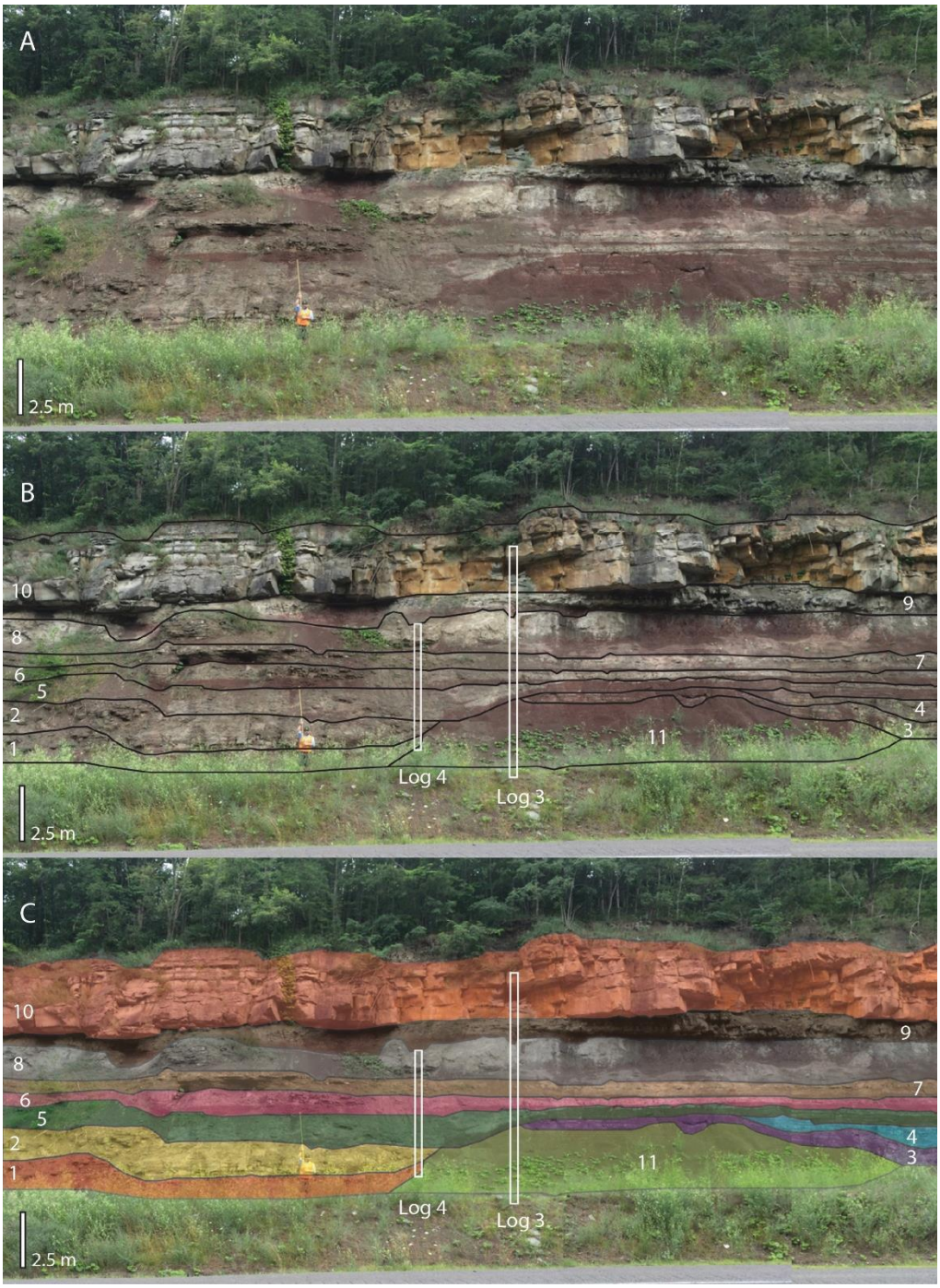

Figure 47: Close-up view of photomosaic of the southern outcrop where logs 3 and 4 were measured (see Box A on Figure 40). (A) Photograph of the site. (B) Line drawing overlay showing the locations of logs and contacts between numbered depositional units (see logs 3 and 4, Figures 30 and 31). (C) Color wash overlay depicting the extent of each depositional unit. Depositional units 1-9 are all assigned to facies association 1, although possible channel geometry can be seen in units 1, 2 and 5 in the middle of the section. Unit 10 belongs to facies association 3, and unit 11 is float.

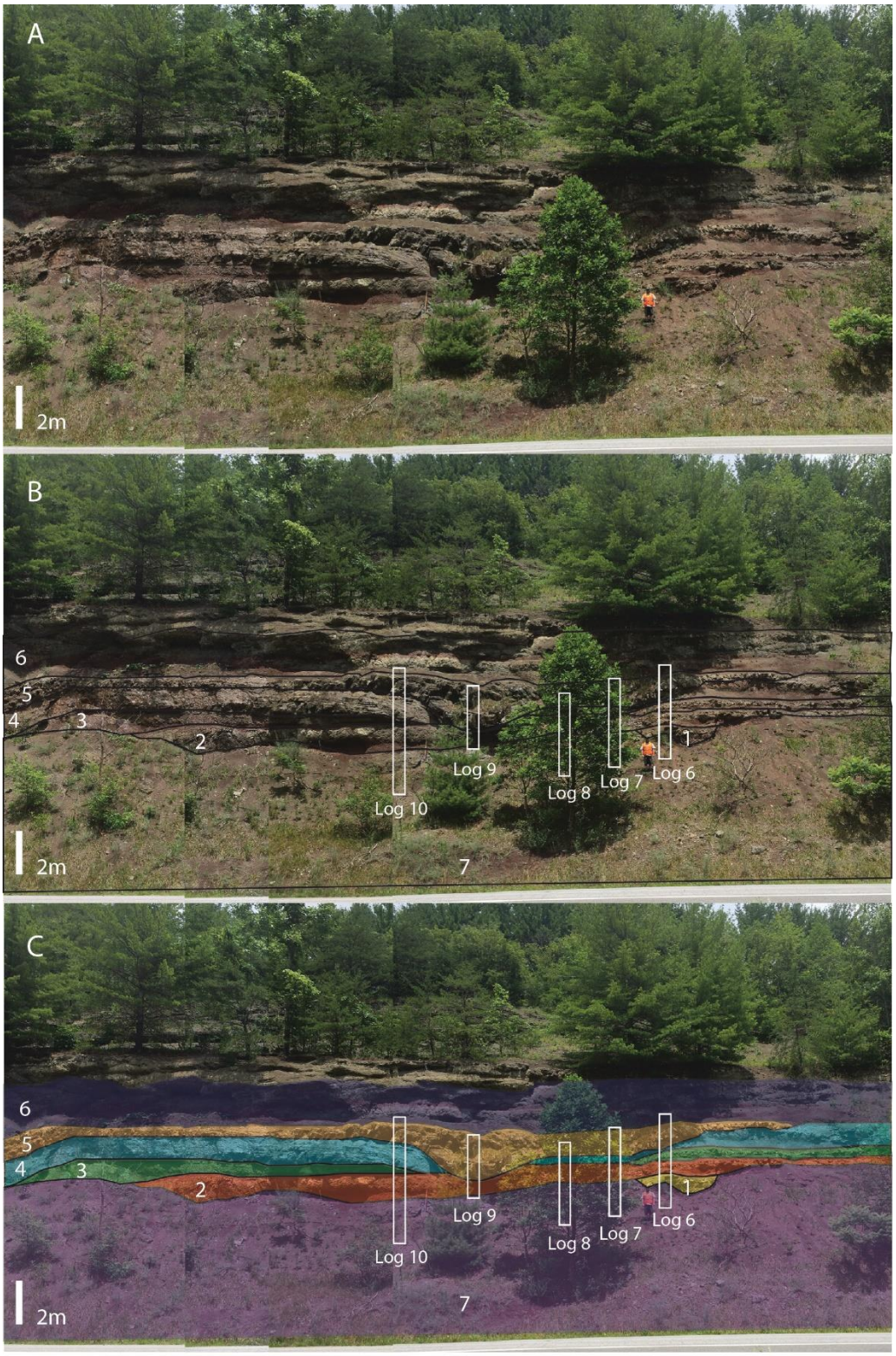

Figure 48: Close-up view of photomosaic of the northern outcrop where logs 6-10 were measured (Box B of Figure 41). (A) Photograph of the site. (B) Line drawing overlay showing locations of logs and contacts between depositional units (see logs 6-10, Figures 32-36). (C) Color wash overlay depicting the extent of each depositional unit. Units 1-4 and 6 are assigned to facies association 1, unit 5 is assigned to facies association 2, and unit 7 is float.

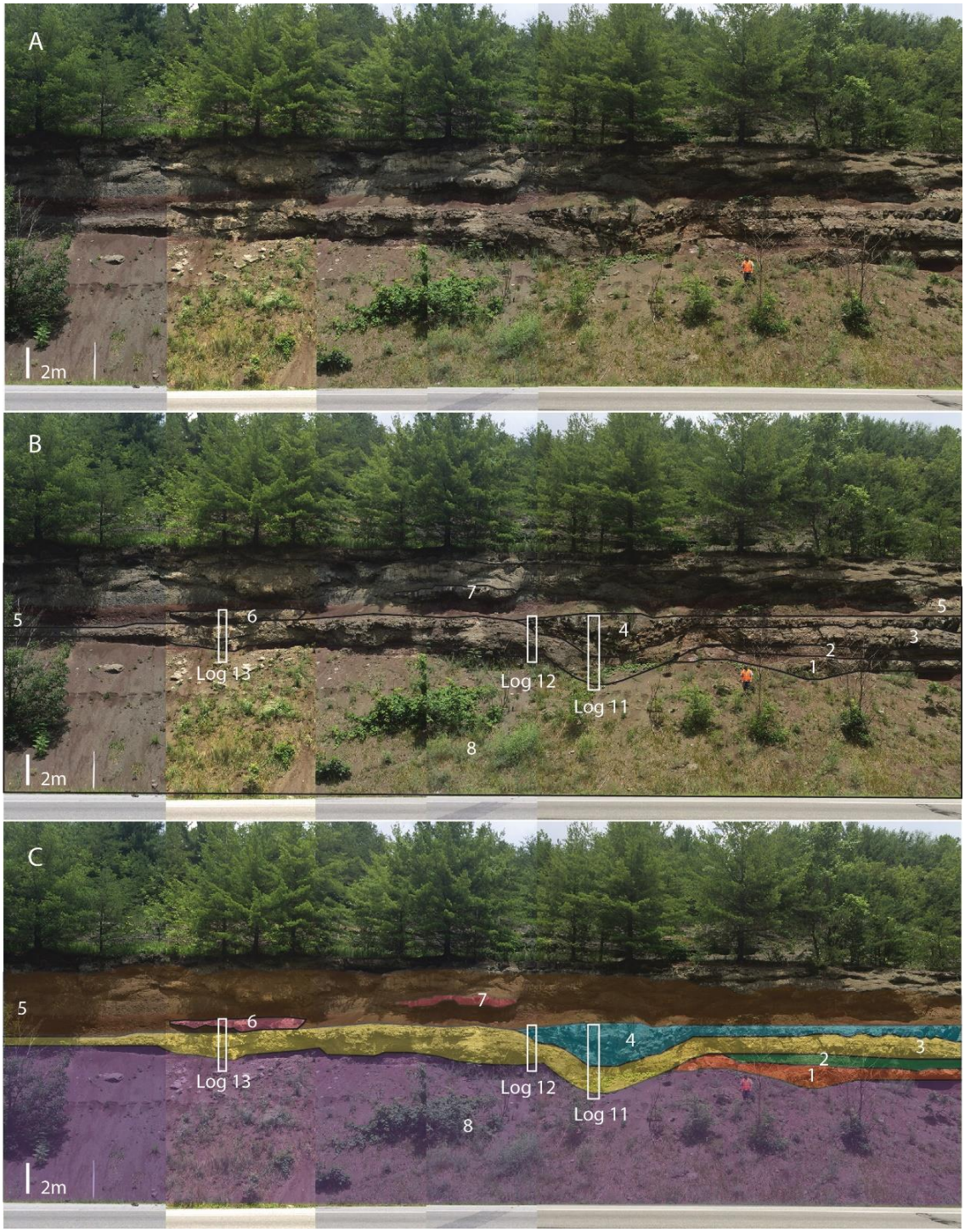

Figure 49: Close-up view of photomosaic in the northern outcrop where logs 11-13 were measured (Box C of Figure 41). (A) Photograph of the site. (B) Line drawing overlay showing locations of logs and contacts between depositional units (see logs 11-13, Figures 37-39). (C) Color wash overlay depicting the extent of each depositional unit. Units 1-3 belong to facies association 1, with unit 3 being deformed due to the presence of unit 4. Unit 4 belongs to facies association 2, and noticeably deforms the units below it. Unit 5 and 7 belong to facies association 1. Units 6 and 7 exhibit lens-shaped geometry, indicative of facies association 2; however, they do not contain the laterally extensive tabular sandstone deposits commonly associated with facies association 2. Unit 8 is float.

4.6 SCANNING ELECTRON MICROPROBE

Samples were selected to represent the composition of the undivided upper Hinton Formation, the channel forms present in that undivided unit, and both base and top of the Princeton Formation (Table 1). At least 200 points were counted per slide to determine average oxide weight percentages (Table 2). From these point counts, selected grains were examined and chemically mapped to show the variations in grain size and shape, with multiple images being taken when available. After examining oxide weight percentages for every point in each slide (available as supplementary file), 19 different minerals were identified (Table 3, Figures 50-70).

Sample	Log #	Unit #	Facies Association	Interpreted Depositional Environment
AM01-05	1	5	1	Floodplain
AM01-09	1	9	1	Floodplain
AM01-11	1	11	1	Floodplain
AM01-16	1	16	1	Floodplain
AM01-18	1	18	1	Floodplain
AM03-09	3	9	3	Trunk Channel
AM08-07	8	7	2	Crevasse Channel
AM09-04	9	4	2	Crevasse Channel
AMPSS-TL	N/A	N/A	3	Trunk Channel
AM460-01	N/A	N/A	3	Trunk Channel
AM460-02	N/A	N/A	3	Trunk Channel
AM460-03	N/A	N/A	3	Trunk Channel

Table 1: List of samples used in thin section analysis. The samples were taken from logs 1, 3, 8, and 9 (refer to Figures 28, 30, 34 and 35, respectively). Sample AMPSS-TL from the type section of the Princeton Formation can be seen in Figure 10. The three Princeton Formation samples from the main study site (the AM460 samples) come from the top of log 3 (Figure 30).

	OXIDE AVERAGE WEIGHT PERCENTAGES													
SAMPLES (with correction type)	FeO	Na_2O	MnO	P_2O_5	CaO	ZrO_2	SiO_2	Al_2O_3	SO_3	K_2O	TiO_2	MgO	Cr_2O_3	SUM
AM01-05 CO_2	1.353	0.275	0.01	0.415	0.52	1.737	84.806	3.692	0.438	0.51	5.881	0.283	0.044	101.386
AM01-09 CO_2	1.877	0.206	0.142	-0.001	1.741	0.59	87.864	1.321	0.4	0.08	2.102	0.461	0.028	100.118
AM01-11 CO_2	5.407	0.253	0.357	0.033	0.81	2.456	80.217	2.4	0.554	0.248	3.076	0.544	0.029	101.031
AM01-16 CO_2	4.035	0.06	0.79	0.008	2.658	0.908	83.663	1.155	0.399	0.074	0.041	0.514	0.021	100.107
AM01-18 H_2O	1.02	-0.005	0.041	0.327	0.093	1.297	94.611	1.142	0.496	0.094	1.269	0.114	0.162	101.337
AM01-18 CO_2	1.004	-0.005	0.04	0.312	0.091	1.296	94.607	1.134	0.495	0.094	1.266	0.113	0.162	101.337
AM03-09 H_20	0.879	0	0.02	-0.004	0.04	1.095	92.639	1.904	0.459	0.204	2.412	0.163	0.028	100.615
AM03-09 CO_2	0.863	0	0.019	-0.004	0.039	1.096	92.603	1.891	0.459	0.202	2.399	0.162	0.028	100.615
AM08-07 H_2O	0.582	0.051	0.019	0.006	0.042	0.874	97.427	0.904	0.486	0.054	0.544	0.123	0.263	101.732
AM08-07 CO_2	0.569	0.051	0.018	0.006	0.041	0.869	97.421	0.903	0.485	0.054	0.537	0.122	0.263	101.732
AM09-04 H_2O	0.471	0	0.042	-0.004	0.058	0.327	97.186	0.841	0.47	0.045	1.135	0.108	0.027	100.93
AM09-04 CO_2	0.461	0	0.041	-0.004	0.056	0.327	97.183	0.841	0.47	0.045	1.133	0.107	0.027	100.93
AMPSS-TL CO_2	5.242	0.066	0.067	0.105	0.069	0.977	81.824	5.129	0.39	0.467	0.559	0.552	0.023	101.585
AM460-01 H_2O	0.148	-0.008	-0.004	0	0.001	2.547	95.738	0.885	0.845	0.029	1.464	0.115	0.201	101.982
AM 460-01 CO_2	0.148	-0.008	-0.004	0	0.001	2.546	95.738	0.885	0.845	0.029	1.463	0.115	0.2	101.982
AM460-02 CO_2	7.015	-0.003	0.161	0.011	0.308	0.357	85.384	3.161	0.4	0.115	0.199	0.835	0.028	101.756
AM460-03 CO_2	3.259	0.001	0.083	0.006	0.259	0.319	92.7	1.489	0.428	0.174	0.107	0.349	0.026	101.545

Table 2: Average oxide weight percentages as measured by an ARL scanning electron microprobe quantometer. Each sample's raw data was either carbon dioxide corrected (CO2) or water corrected (H2O). These were done to account for carbonate minerals and hydrous minerals, respectively.

Mineral	Ig.	Met.	Sed.	Notes
Albite	X			Magmatic and pegmatitic rocks
Apatite	X	X		Granite pegmatites, contact metamorphics, igneous diabases, ore veins.
Barite			X	Sedimentary rocks and late gangue mineral in ore veins
Calcite	X	X	X	Found in sedimentary, igneous, and metamorphic rocks
Chromite	X			Cummulate (magmatic segregation) mineral found in ultramafic portions of layered mafic intrusions. Common in meteorites
Ilmenite	X	X		Common accessory mineral in igneous and metamorphic rocks. Commonly concentrated in placers as "black sand" deposits
Kaolinite				Secondary mineral derived from the weathering of alumino-silicate minerals
Monazite	X			Granitic pegmatites
Muscovite	X			Granites and Pegmatites
Orthoclase	X	X		Intrusive and extrusive igneous, and metamorphic rocks
Palermoite	X			In cavities in a pegmatite
Pseudorutile				Alteration in ilmenite placers and beach sands
Pyroxene	X	X		High temperature and/or pressure, mafic/ultramafic igneous, high-grade metamorphism.
Quartz	X	X	X	Sedimentary, metamorphic, and igneous rocks
Rutile	X			High pressure and temperature accessory mineral in igneous rocks. Common detrital mineral
Siderite	X	X	X	Primarily bedded, biosedimentary deposits, also in metamorphic and igneous rocks. Forms a series with rhodochrosite.
Tourmaline	X	X		Produced in pegmatites. Generally surrounded by granite or schists, occasionally grow in metamorphics such as marble
Xenotime	X			Minor accessory mineral in both acidic and alkalic igneous rocks and their pegmatites
Zircon	X	X	X	Magmatic, metamorphic, pegmatitic, and alluvial rocks. Zircons are commonly slightly radioactive due to trace amounts of uranium and make prime, geochronological age indicators

Table 3: Minerals identified within the twelve thin sections by ARL-SEMQ. Each mineral is assigned to the major rock type it comes from, as well as notes. Two minerals without major rock type designations (kaolinite and pseudorutile) are formed through diagenetic processes, and therefore are not classified. (Information from webmineral.com, minerals.net, and britannica.com).

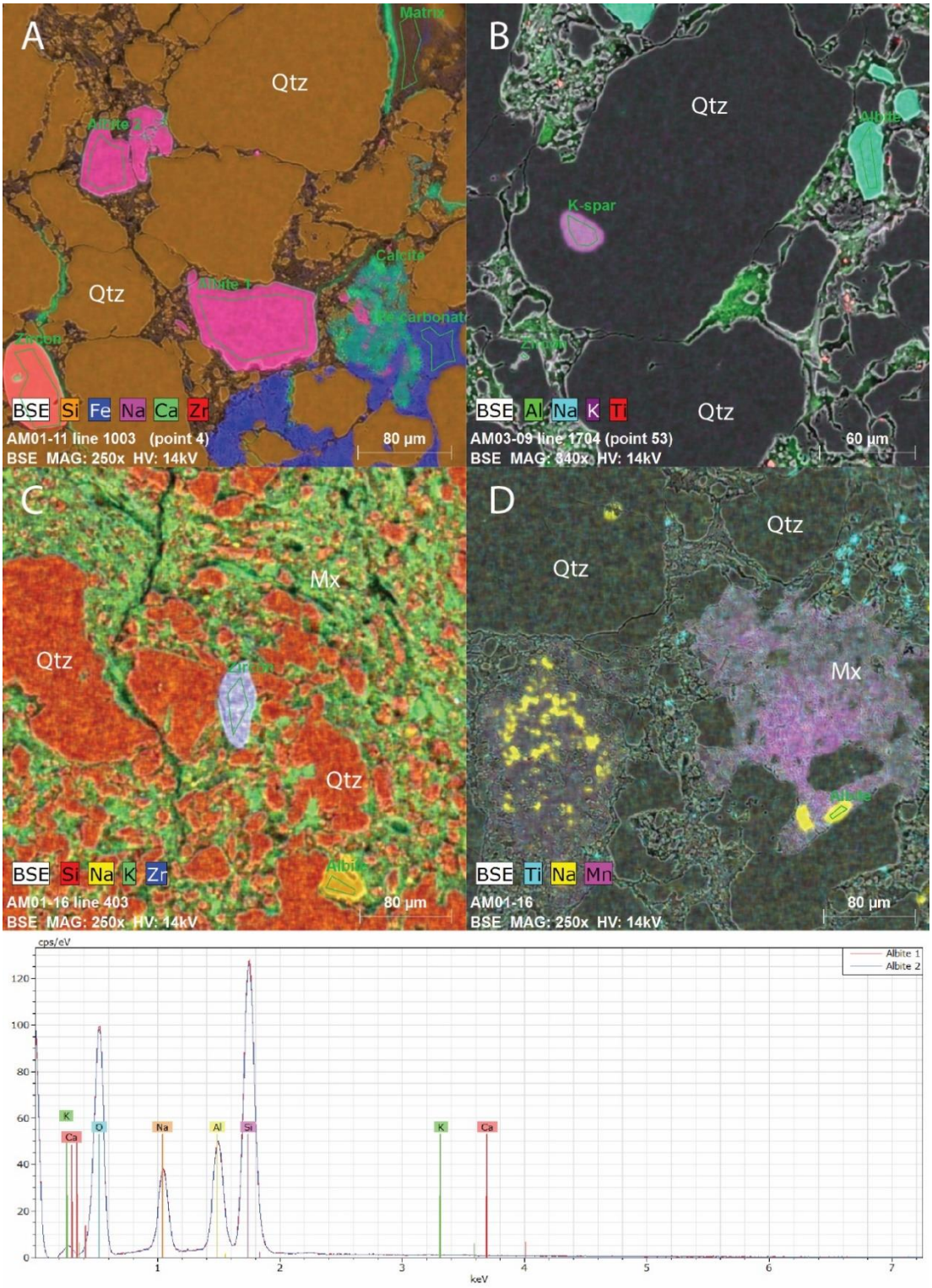

Figure 50: Scanning electron microprobe images of the mineral albite from samples (A) AM01-11, (B) AM03-09, and (C and D) AM01-16. Albite grains appear as (A) pink, (B) teal, and (C and D) yellow. Below the microprobe images, an energy dispersive spectroscopy readout shows the elemental peaks of the albite grains identified in the sample from (A) AM01-11. Quartz (Qtz), matrix (Mx), albite, calcite, orthoclase, and zircon are identified as well.

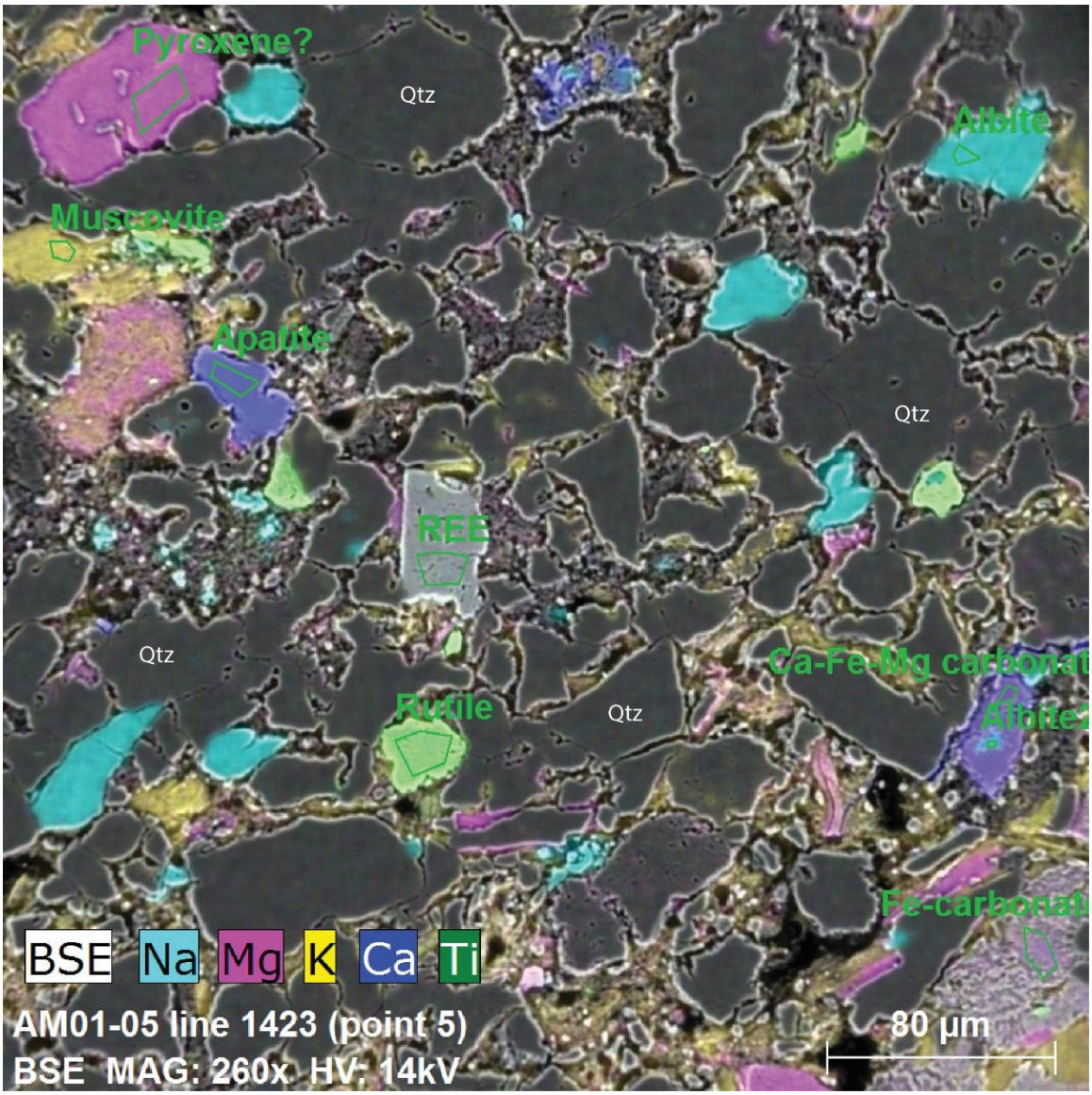

Figure 51: Scanning electron microprobe image of apatite near the upper left quadrant in blue-purple from sample AM01-05. Other minerals identified in this image are muscovite, pyroxene, albite, rutile, and quartz (Qtz). Various carbonates (Fe and Ca-Fe-Mg dominant) are labeled.

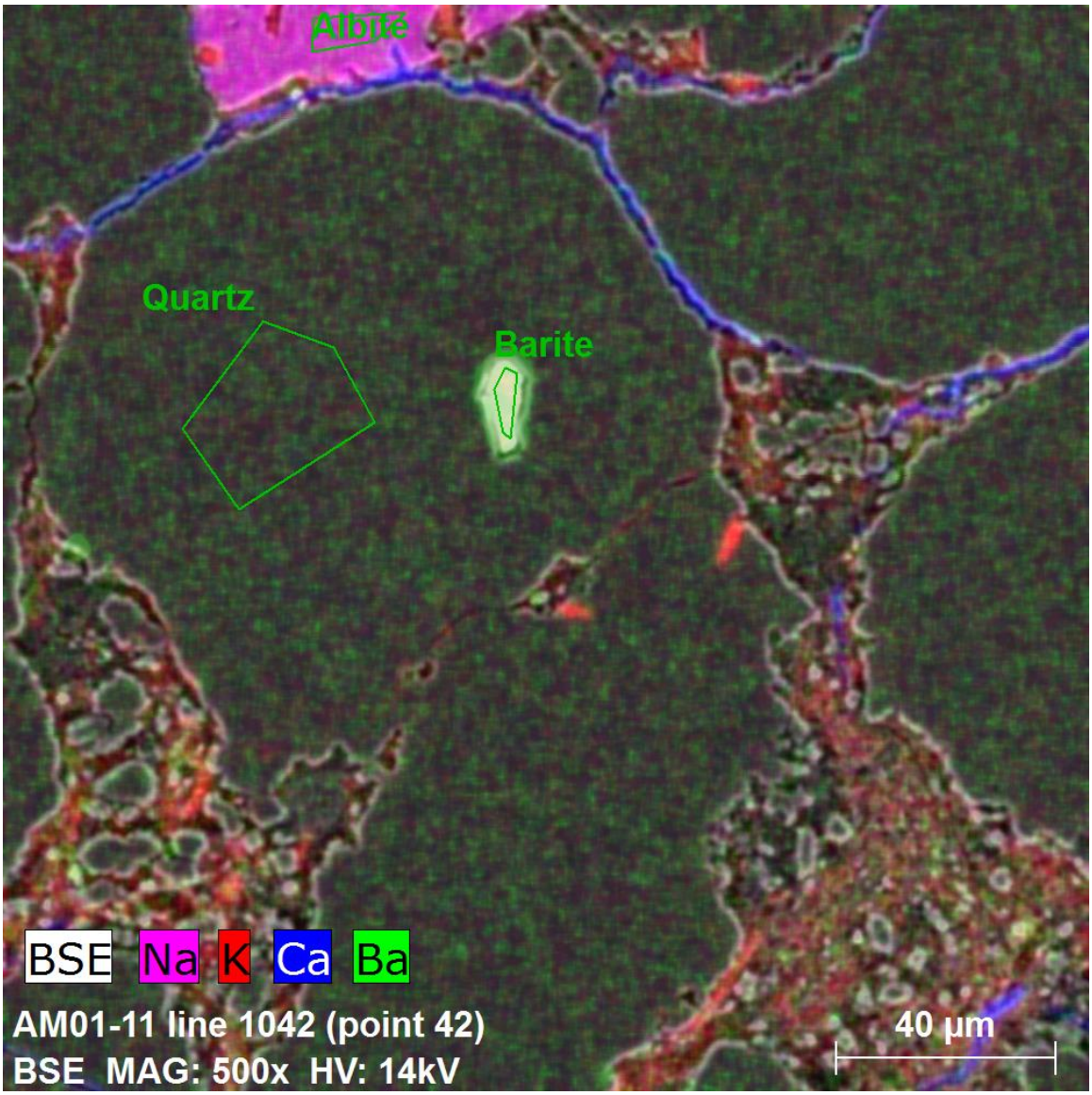

Figure 52: Scanning electron microprobe image of the mineral barite from sample AM01-11. Since the barite is an ingrowth of the surrounding quartz mineral, it is indicative of formation in a hydrothermal quartz vein. The mineral albite is also present in this image at the top center in pink. The red shows areas of potassium-rich matrix, while the larger green-purple grains are all quartz.

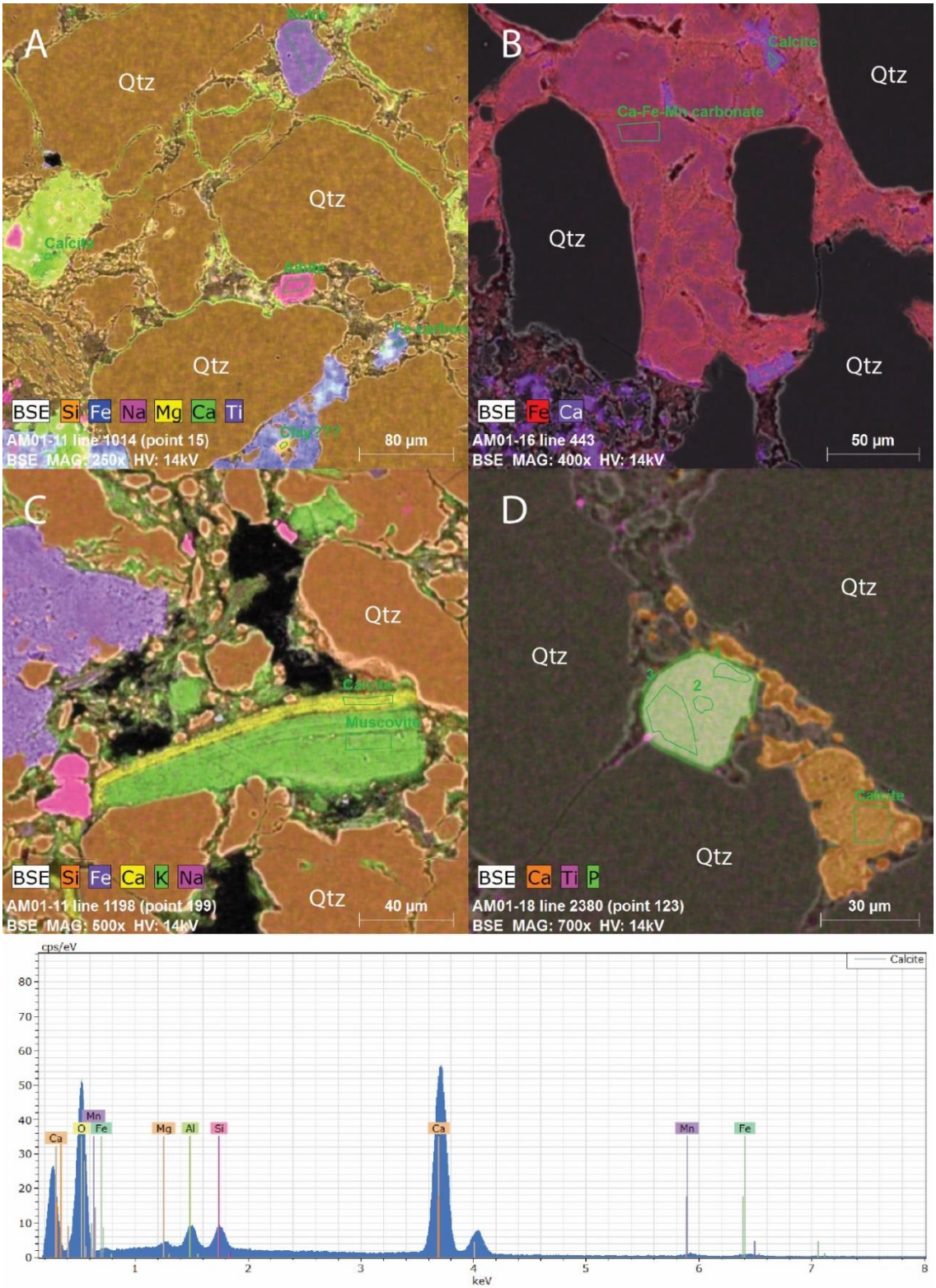

Figure 53: Scanning electron microprobe images of the mineral calcite from samples (A) AM01-11, (B) AM01-16, (C) AM01-11, and (D) AM01-18. The calcite grains appear as (A) green, (B) purple, (C) yellow, and (D) orange. Below the microprobe images, an energy dispersive spectroscopy readout shows the elemental peaks of the calcite grain identified in (D) sample AM01-18. Quartz (Qtz), calcite, rutile, muscovite, and various carbonates (Fe and Ca-Fe-Mg) have also been identified in each sample.

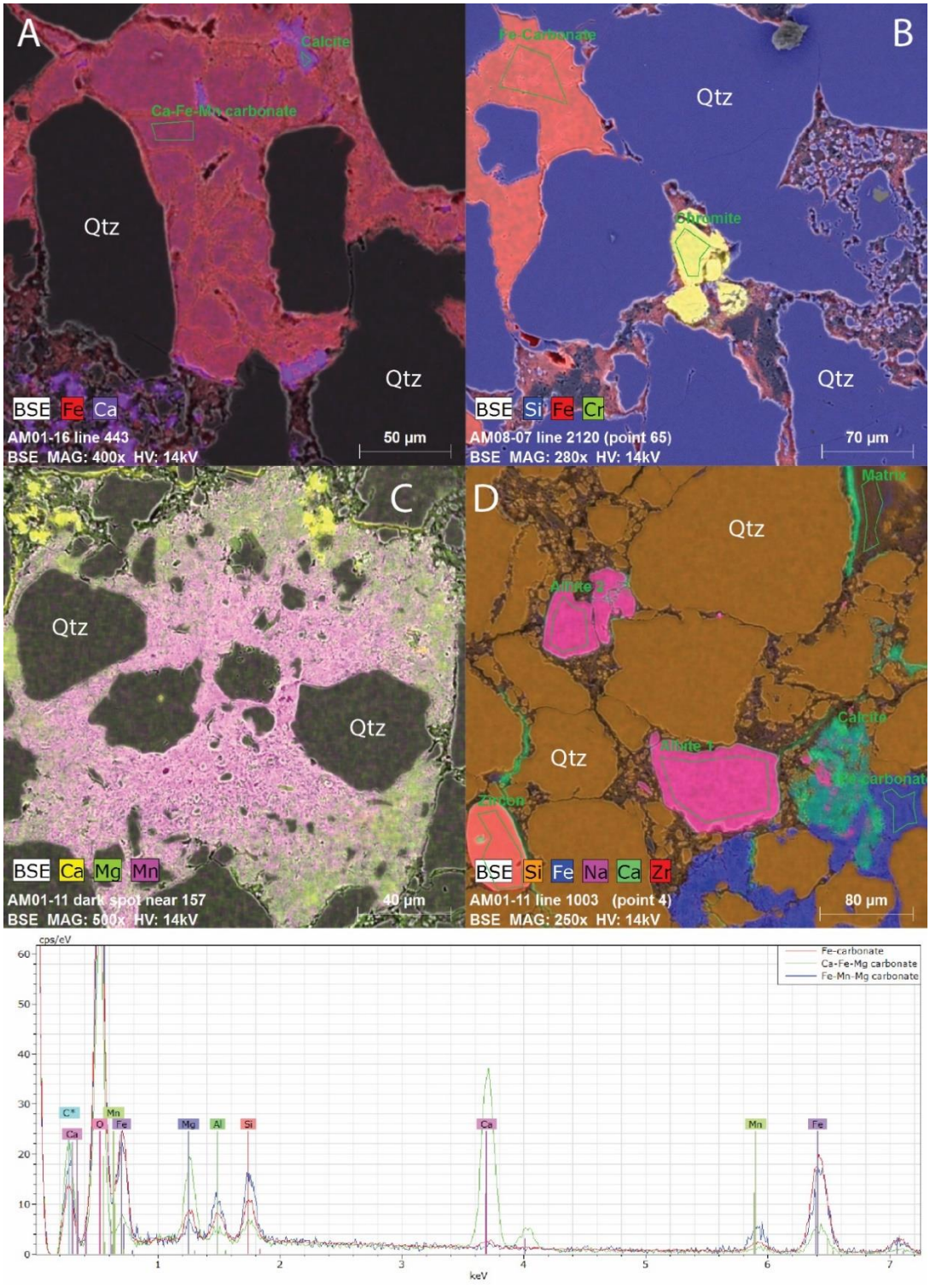

Figure 54: Scanning electron microprobe images of the various carbonates found within the grains from samples (A) AM01-16, (B) AM08-07, (C) AM01-11, and (D) AM01-11. (A) A mixture of calcium-iron-manganese carbonate appears in red. (B) A dominantly iron-carbonate appears in red. (C) A mixture of magnesium-manganese carbonate appears in green and pink, respectively. (D) A dominantly iron-carbonate appears in purple. Below the microprobe images, an energy dispersive spectroscopy readout shows the elemental peaks of the various carbonates identified in (D) sample AM01-11. Minerals identified include chromite, albite, calcite, zircon, and quartz (Qtz).

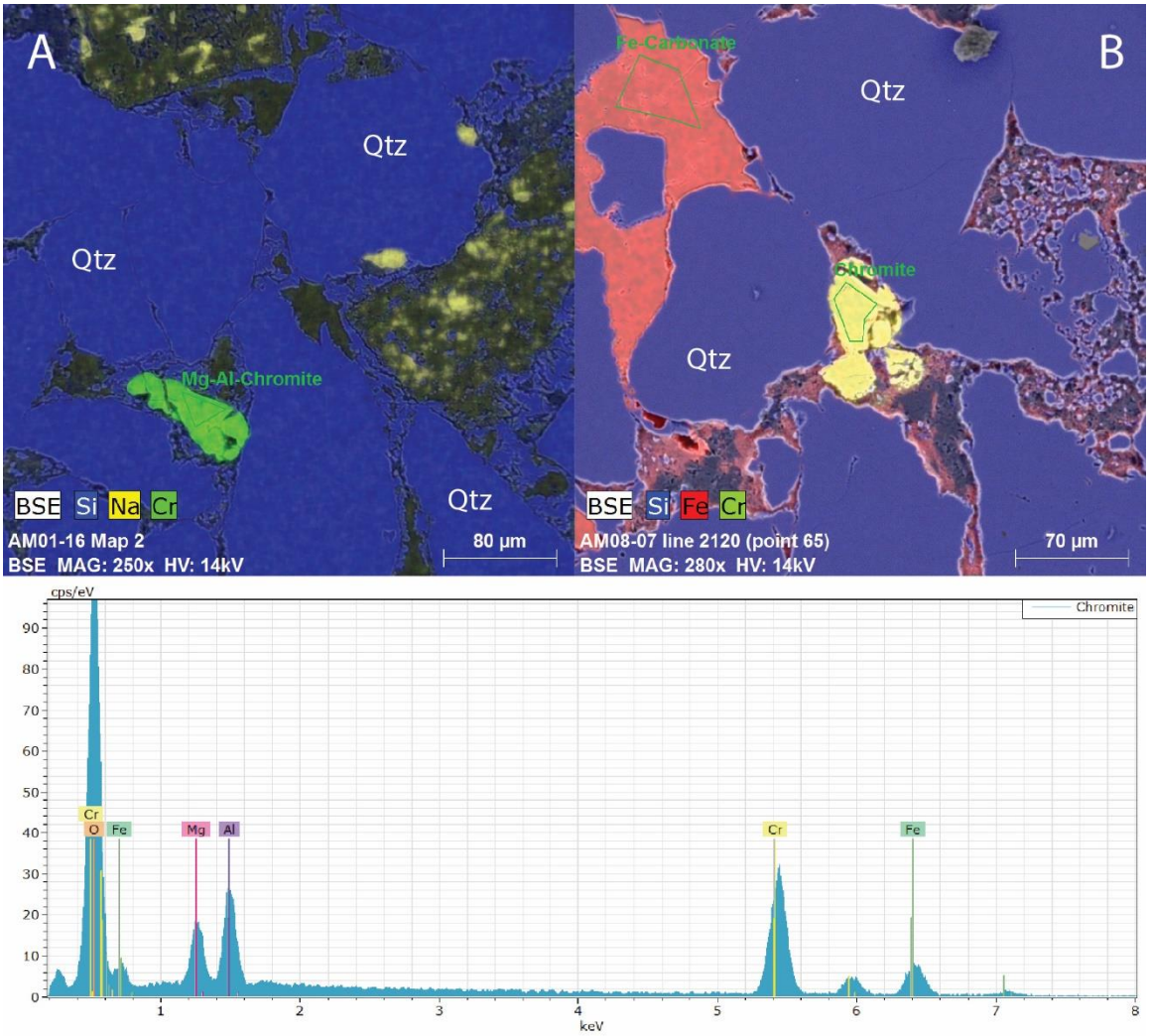

Figure 55: Scanning electron microprobe images of the mineral chromite from samples (A) AM01-16 and (B) AM08-07. The chromite grains appear as (A) green, and (B) yellow. Below the microprobe images, an energy dispersive spectroscopy readout shows the elemental peaks of the chromite grain identified in (B) sample AM08-07. Quartz (Qtz) and Fe-carbonate are also identified.

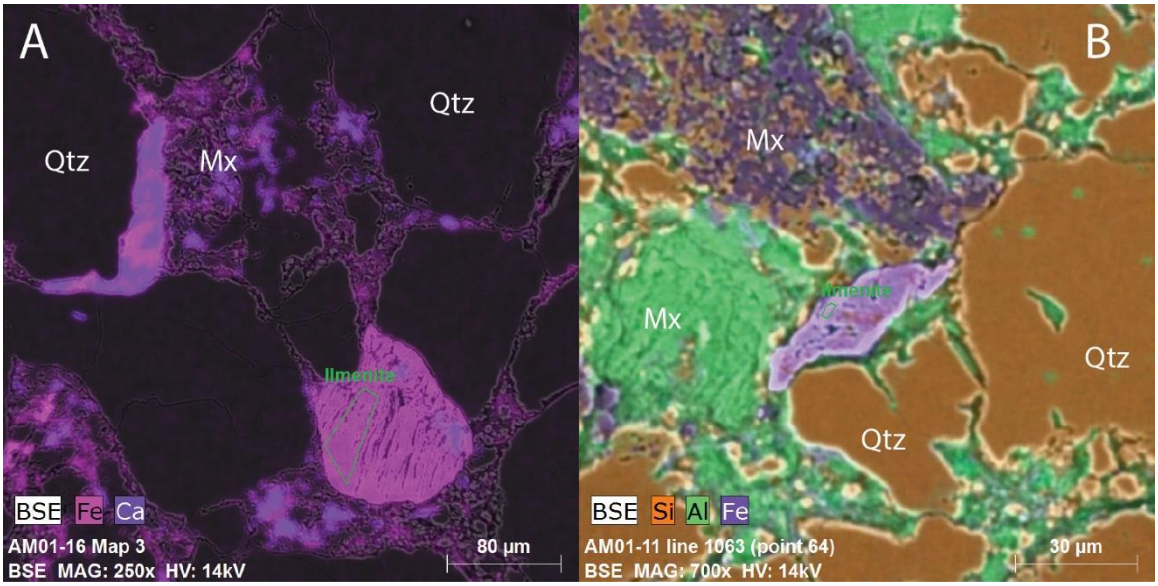

Figure 56: Scanning electron microprobe images of the mineral ilmenite from samples (A) AM01-16 and (B) AM01-11. Ilmenite grains appear as purple (A and B). Quartz (Qtz) and matrix (Mx) are identified.

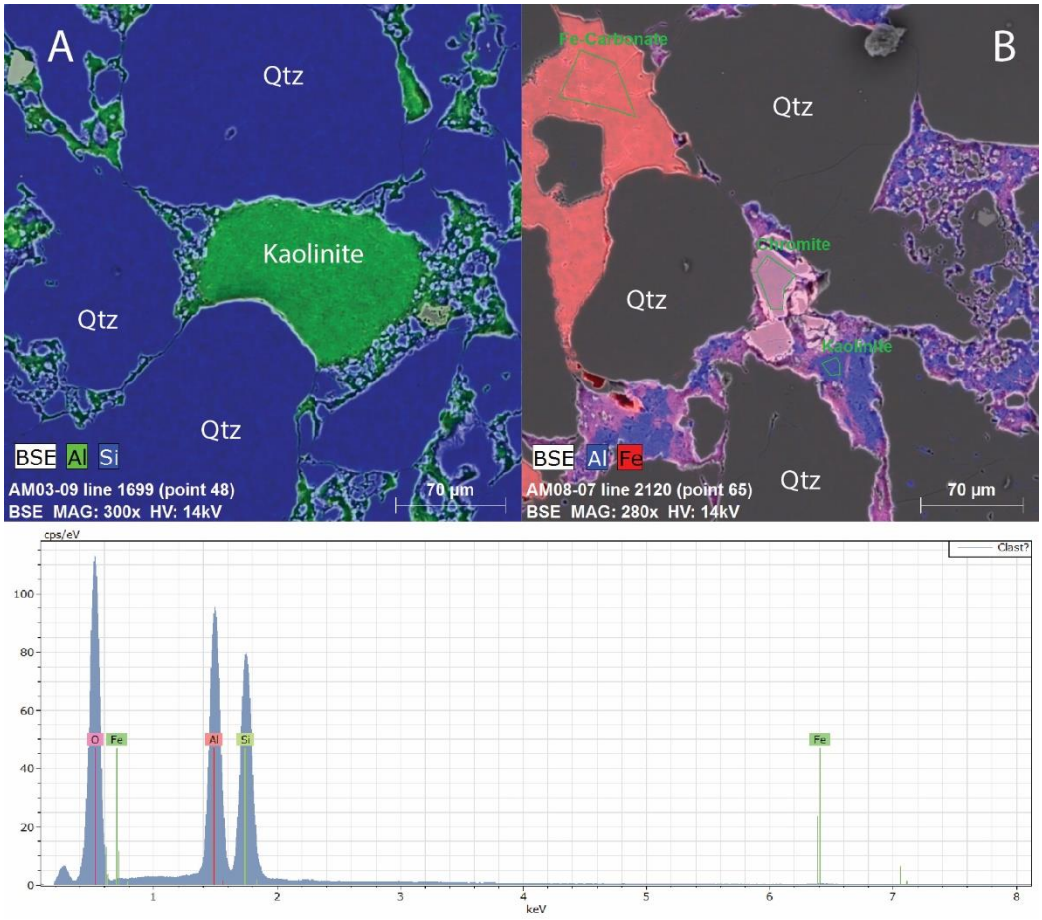

Figure 57: Scanning electron microprobe images of the mineral kaolinite from samples (A) AM03-09 and (B) AM08-07. Kaolinite grains appear as (A) green and (B) dark blue-purple. Below the microprobe images, an energy dispersive spectroscopy readout shows the elemental peaks of the kaolinite grain identified in (A) sample AM03-09. Quartz (Qtz), chromite, and Fe-carbonate are also identified.

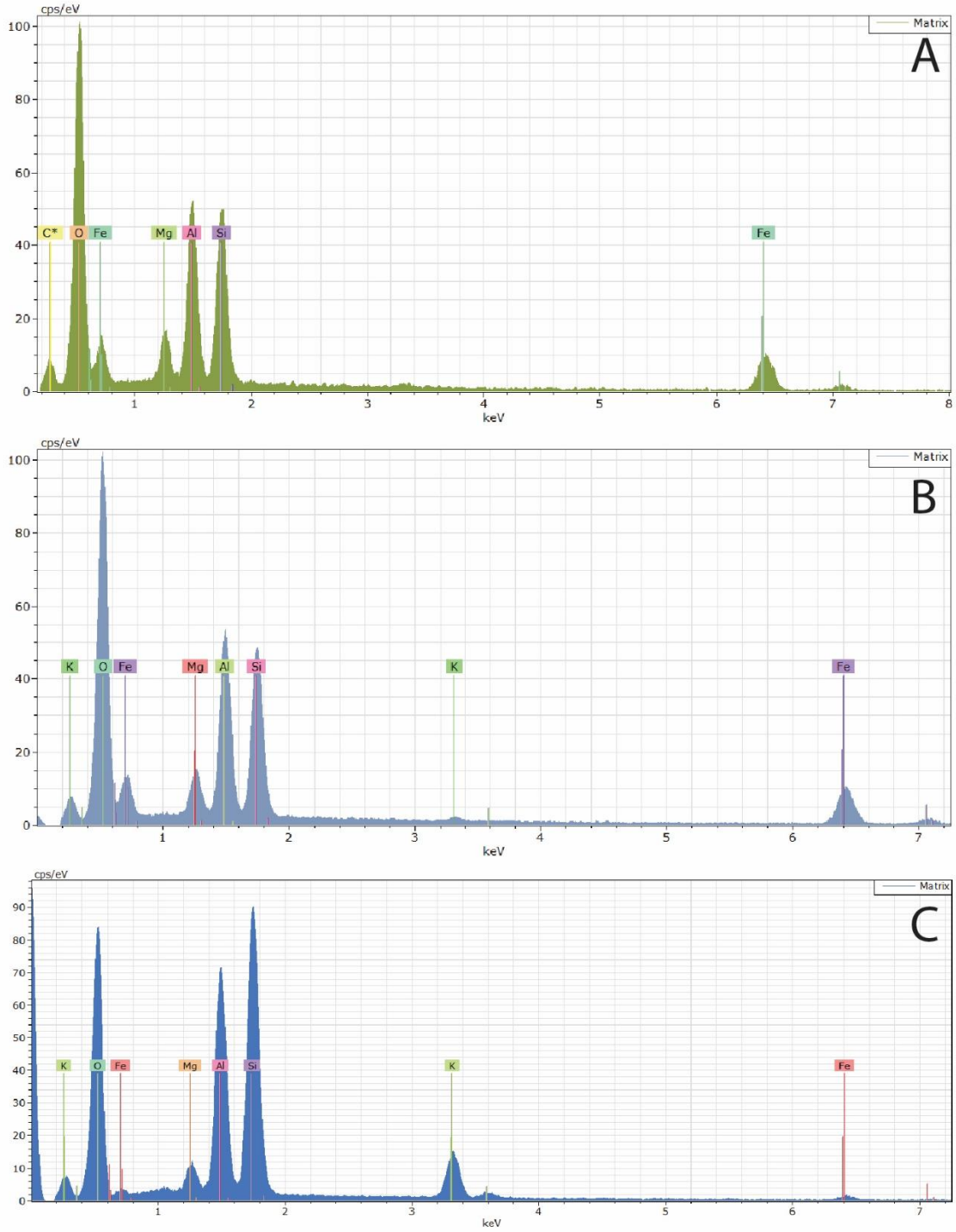

Figure 58: Energy dispersive spectroscopy readouts for the various matrix compositions from (A and B) sample AM460-02 and (C) sample AM01-11.

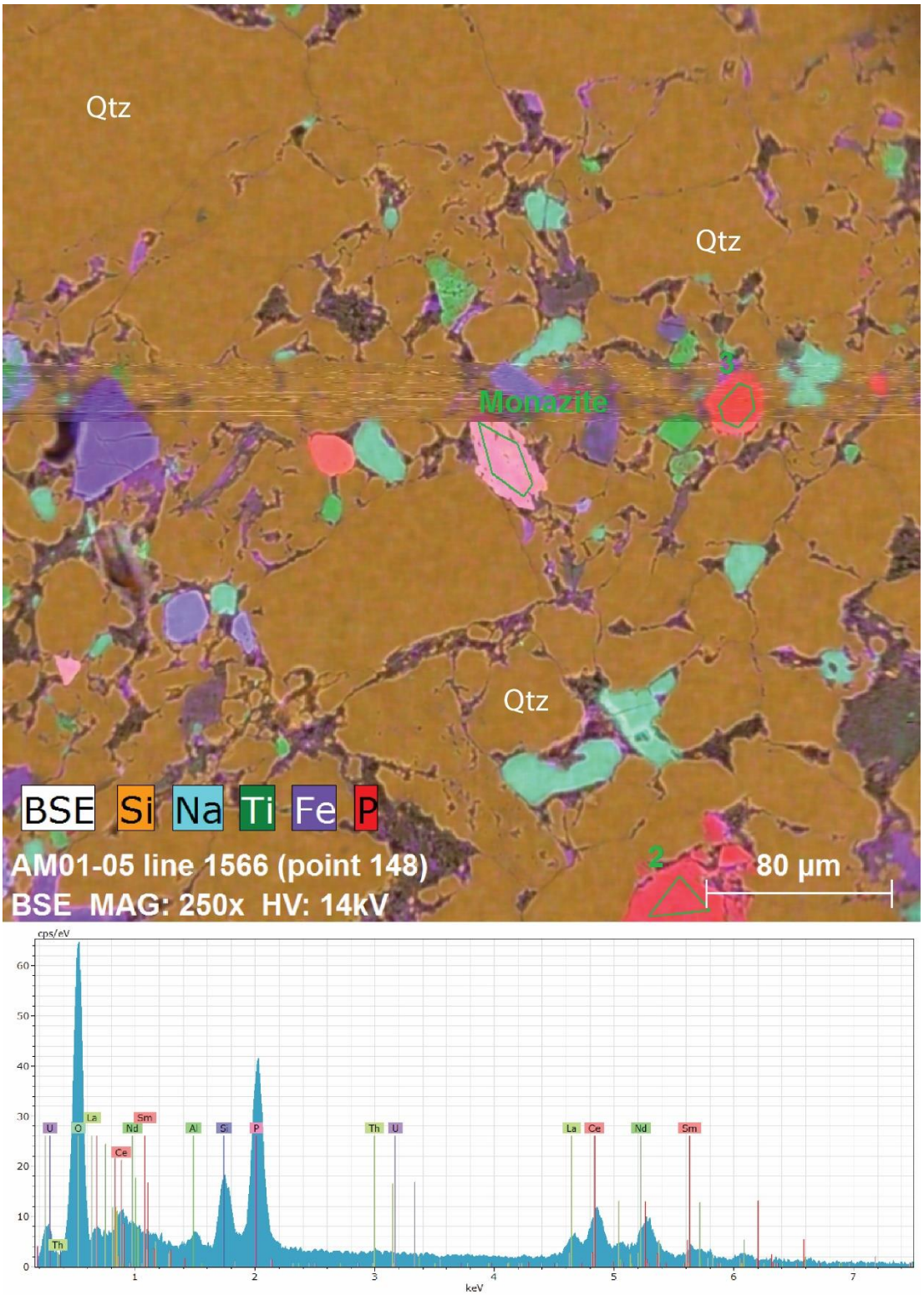

Figure 59: Scanning electron microprobe image of the mineral monazite from sample AM01-05. Grain appears as pink in the center of the image. Below the microprobe images, an energy dispersive spectroscopy readout shows the elemental peaks of the monazite grain identified in (A) sample AM01-05. Quartz (Qtz) is also identified.

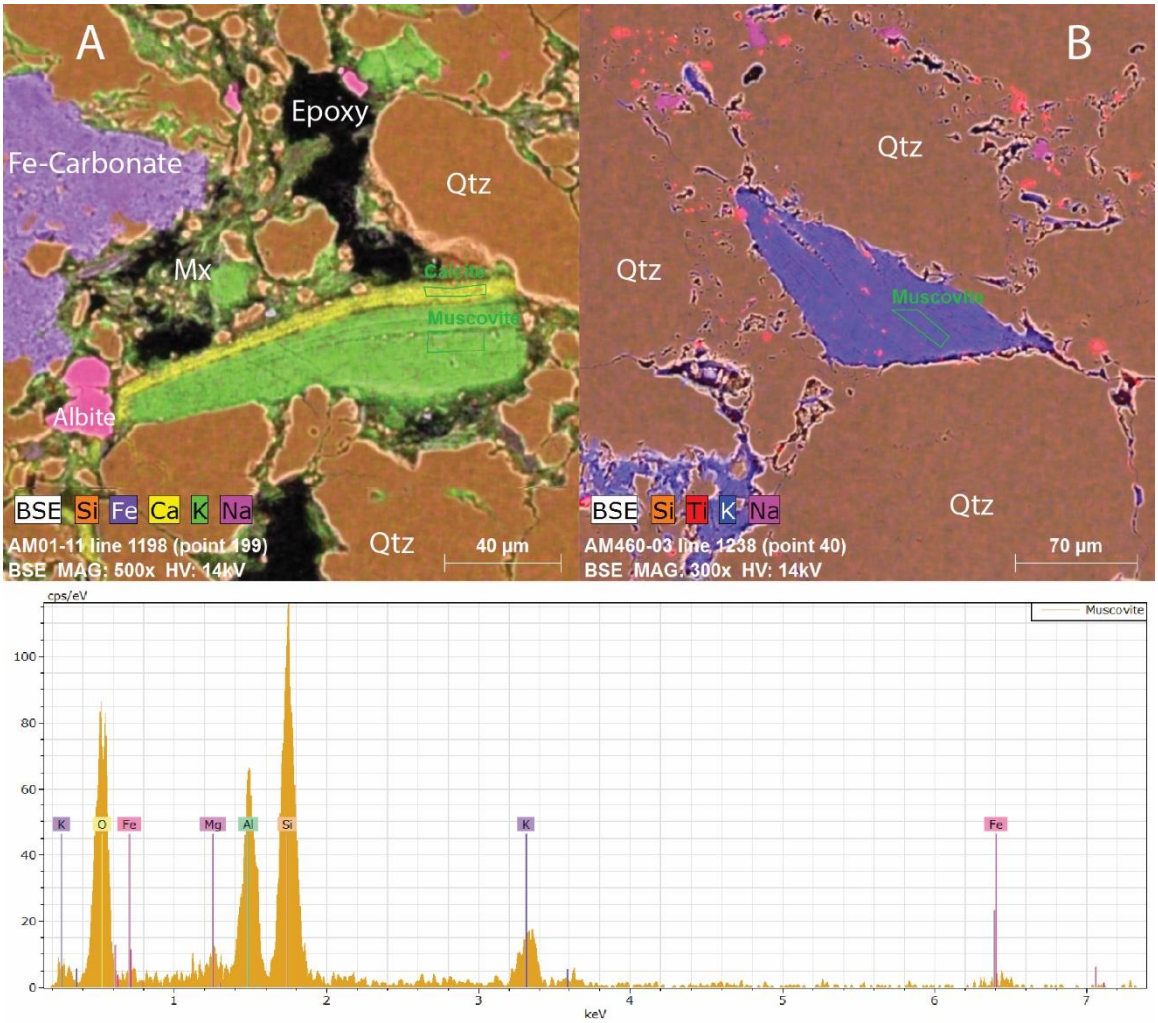

Figure 60: Scanning electron microprobe images of the mineral muscovite from samples (A) AM01-11 and (B) AM460-03. Grains appear as (A) yellow and (B) purple. Below the microprobe images, an energy dispersive spectroscopy readout shows the elemental peaks of the muscovite grains identified in (A) sample AM01-11. Quartz (Qtz), matrix (Mx), iron carbonate (Fe-carbonate), albite, calcite and rutile (red in image B) were also identified. Black areas are epoxy.

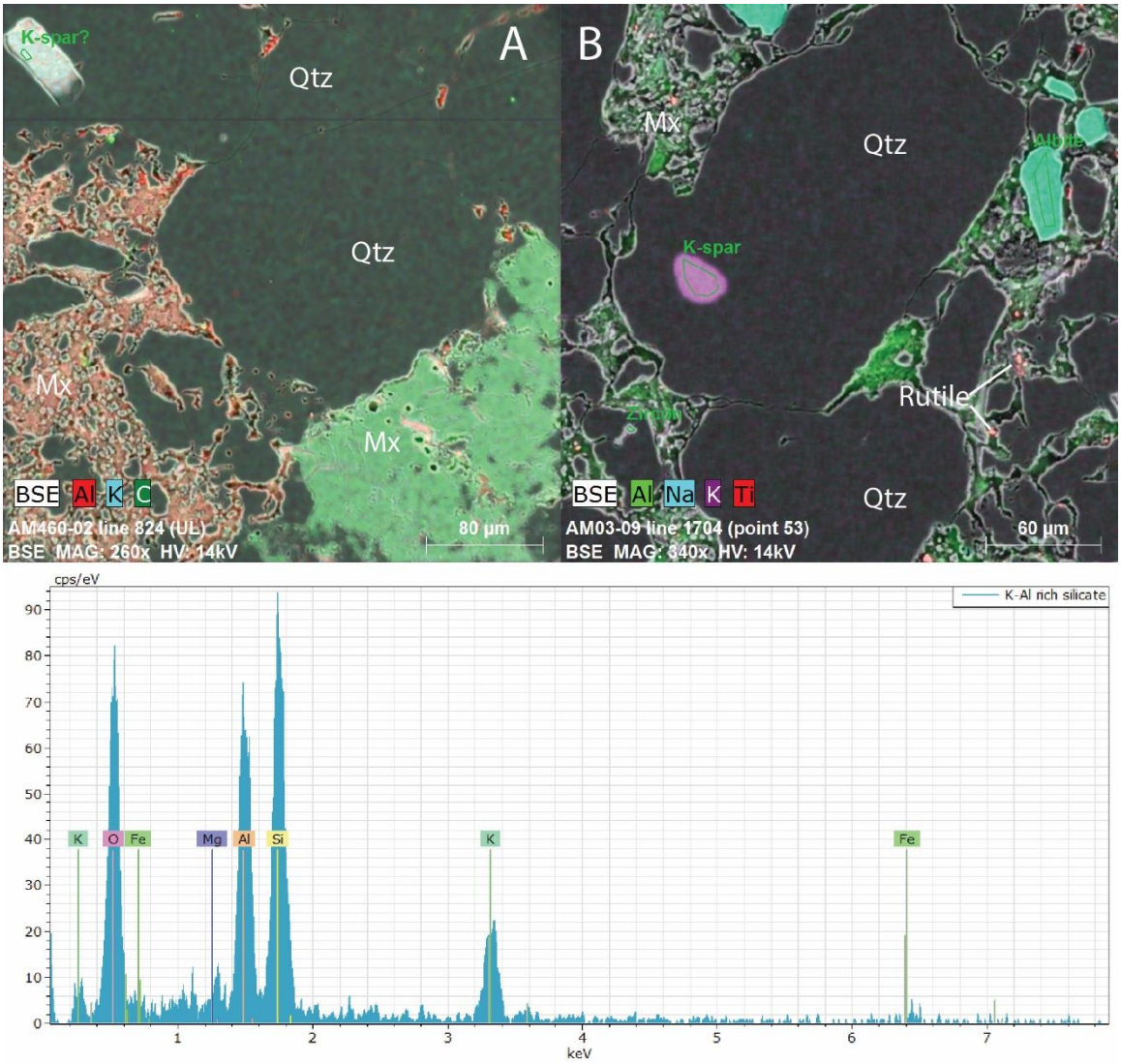

Figure 61: Scanning electron microprobe images of the mineral orthoclase feldspar from samples (A) AM460-02 and (B) AM03-09. The orthoclase grains appear as (A) light teal to white, and (B) pink. Below the microprobe images, an energy dispersive spectroscopy readout shows the elemental peaks of the orthoclase grain identified in (A) sample AM460-02. Quartz (Qtz), matrix (Mx), albite, and rutile are also identified.

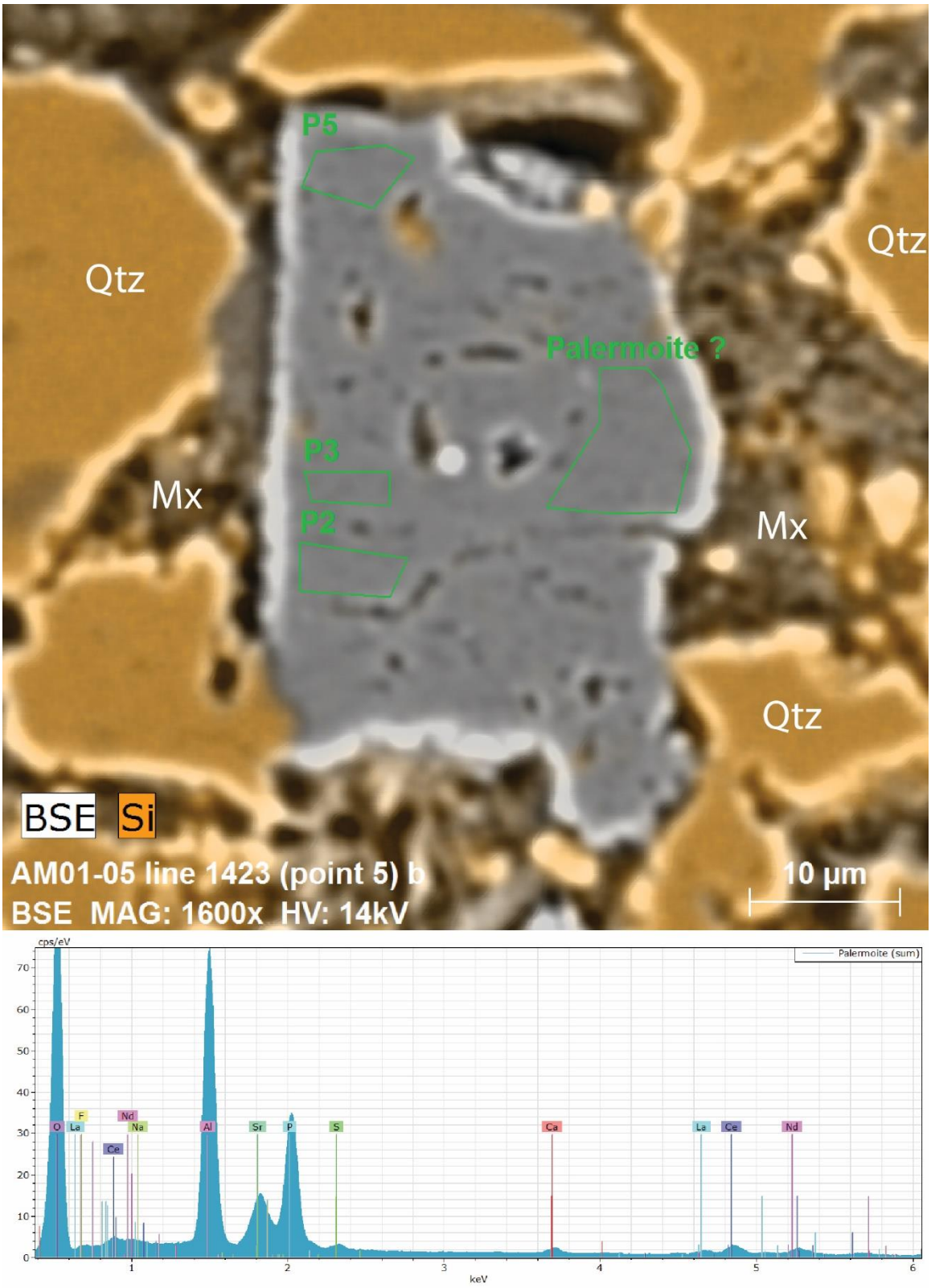

Figure 62: Scanning electron microprobe image of the mineral palermoite from sample AM01-05. Grain appears as gray. Below the microprobe images, an energy dispersive spectroscopy readout shows the elemental peaks of the palermoite grain identified in sample AM01-05. Quartz (Qtz) and matrix (Mx) are also identified.

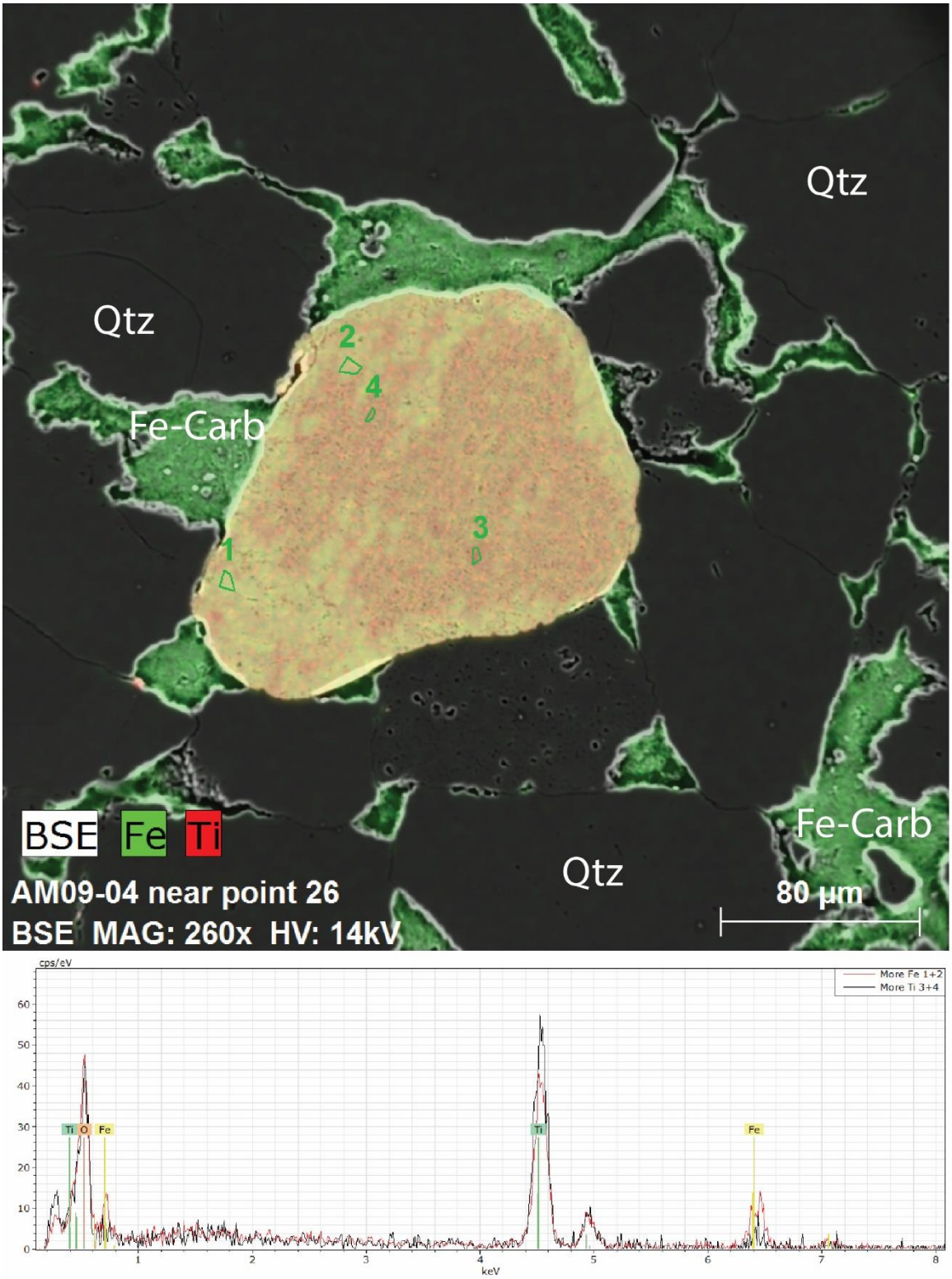

Figure 63: Scanning electron microprobe image of the mineral pseudorutile from sample AM09-04. The pseudorutile grain appears as a red-yellow mixture. Below the microprobe image, an energy dispersive spectroscopy readout shows the elemental peaks of the pseudorutile grain identified in sample AM09-04. Quartz (Qtz) and iron carbonate (Fe-Carb) are also identified.

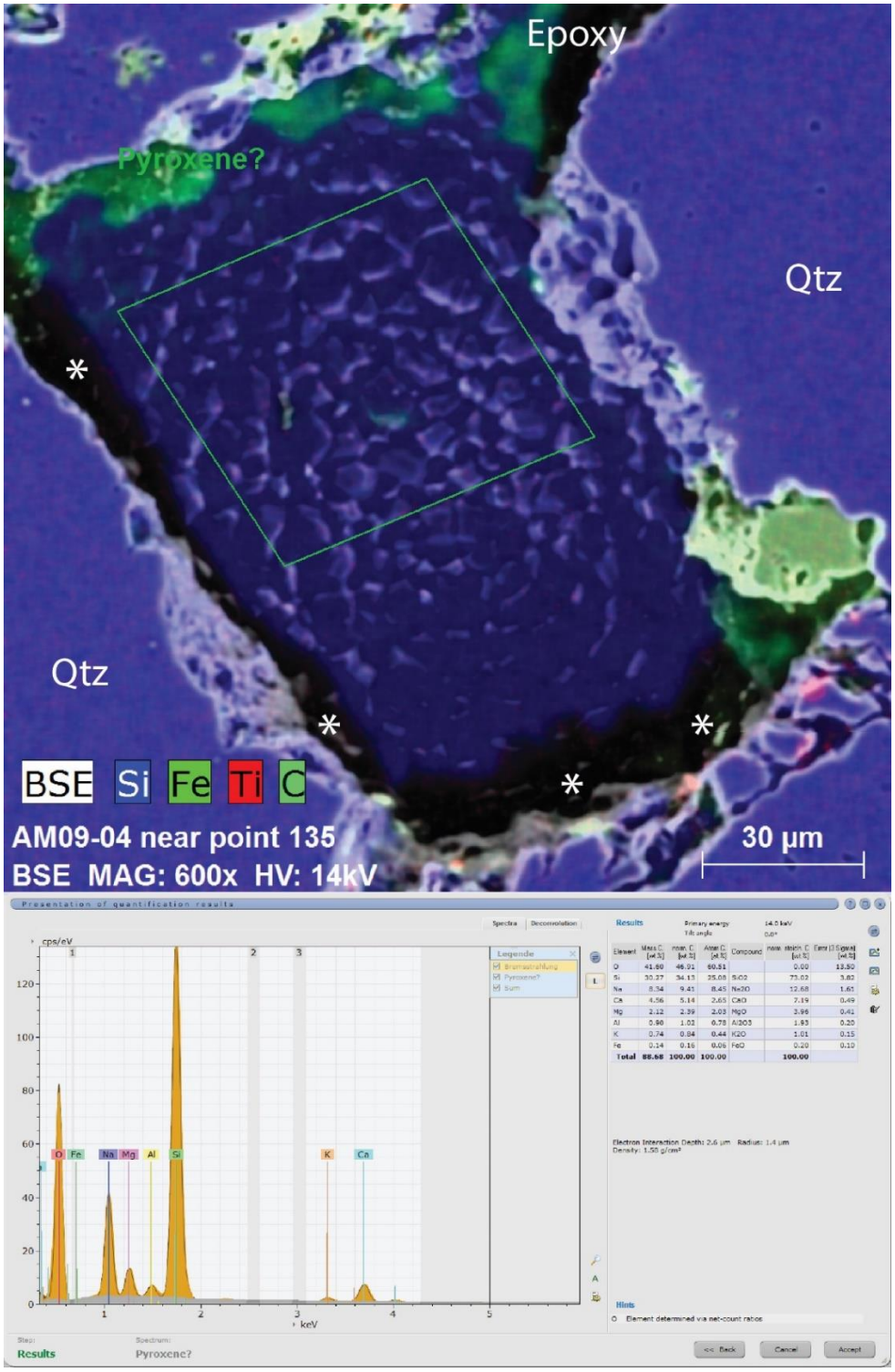

Figure 64: Scanning electron microprobe image of the mineral class pyroxene from sample AM09-04. The pyroxene grain appears as a dark, textured purple, and is at a lower elevation than the surrounding quartz grains, as is evident by the shadow cast along the bottom and left side of the grain, noted by the asterisks. Below the microprobe image, an energy dispersive spectroscopy readout shows the elemental peaks of the pyroxene grain identified within the green polygon in sample AM09-04. Quartz (Qtz) is identified, and epoxy is noted as the black area at the top of the image.

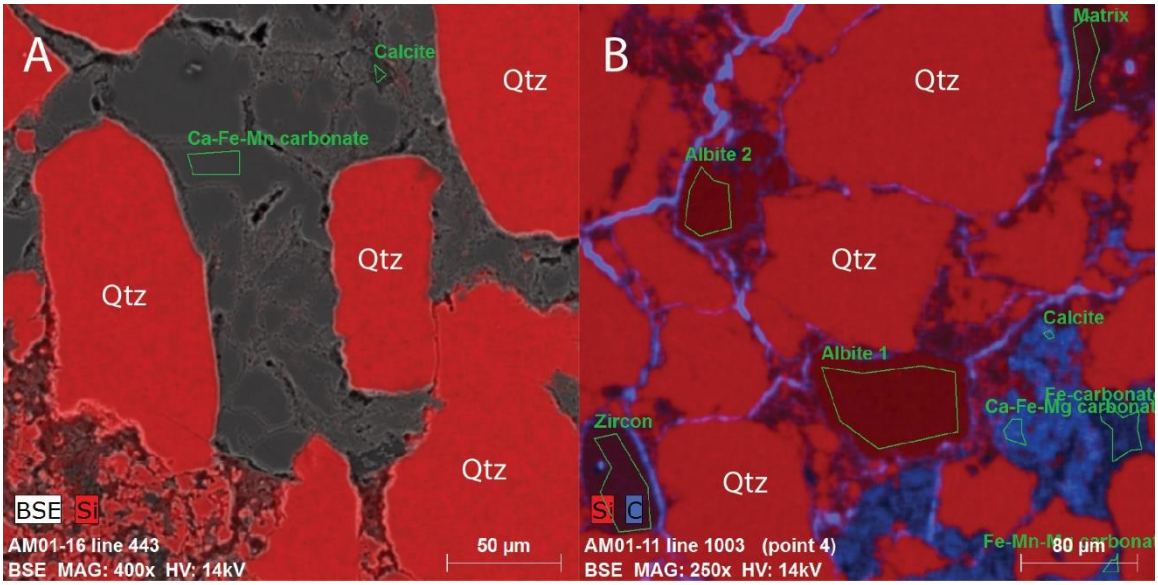

Figure 65: Scanning electron microprobe images of the mineral quartz (Qtz) from samples (A) AM01-16 and (B) AM01-11. Grains appear as red (A and B). This was the dominant mineral found in every thin section sampled. Calcite, albite, and zircon are also identified, as well as various carbonates.

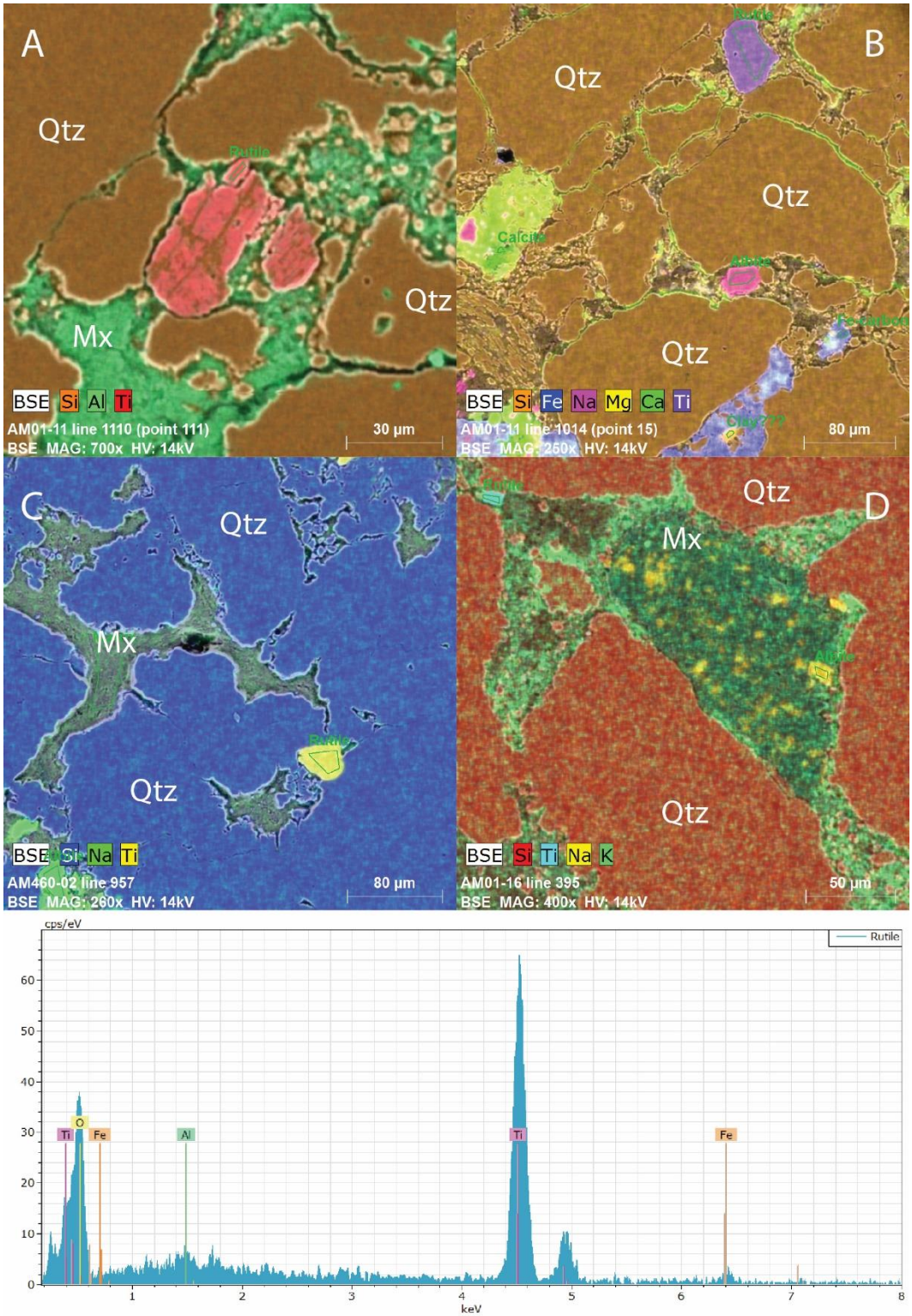

Figure 66: Scanning electron microprobe images of the mineral rutile from samples (A-B) AM01-11, (C) AM460-02, and (D) AM01-16. The rutile grains appear as (A) red, (B) purple, (C) yellow, and (D) blue. Below the microprobe images, an energy dispersive spectroscopy readout shows the elemental peaks of the rutile grain identified in (C) sample AM460-02. Quartz (Qtz), matrix (Mx), calcite, and albite are also identified.

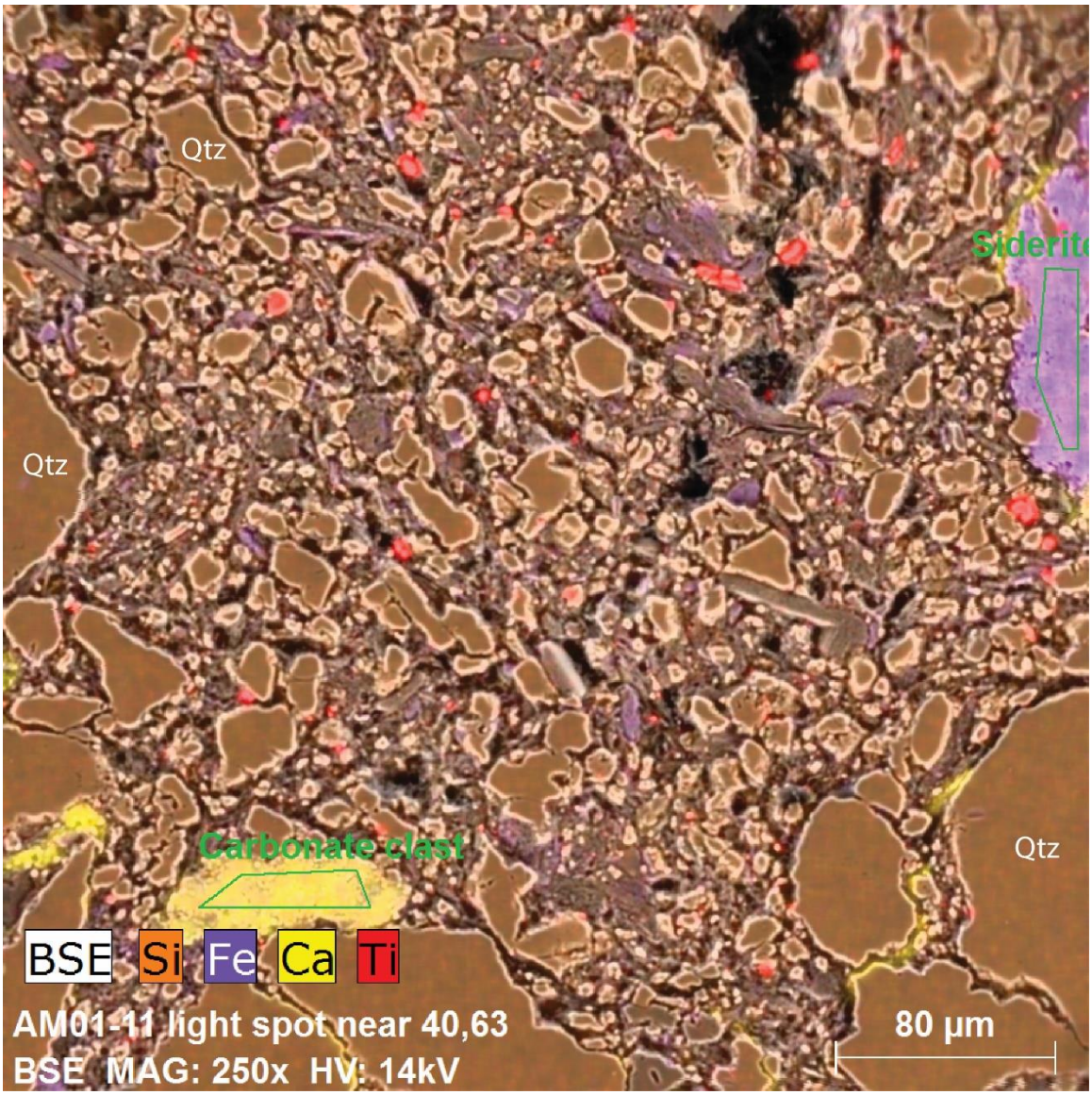

Figure 67: Scanning electron microprobe images of the mineral siderite from sample AM01-11. The siderite grain appears as purple along the right side. Quartz (Qtz), a carbonate clast, and rutile (red) are also identified.

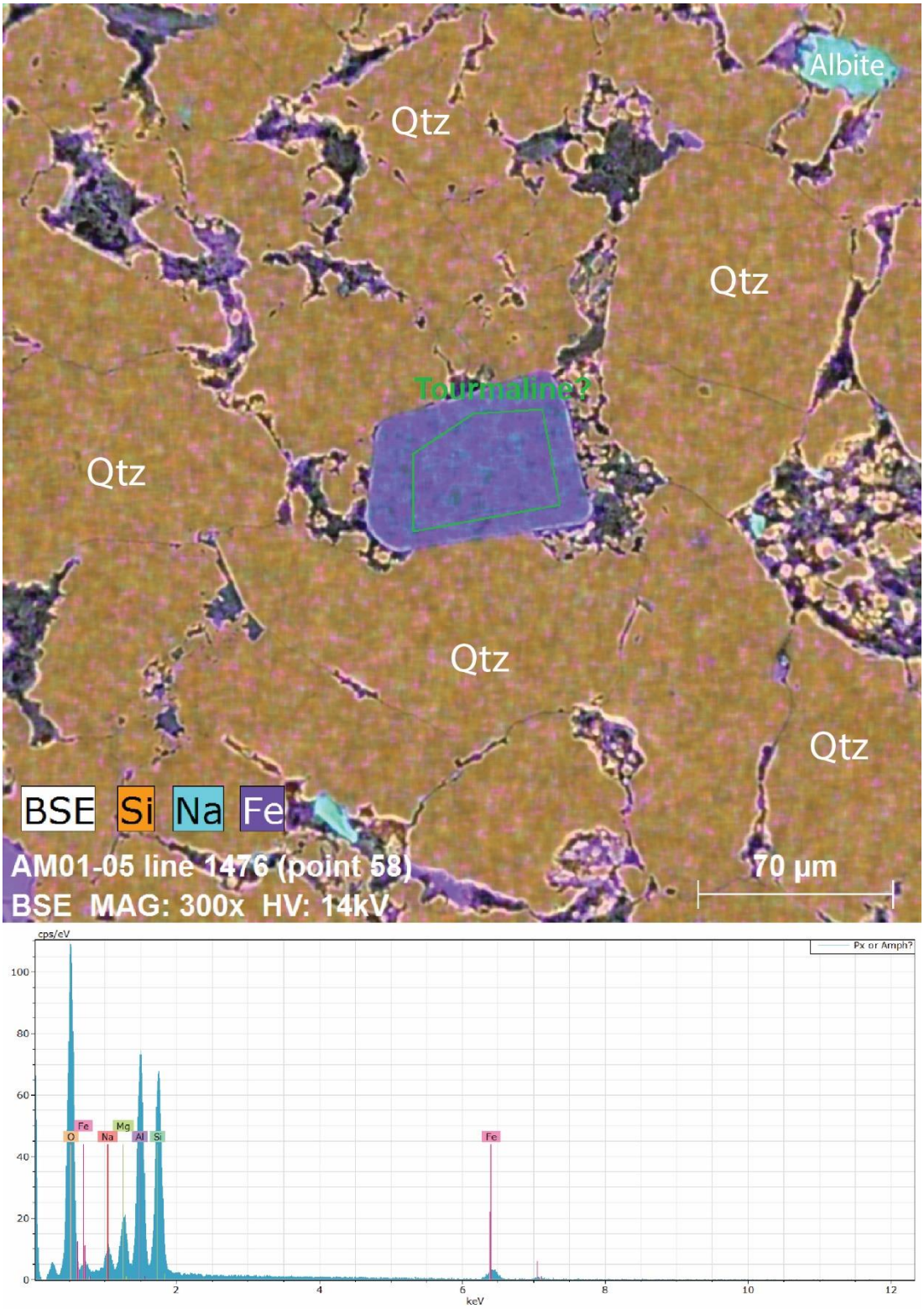

Figure 68: Scanning electron microprobe image of the mineral tourmaline from sample AM01-05. The tourmaline grain appears as purple in the center of the image. Below the microprobe image, an energy dispersive spectroscopy readout shows the elemental peaks of the tourmaline grain identified in sample AM01-05. Quartz (Qtz) and albite are also identified.

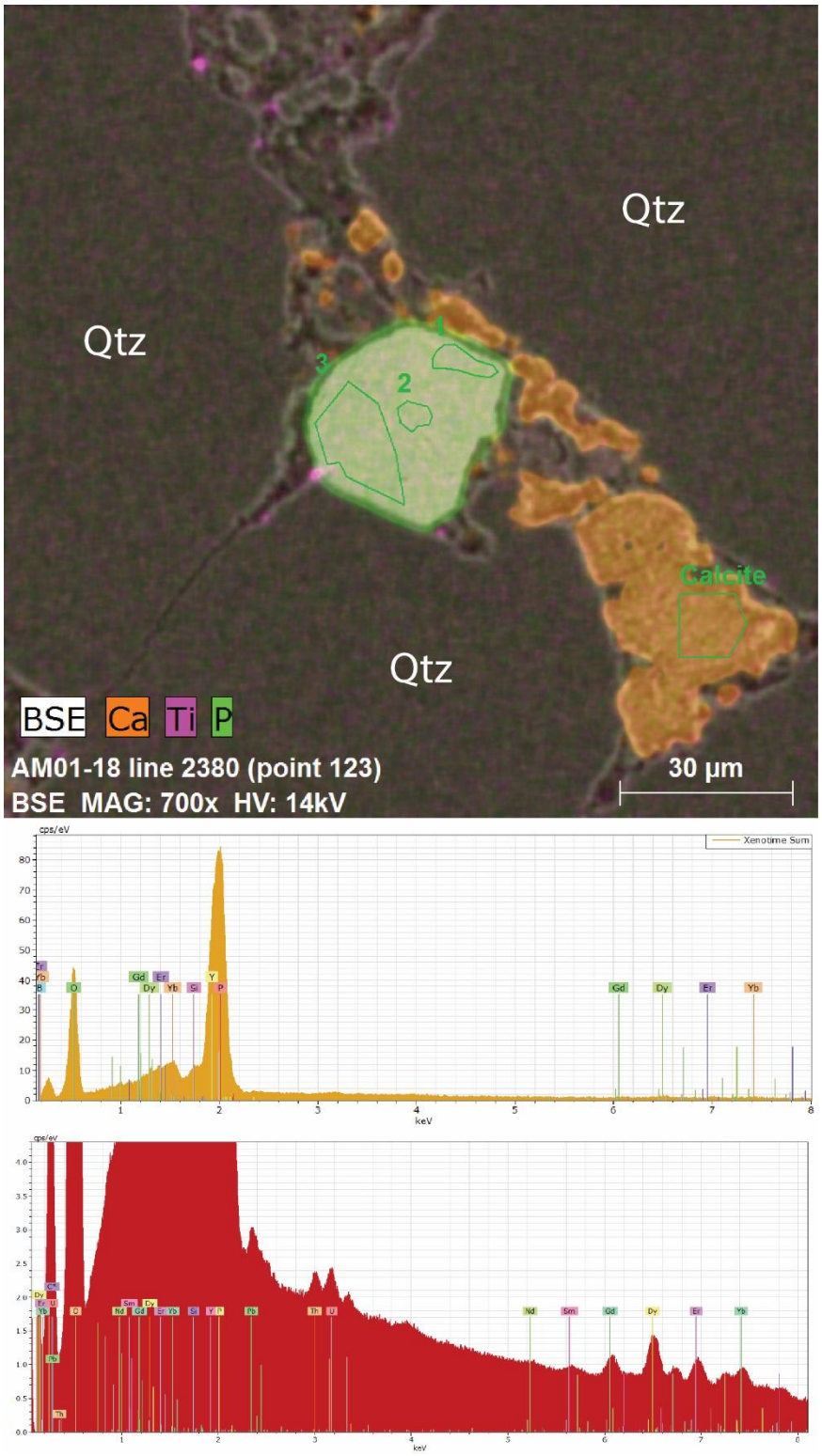

Figure 69: Scanning electron microprobe images of the mineral xenotime from sample AM01-18. The xenotime grain appears as green in the center of the top image. Below the microprobe image, an energy dispersive spectroscopy readout shows the elemental peaks of the grain identified in sample AM01-18. The bottom chart is a high-resolution, 300 second point count with 60k counts per second. This readout shows the elemental peaks of uranium, thorium, and lead. Quartz (Qtz), rutile (pink), and calcite are also identified.

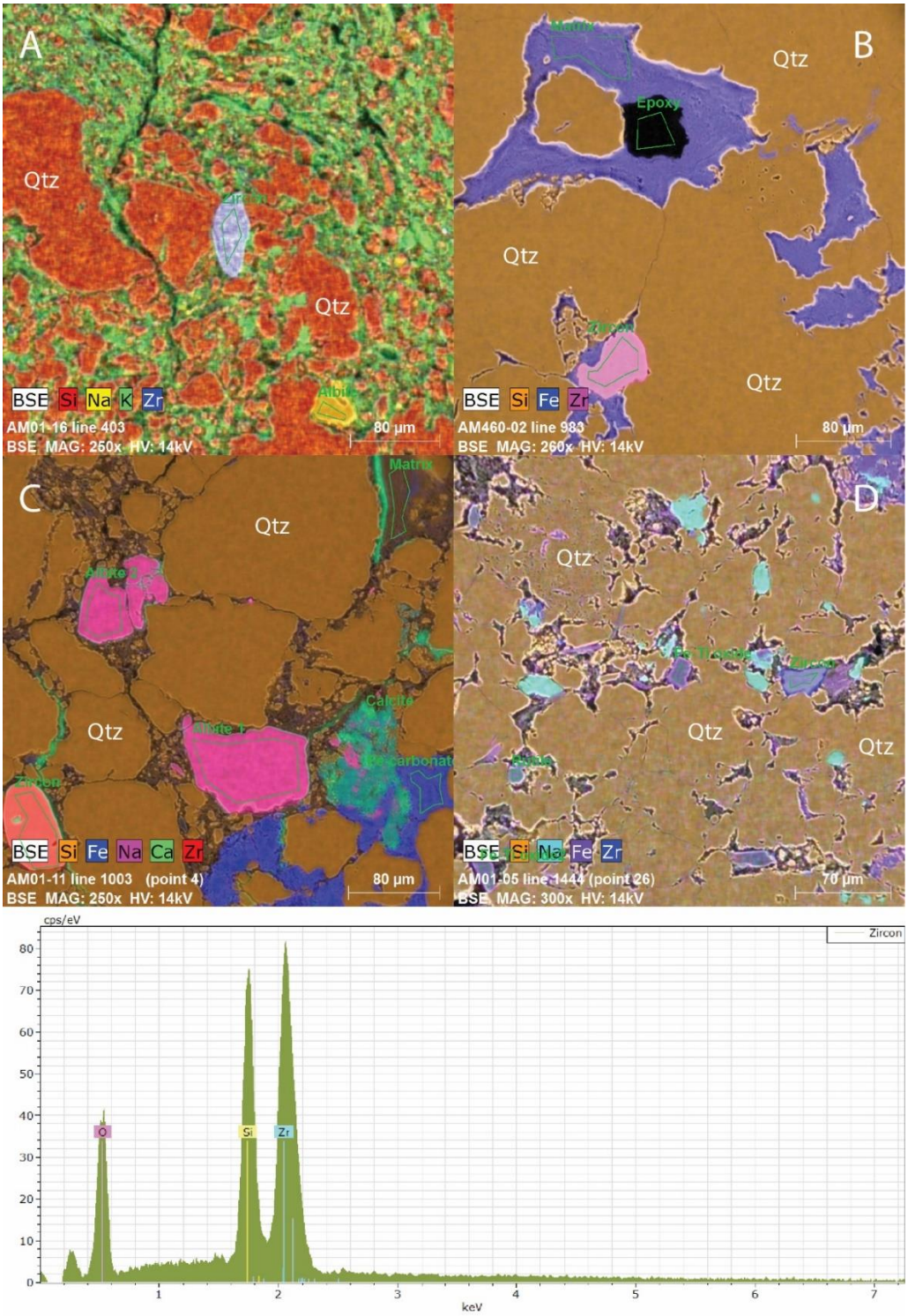

Figure 70: Scanning electron microprobe images of the mineral zircon from samples (A) AM01-16, (B) AM460-02, (C) AM01-11, and (D) AM01-05. Zircon grains appear as (A) purple, (B) pink, (C) red, and (D) blue. Below the microprobe images, an energy dispersive spectroscopy readout shows the elemental peaks of the zircon grain identified in (B) sample AM460-02. Quartz (Qtz), albite, matrix, epoxy, calcite, and various carbonates are also identified.

4.7 EDS CHEMICAL MAP

Of particular interest was the thin section from the type section of the Princeton Formation (AMPSS-TL) due to its high level of heterogeneity. Scans were taken both in plane polarized light and cross-polarized light (Figure 71a-b). In the cross-polarized scan, the larger clasts can be seen to have multiple zones in them, showing both monocrystalline and polycrystalline quartz grains. Then, the thin section was chemically mapped using energy dispersive spectroscopy (Figure 72).

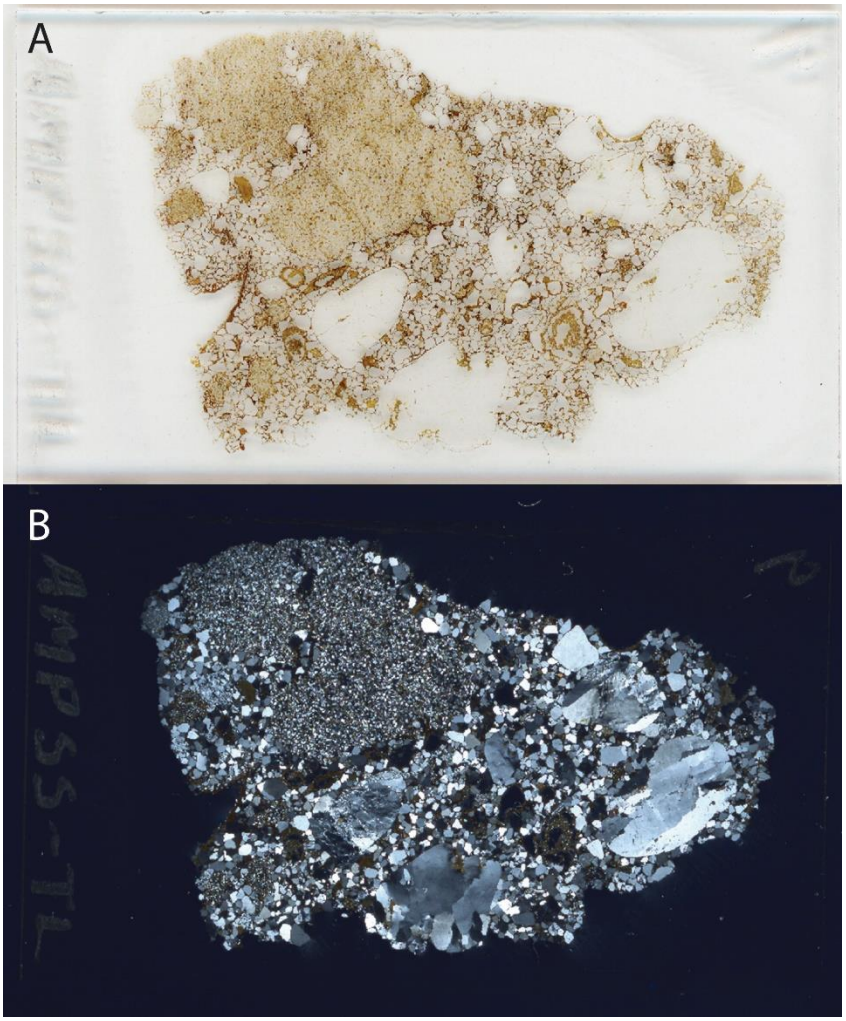

Figure 71: (A) Plane-polarized scan of thin section AMPSS-TL. The red-brown color is iron oxide, and the clear clasts are dominantly quartz. (B) Cross-polarized scan of thin section AMPSS-TL. Quartz grains show up as a gray-white gradient, with variable monocrystalline and polycrystalline quartz grains.

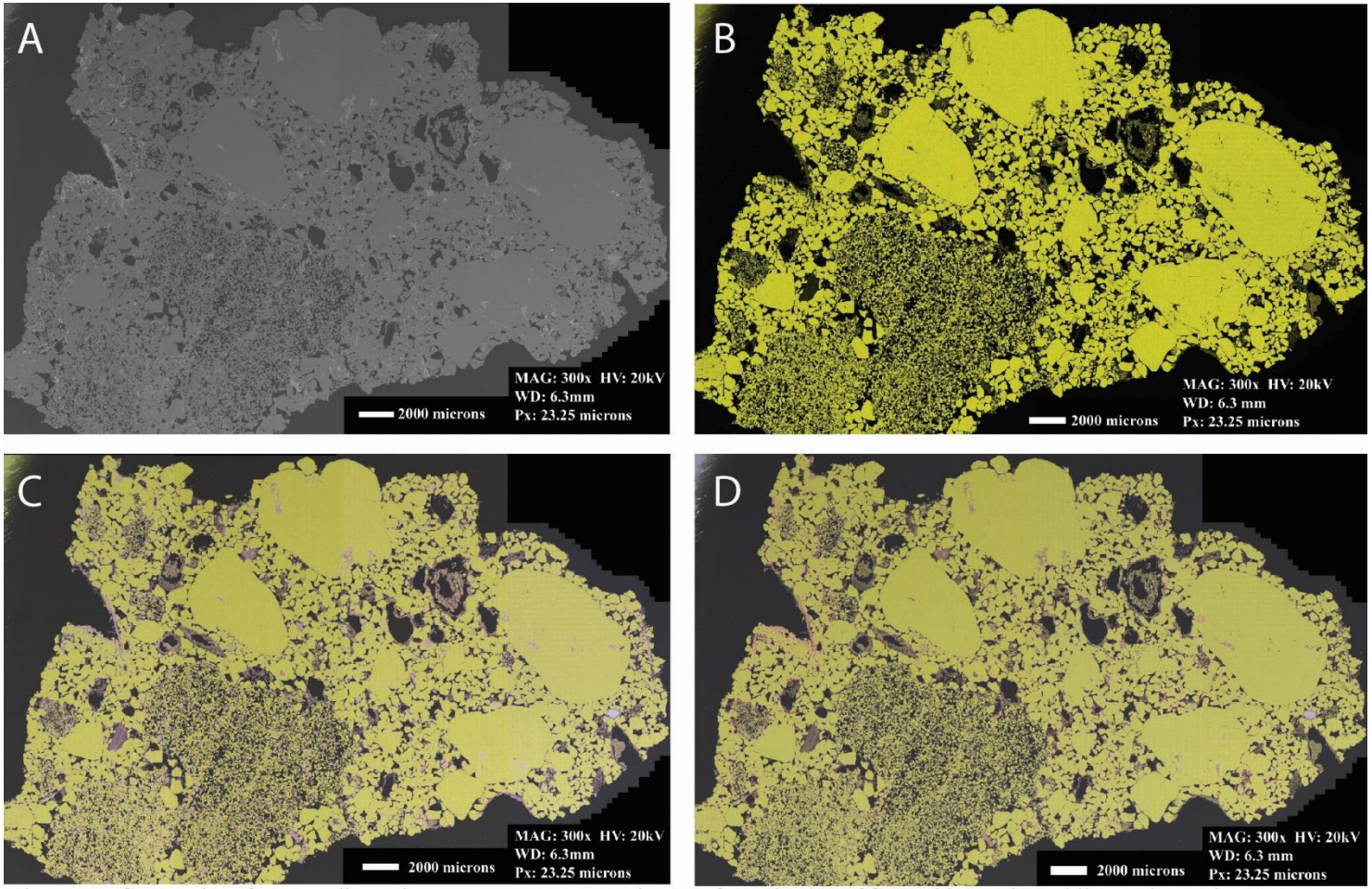

Figure 72: Composite of energy dispersive X-ray spectroscopy images from the AMPSS-TL thin section. All samples under 300x magnification, 2,000 micron scale bar, HV of 20kV, WD of 6.3mm, and Px of 23.25 microns. (A) Backscatter energy showing the rock (light gray), epoxy (dark gray), and void space (black). (B) Elemental map showing silicon (yellow) and epoxy (black). (C) Elemental map showing silicon (yellow), iron (red), sodium (blue), and backscatter (gray). (D) Elemental map showing silicon (yellow), aluminum (pink), magnesium (green), and backscatter (gray).

CHAPTER 5: INTERPRETATION

5.1 FACIES

The siltstone facies is interpreted as floodplain deposits with local development of paleosols. The tubules that are locally present in this facies are interpreted as root casts or possibly animal burrows. The blocky structures present are the result of cyclic wetting and drying, which causes the clay component to swell and shrink. As this process continued, fractures occurred along the clay-rich areas, causing blocky ped structures to form. The siltstone is composed of clay to silt sized grains, which would have been deposited out of suspension from flood waters where the stream energy would have been strong enough to carry suspended sediment over the banks of a channel and then, once the flow slowed, deposit the fine sediments in relatively quiet settings.

The thin-bedded sandstone facies is interpreted as floodplain deposits. During times of increased stream energy, the size of sediments in transport would increase from clays and silts to sands, resulting in the suspended and bedload transport of fine to medium grained sand, and subsequent deposition where flow velocities decreased. Cross-laminated beds are common in this facies due to the migration of ripples.

The medium-bedded sandstone facies is interpreted as small crevasse channel and associated splay deposits. Where this facies has a lenticular geometry, it is consistent with crevasse channel forms. As the flow in the channels decreased, the fine- to coarse-

grained sandy sediments were deposited in cross-bedded, fining-upward, medium-bedded sandstones. The fining-upward nature of this facies may record decreasing flow velocity and discharges as the flood conditions waned after cutting the crevasse channels. Where the medium-bedded sandstone facies is planar stratified, it is interpreted as splay deposits associated with the crevasse channels. As the crevasse channels cut through the levees, the flood water could spill out onto, and spread out over, the floodplain. These planar bedded deposits formed flat-lying and laterally extensive tabular sands which extend beyond the crevasse channel.

The thick, cross-bedded sandstone facies is interpreted as deposition by dunes in large channels. This facies is only associated with the Princeton Formation. In outcrop view, this unit is laterally extensive for hundreds of meters. The Princeton Formation can be traced over 227 kilometers on the West Virginia state geological map (Cardwell *et al.*, 1968) near the eastern border from Mercer County in the south to Tucker County in the north. This unit contains multiple cross-bedded sets of sandstone where the co-sets are decimeters to meters in thickness.

5.2 FACIES ASSOCIATIONS

Facies association 1 is interpreted as having formed in a floodplain depositional setting. As flooding events occurred, clay and silt sized particles were suspended in the flood waters that spread over the banks of the channel, and then the fine sediments were deposited on the levees and floodplains. During times of large floods, fine to medium sand grains could have been carried as suspended and bedload over the banks of the channel and deposited as cross-laminated layers on top of the silts and clays on both the levees and floodplains. Since the sandstone units are not as thick as the siltstone units, it

can be inferred that high-discharge flooding events were less frequent. The intervals between flood events allowed for the development of paleosols and for flora to grow. The root casts present at the top of multiple siltstone units show evidence for abundant flora and possibly the activity of burrowing creatures.

Facies association 2 is interpreted as crevasse channels and associated splay deposits. The channels eroded into the underlying levee units, and developed a lenticular geometry consistent with single narrow, incised channels. As the channels filled with sediment, they aggraded vertically, eventually spilling water and suspended sediment out onto the surrounding floodplains. This overbank spillage resulted in the splay deposits, which are decimeters thick and extend laterally for tens of meters before pinching out. The grain size distributions in the crevasse splay deposits exhibit a fining-upward and distally fining sequence, indicative of decreasing flow velocity during the waning stages of flood events.

Facies association 3 is interpreted as a large, single channel that was possibly the trunk channel for the region. The sandstone is thick bedded, with multiple generations of cross-stratification present. This channel eroded into the underlying floodplain facies association easily, with paleoflow directions to the south-southwest. In the US-460 outcrop, the margin of the trunk channel system may be present. In contrast, at the type section for the Princeton Formation, the central part of the system may be exposed. As the trunk channel transitions from base to top, grain size fines upward from a pebble conglomerate at the base to a medium sand at the top.

5.3 DEPOSITIONAL HISTORY

This section of the paper will attempt to reconstruct the depositional history of the outcrops along US-460. Because there is a low-angle southward dip, the oldest rocks are exposed at the base of the northern outcrop. Deposition at the base of the outcrop began on a floodplain, as is evidenced by the multiple successions of siltstone and thin-bedded sandstone (facies association 1) in the eastern-most section of the northern outcrop. These lower units were measured at an elevation of 743.1m above sea level. After deposition of these floodplain deposits, faulting occurred, as evidenced by the single normal fault causing less than one meter of offset in the outcrop (Figure 73). In the northern outcrop, the amount of offset appears to be uniform going up-section along the fault. This suggests that faulting occurred after the last of the faulted layers was deposited.

In contrast to the northern outcrop, the presence of a faulted horst and graben in the southern outcrop (Figure 74) implies that deposition of the floodplain deposits (facies association 1) occurred during on-going fault movement (growth faulting). In Figure 74, the horst and graben structure is well exposed. The amount of offset between correlative layers cut by the fault decreases up-section along both sides of the graben. There is also a thickening of depositional units within the graben, as compared to correlative units outside the graben. Taken together, this implies that faulting was occurring episodically at the same time as deposition was taking place. Furthermore, the land surface was likely offset by the active faulting, producing topographic lows that could influence subsequent deposition. This control of the site of deposition may have acted to influence the location of the thick-bedded sandstone (facies association 3) at the top of Figures 74 and 75.

Figure 75 shows the possible location of the uppermost part of the normal fault (dashed fault line), which could account for why the facies association 3 sandstone pinches out at that point.

Figure 73: Fault near the eastern extent of the northern outcrop. The yellow line indicates fault position, the arrows represent movement direction, and the black lines correlate similar units on either side of the fault. Note that the amount of offset between correlative units appears to be the same from bottom to top of the fault. This implies that fault motion occurred after the last of the correlative units was deposited (photograph courtesy of Jordan Smith).

Figure 74: Horst and graben near the eastern extent of the southern outcrop. The yellow lines indicate observed faults, the arrows indicate movement direction, and the black lines correlate similar units on both sides of the faults. The lengths of the blue lines show that sandstone thickness is greatest within the graben and decreases when moving across faults toward the horst. The pink lines show decreasing siltstone unit thicknesses moving from the graben to a location outside the graben. Note that the diminishing offsets going up-section along the bounding faults implies that growth-faulting was concurrent with deposition. This observation is supported by the increased thickness of depositional units within the graben as compared to correlative units outside of the graben. Field assistant for scale (approximately 1.75 meters tall).

Figure 75: Alternative interpretation of the horst and graben near the eastern extent of the southern outcrop. The yellow lines indicate observed faults, the arrows indicate movement direction, and the black lines correlate units on both sides of the faults. The dashed yellow line at the top of the outcrop indicates possible continuation of a fault to the top of the section. The blue lines show decreasing sandstone unit thickness moving out of the graben, while the pink lines show decreasing siltstone unit thickness moving out of the graben. Note that the location of the uppermost part of the fault (dashed line) coincides with the pinch out of the thick-bedded sandstone (facies association 3) at the top of the exposure. This implies that growth-faulting may have created contemporary topographic lows that influenced the position of the thick-bedded sandstone (facies association 3). Field assistant for scale (about 1.75 meters tall).

Once faulting was completed and the area stabilized, three distinct channels developed in the northern outcrop (Figure 76). These contain deposits belonging to facies association 2. The western-most and central channels (Figure 76 A-B, respectively) show single, symmetrical, incised channels with no lateral movement, while the eastern-most channel (Figure 76 C) exhibits an asymmetric form with evidence for lateral migration to the east. This is suggested by the secondary channel form connected to the right side of the larger one. The channel fills are composed of fining-upward

sequences from coarse to fine grained sandstones and belong to facies association 2. Paleoflow directions observed in outcrop were to the south-southwest. There is evidence of facies association 2 channels within the southern outcrop which vary in width and depth, but maintain a single location with no evidence for lateral migration (Figure 40).

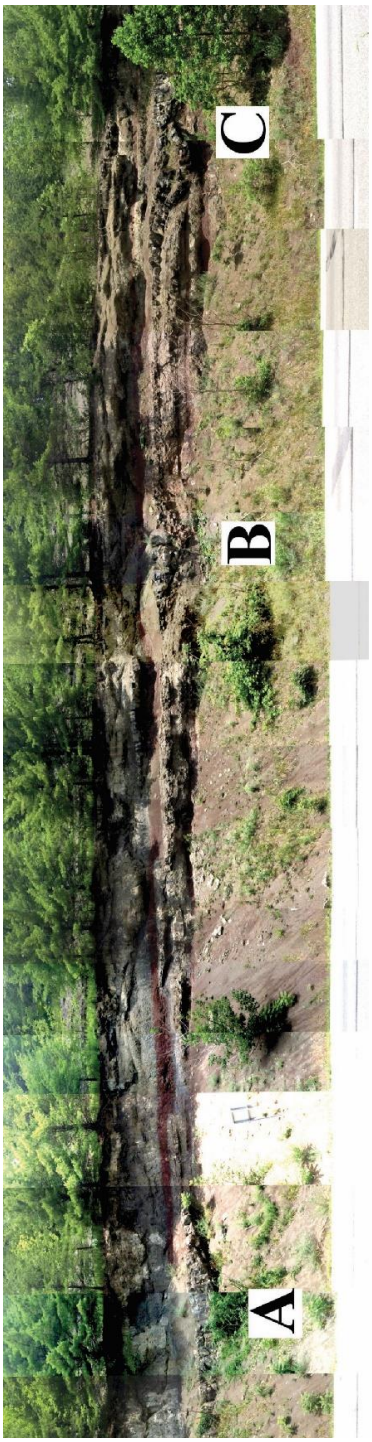

Figure 76: Three distinct incised channels in the northern outcrop of US-460. Two channelss consist of single incised channels with no evidence of lateral movement (A and B), while the third channel displays evidence for a small amount of lateral accretion before the channel was abandoned (C).

Above the channel fills on the northern outcrop, more floodplain sediments were deposited throughout the rest of the upper Hinton Formation. Taken together, the floodplain deposits (facies association 1) in the lower part of the northern outcrop, overlain by the channel fills (facies association 2), which are in turn overlain by more floodplain deposits (facies association 1) in the upper part of the northern outcrop all account for approximately 13 meters of section (Beuthin and Blake, 2004). During this time, there is a clear transition from dominantly siltstone to dominantly sandstone, with a return to siltstone at the very top of the northern outcrop. This is indicative of increasing discharge from the source, followed by a decrease in discharge.

The southern outcrop exhibits uniform floodplain deposits (facies association 1), which are dominant except for the thick-bedded sandstone (facies association 3) at the top of the outcrop. Present within the floodplain deposits are two fine-grained channel fills composed of facies association 1 (see Figure 24). These fine-grained channel fills may be correlative distal extensions of the coarser grained crevasse channels of the northern outcrop (facies association 2 of Figure 40 and Figure 76). The Princeton Formation observable at the top of the southern outcrop marks a sharp transition to higher energy flow conditions of a possible trunk channel.

The horst and graben structure near the eastern end of the southern outcrop (Figures 74-75) shows evidence for growth faulting. As the graben dropped, a topographic low was created, which resulted in the thickening of facies association 1 deposits within the graben, but may also have influenced the migration of the facies association 3 unit to this location. This growth faulting was apparently active at the southern outcrop throughout the interval during which facies association 1 was being

deposited. It is possible that the fault then propagated laterally and reached the location of the northern outcrop, where faulting appears to post-date the deposition of the units it offsets (Figure 73). This would have marked the last faulting event to affect the contemporaneous topographic relief at the study site. Figure 75 shows how that last faulting event may have extended to the top of the section and thereby influenced the relocation of the Princeton Formation channel to the site.

Finally, the Princeton Formation was deposited. It has a sharp erosive base with decimeters of relief. It could represent the trunk channel that fed the crevasse splay and floodplain sedimentation visible in the lower parts of the outcrop both on the northern and southern sides of the road. Over time, that channel could have migrated across the alluvial plain and its final arrival at the study site is documented by this facies association 3 deposit. The base of the Princeton Formation at the US-460 outcrop has an elevation of 764 meters above sea level, and the top of the unit has an elevation of 774 meters above sea level, for a total thickness of 10 meters.

Elsewhere in the region, at the type location, in the town of Princeton, West Virginia, which is 9.6 kilometers west of the US-460 outcrop, the base of the Princeton Formation has an elevation of 751 meters above sea level with a thickness of 5 meters. The Princeton Formation at the type section is coarser than at the US-460 outcrop. At the type section, the Princeton Formation is composed of a quartz pebble conglomerate. Based on its lower basal elevation and coarser grain size, the Princeton Formation at the type locality may represent the channel that began the initial filling of the incised valley fill. As the valley filled over time, the grain size would have decreased and the channel could have migrated across the valley floor (see Figure 6). Thus, the transition to a

medium-grained sandstone at a higher elevation at the US-460 outcrop, may record the progressive filling of the incised valley. The change in grain size indicates that flow velocities decreased as the site of deposition moved towards the US-460 outcrop. By combining the elevations of the Princeton Formation at the type locality with the US-460 outcrop, it appears that the total thickness of the Princeton Formation was about 23 meters, with an intermediate 8 meters of the formation not visible at either outcrop.

5.4 MINERAL ANALYSIS

A total of 2,442 points were analyzed from the twelve thin sections in order to develop a better understanding of the elements and minerals present, as well as to document any trends for the average oxide weights between samples. During the counts, 19 different minerals were identified (Table 3). Of these minerals, only three could not be formed through igneous processes, those being barite, kaolinite, and pseudorutile. However, barite can form in hydrothermal quartz veins, while kaolinite and pseudorutile form through diagenetic processes.

The average oxide weight percentages (Table 2), as a whole, did not show significant trends as far as stratigraphic correlation; however, units that were relatively high in chrome oxide (Cr_2O_3) tended to also be relatively high in zirconium oxide (ZrO_2). When examining the sandstone units not associated with channel fills (AM01-05 through AM03-09, facies association 1), there is a trend of increasing silicon oxide content up-section. In contrast, iron oxide, calcium oxide, and titanium decrease in abundance up-section.

When examining the crevasse channel fill mineralogy (facies association 2), both samples AM08-07 and AM09-04 exhibit very high abundances of silicon dioxide

(~97%). These two channel fills are part of crevasse channel C in Figure 76, with AM09-04 being the original channel and AM08-07 being from the secondary laterally accreted channel. While both channels show approximately 0.5% iron oxide, the relative abundance of zirconium oxide and titanium oxide switches as the channel migrated laterally. The early part of the channel fill (AM09-04) had a higher abundance of titanium dioxide (1.1% vs. 0.5%), while the later part of the channel fill (AM08-07) has a higher abundance of zirconium oxide (0.9% vs. 0.3%).

The Princeton Formation mineralogy varies greatly between the basal unit at the type location (sample AMPSS-TL) and the upper portion that occurs at the US-460 outcrop (AM460-01 through AM460-03). The basal unit had the second lowest concentration of silicon oxide (~82%), while having the highest aluminum oxide (5.1%) and the second highest iron oxide (5.2%) concentrations. Moving stratigraphically up to the US-460 outcrop of the Princeton Formation (where AM460-01 is at the base and AM460-03 is approximately halfway up the outcrop), the silicon oxide concentrations vary enough so a trend could not be established. However, zirconium oxide and titanium oxide concentrations decreased, while sodium oxide and potassium oxide increased going up-section.

CHAPTER 6: DISCUSSION AND CONCLUSIONS

In examining the hypotheses presented at the beginning of the study, both allocyclic and autocyclic processes contributed to the deposition of the upper Hinton Formation and the Princeton Formation. After the deposition of the marine Eads Mill Member (Beuthin and Blake, 2004), there was a small-scale regression driven by allocyclic processes. This regression likely increased the topographic relief in the region, which allowed a braided river system to develop and an incised valley to form. After the incised valley formed, a subsequent transgression resulted in the aggradation within the valley. This resulted in the deposits of the upper Hinton Formation and the Princeton Formation. During this period of transgression, the braided rivers were able to transport siliciclastics ranging in size up to gravels southward from the source area. With the Laurentian supercontinent being near the equator (Blakey, 2014), more temperate and semi-tropical climates were able to sustain high precipitation rates, which led to frequent flooding events. This type of environmental control falls under the heading of autocyclic processes. While there was likely a main channel system present near the US-460 outcrop location, the earliest deposits were fine-grained floodplain deposits (facies association 1), including evidence for paleosols and root casts.

Deposition of fine sediments on the floodplain was interrupted by some higher energy events. This period can be seen by the development of the crevasse channels

present approximately halfway up the US-460 outcrop on the north side. Crevasse channels during this stage were able to incise and then aggrade vertically. In one case, the channel migrated laterally before filling and abandoning the site. These features are likely due to autocyclic processes associated with the action of a nearby trunk channel. As that trunk channel and its channel belt aggraded, it produced its own levee system. During a flood event, the levees could have been breached by crevasse channels that fed splay deposits onto the floodplain. The crevasse channels could have formed during an interval when the main trunk channel approached this location. If the trunk channel approached, then receded once more, this site could have reverted to fine-grained vertical aggradation on the floodplain. This could account for alluvial architecture exhibited in the northern outcrop where facies association 1 grades up into facies association 2, and is in turn overlain by more facies association 1. The main trunk channel for much of the time represented by the US-460 outcrop may have been located further north and west. It is possible that the basal portion of the Princeton Formation visible at the type location, a quartz pebble conglomerate with high levels of iron oxide, was the trunk channel at that time.

In calculating incision depth, the US-460 outcrop showed a base elevation for the visible siltstone units of the northern outcrop at 743 meters above sea level, with the base elevation of the Princeton Formation at the US-460 southern outcrop at 764 meters above sea level. In contrast, the basal Princeton Formation at the type location is 751 meters above sea level. Assuming no post-depositional tilting, this suggests that at least 13 meters of down cutting into the floodplain deposits occurred at the type location. After incision of the valley, the Princeton Formation at the type location could have developed

into a multi-storey sandstone, with paleoflow directions to the south-southwest. With time, the channel system responsible for the Princeton Formation aggraded and avulsed to new locations. Eventually, the Princeton Formation avulsed to a position represented by the facies association 3 deposits at the top of the southern outcrop along US-460. These findings help to answer hypotheses 1-4 by showing that autocyclic processes could have dominated during deposition of the upper Hinton Formation and the Princeton Formation.

The final hypothesis addressed the issue of mineralogy and the ability to both determine source provenance and the possibility of tying the crevasse channels and the trunk channel sandstones to a similar system. The point count average oxide weight percentages do not provide enough information to be able to tie all of the sandstones to a similar system during deposition of both the crevasse channels and the trunk channels. However, the presence of 19 minerals (see Table 3) show a provenance derived from a combination of igneous and metamorphic rocks. When looking at the trend, extent and paleoflow indicators of the Princeton Formation, it is likely that the sediment was derived in part from areas affected by the Grenville Orogeny (Figure 77), which occurred from 1,200 – 900 mya. This would imply that basement rocks belonging to the Grenville orogeny were unroofed during events such as the Taconic Orogeny or the Alleghanian Orogeny (Figure 78) to provide a source for the upper Hinton Formation and Princeton Formation. The eroded debris was then transported to the south-southwest and deposited at the study site.

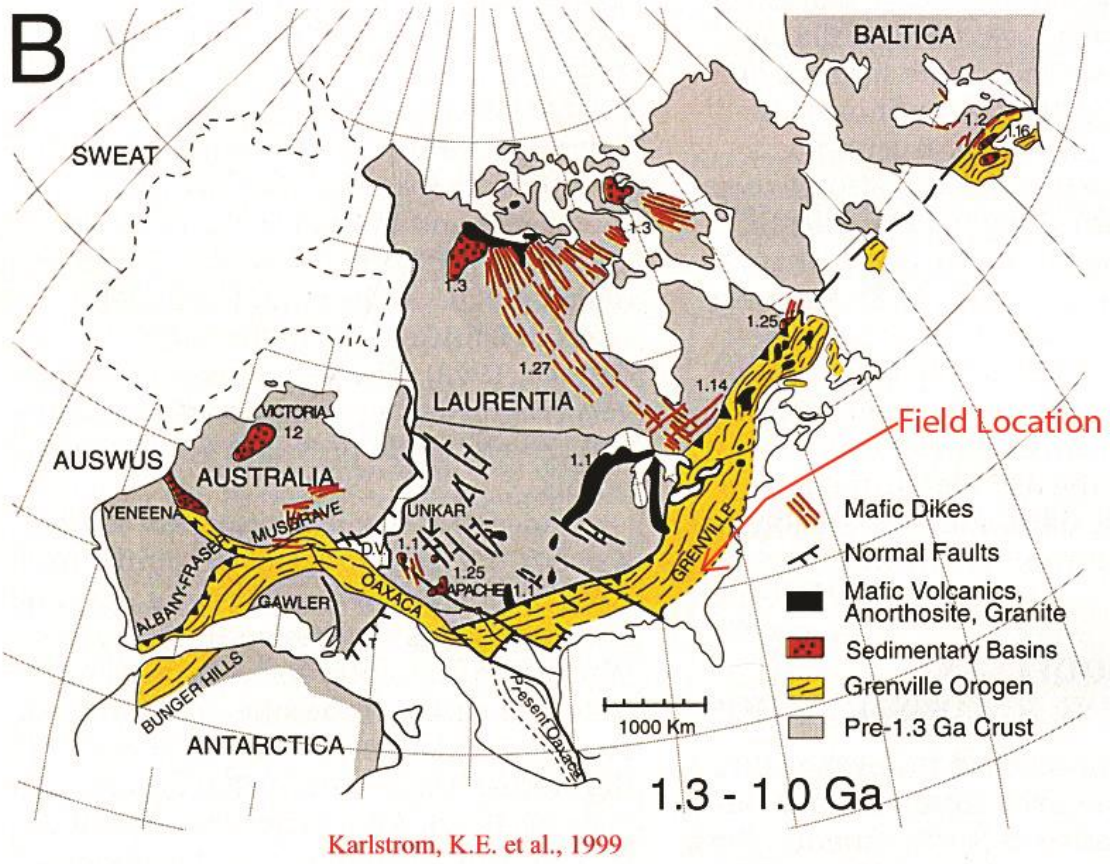

Figure 77: Outline of the extent of the Grenville Orogeny shown in yellow (from Karlstrom *et al.,* 1999).

When viewing the upper Hinton Formation and Princeton Formation together, the facies architecture suggests a single regression set off a period of incision to form a paleovalley. This was followed by a transgression that set off an interval of aggradation. This does not agree with the findings of Miller and Eriksson (2000, p. 210), and suggests a lesser number of transgressive and regressive sequences during the interval recorded by the stratigraphy at the study site. However, the findings of this research help to corroborate the findings of Miller and Eriksson (2000, p. 215) in that the Princeton Formation began as an incised valley which then filled with an overall fining upward sequence during the subsequent transgression, although the geometry of this valley fill complex differs from those presented by Weber and others (2004, p. 35). Further, the

facies architecture of the upper Hinton Formation outcrops do agree with the findings of Miller and Eriksson (2000, p. 215) in that the system developed as a braided-fluvial system.

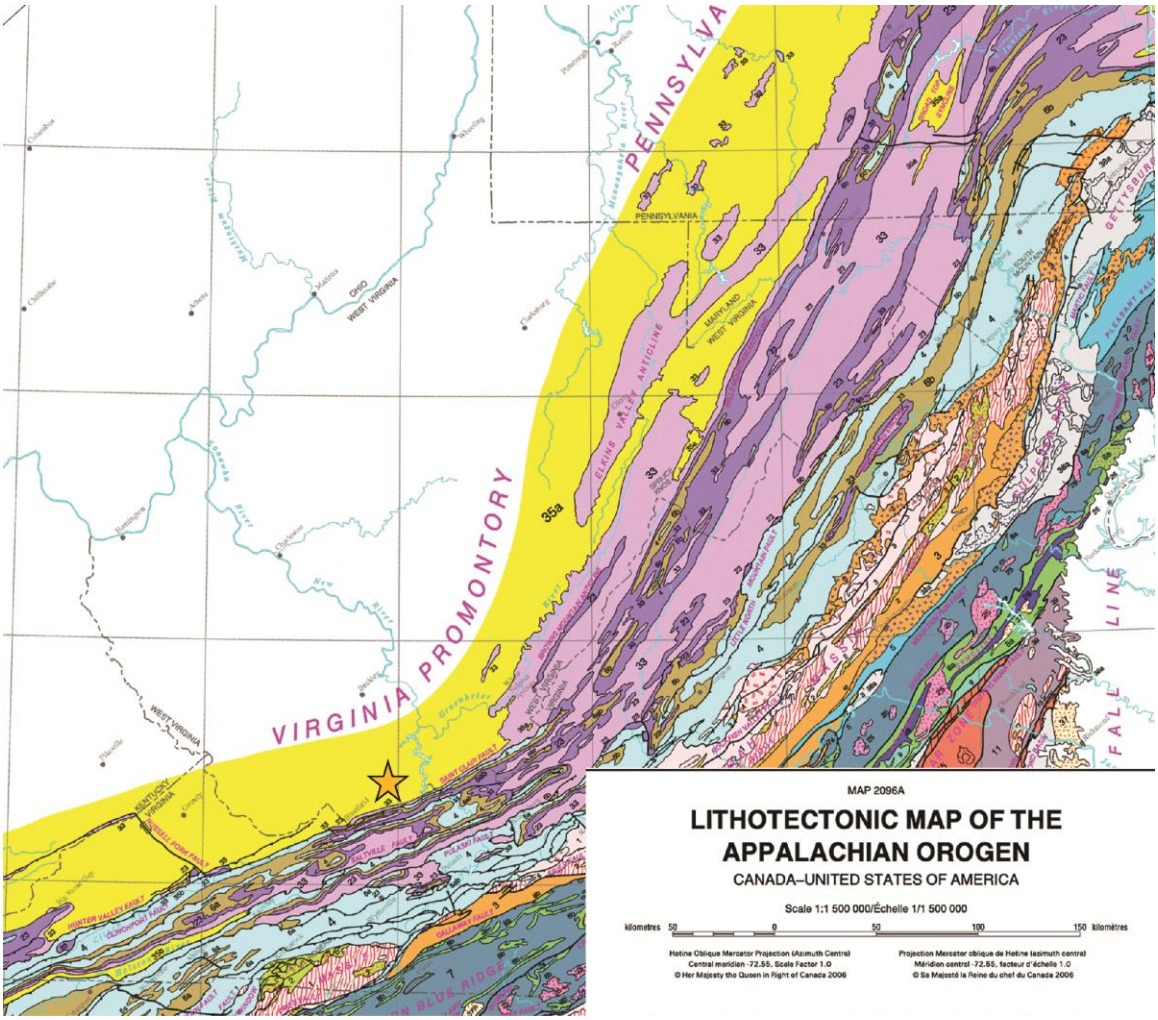

Figure 78: Lithotectonic map of the Appalachian Orogen (modified from Hibbard *et al.,* 2006). Field area noted by yellow star, and north is to the top of the image.

One area of interest that was not foreseen in this study is the impact that faulting could have on the preferred locations of deposition. As discussed by Alexander and Leeder (1987, p. 247), "a river tends toward the position of topographic minimum, which is commonly the site of maximum subsidence". The southern outcrop shows a horst and graben feature indicative of a growth fault, implying contemporaneous faulting as deposition was occurring. On the northern outcrop, a single fault, along the same trend as

the eastern-most faults from the southern horst and graben, also shows the potential for growth faulting. With growth faulting occurring during deposition, a topographic low would have been created at the site of the US-460 outcrop as a result of tensile stresses. With the understanding that rivers will migrate towards topographic lows (Alexander and Leeder, 1987), it can be argued that the location of the Princeton Formation at the US-460 outcrop was due to a topographic low caused by extensional faulting. This has not been addressed in the previous literature of the Mauch Chunk Group, and could be an area for further research.

BIBLIOGRAPHY

Alexander, J., and Leeder, M.R. 1987. Active tectonic control on alluvial architecture: *Society of Sedimentary Geology Special Publication* 39: 243 – 252.

Allen, J.R.L. 1966. On bed forms and paleocurrents. *Sedimentology* 6: 153 – 190.

Allen, G.P., and Posamentier, H.W. 1994. Transgressive facies and sequence architecture in mixed tide and wave-dominated incised valleys: Example from the Gironde estuary, France. *In:* Dalrymple, R.W., Boyd, and Zaitlin, B.A. (eds), *Incised Valley Systems: Origin and Sedimentary Sequences*. Society of Sedimentary Geology Special Publication 51: 226 – 240. Tulsa: SEPM.

AMETEK, Inc – CAMECA SAS, 2016, Electron Probe Micro-Analysis: http://www.cameca.com/instruments-for-research/epma.aspx (accessed April 2017).

Ashley, G.M., and Sheridan, R.E. 1994. Depositional model for valley fills on a passive continental margin. *In*: Dalrymple, R.W., Boyd, R.J., and Zaitlin, B.A. (eds.), *Incised Valley Systems: Origin and Sedimentary Sequences*, Society of Sedimentary Geology Special Publication 51: 285– 301. Tulsa: SEPM, Tulsa, p..

Bates, R. L., and Jackson, J. A., (eds.). 1984. *Dictionary of Geological Terms of the American Geological Institute*. New York: Anchor Books.

Beuthin, J.D. and Blake, B.M. 2001. Bedrock geologic map of the Athens Quadrangle, West Virginia: *West Virginia Geological and Economic Survey Open File Report OF-0104*, scale 1:24000.

Beuthin, J.D. and Blake, B.M. 2002. Bedrock geologic map of the Lerona Quadrangle, West Virginia: *West Virginia Geological and Economic Survey Open File Report OF-0203*, scale 1:24000.

Beuthin, J. D. and Blake, B.M. 2004. Revised stratigraphy and nomenclature for the upper Hinton Formation (Upper Mississippian) based on recognition of regional marine zones, southern West Virginia: *Southeastern Geology* 42(3): 165-178.

Blakey, R. 2014. North American Paleogeography, Colorado Plateau Systems, INC: http://cpgeosystems.com/nam.html (accessed October 2015).

Bogdanoff, A.A. 1960. On the term "structural stages": *International Geological Congress, Committee for Geologic Map of World, Subcommittee for Tectonic Map of World,* Moscow, p. 1-23.

Boggs, S. Jr. 2001. *Principles of Sedimentology and Stratigraphy,* New Jersey: Prentice-Hall Inc.

Cardwell, D.H., Erwin, R.B, and Woodward, H.P., compilers, Lotz, C.W., cartographer. 1968. Geologic Map of West Virginia: *West Virginia Geological and Economic Survey*, scale 1:250,000, 2 sheets.

Cawthern, T. R. 2007. Marine Paleoecology of the Fivemile Member of the Hinton Formation, Upper Mississippian, West Virginia and Virginia [Master's thesis]: Morgantown, West Virginia University.

Cotter, E. 1978. The evolution of fluvial style, with special reference to the central Appalachian Paleozoic. *In*: Miall, A.D. (ed.) Fluvial Sedimentology. *Canadian Society of Petroleum Geology Memoir* 5: 361 – 383.

Davidson, S.K., Hartley, A.J., Weissmann, G.S., Nichols, G.J., and Scuderi, L.A. 2013. Geomorphic elements on modern distributive fluvial systems: *Geomorphology* 180-181: 82-95.

Davidson, S.K. and Hartley, A.J. 2014. A quantitative approach to linking drainage area and distributive-fluvial-system area in modern and ancient endorheic basins. *Journal of Sedimentary Research* 84: 1005-1020.

Emery, D., and Myers, K.J., (eds.). 1996. *Sequence Stratigraphy.* Oxford: Blackwell Science Ltd.

Englund, K. J. 1968. Geologic map of the Bramwell quadrangle, West Virginia – Virginia: *U.S. Geological Survey Map GQ-745*, scale 1:24000.

Friend, P.F. 1983. Towards the field classification of alluvial architecture or sequence. *In*: Collison, J.D., Lewin, J. (eds.) Modern and Ancient Fluvial Systems. *International Association of Sedimentology Special Publications* 6: 345 – 354.

Friend, P.F., Slater, M.J., and Williams, R.C. 1979. Vertical and lateral building of river sandstone bodies, Ebro Basin, Spain. *Journal of the Geological Society of London* 136: 39 – 46.

Hartley, A.J., Weissmann, G.S., Nichols, G.J., Warwick, and G.L. 2010. Large distributive fluvial systems: Characteristics, distribution, and controls on development. *Journal of Sedimentary Research* 80: 167 – 183.

Hibbard, J.P., van Staal, C.R., Rankin, D.W., and Williams, H. 2006. Lithotectonic map of the Appalachian Orogen, Canada – United States of America: *Geological Survey of Canada "A" Series Map 2096A,* scale 1:1500000.

Horton, B.K. and DeCelles, P.G. 2001. Modern and ancient fluvial megafans in the foreland basin system of the central Andes, southern Bolivia: Implications for drainage network evolution in fold-thrust belts. *Basin Research* 13: 43 – 63.

Karlstrom, K.E., Harlan, S.S., Williams, M.L., McLelland, J., Geissman, J.W., and Ahaell, K. 1999. Refining Rodinia: Geologic Evidence for the Australia Western U.S. (AUSWUS) connection for Proterozoic Supercontinent Reconstructions. *GSA Today* 9 (10): 1 – 7.

Krebs, C. E., and Teets, D. D., Jr. 1916. Raleigh County and the western portions of Mercer and Summers Counties. *West Virginia Geological Survey County Reports*, 778.

Leier, A.L., DeCelles, P.G., and Pelletier, J.D. 2005. Mountains, monsoons, and megafans. *Geology* 33(4): 289 – 292.

Long, D.G.F. 1978. Proterozoic stream deposits: some problems of recognition and interpretation of ancient sandy fluvial systems. *In*: Miall, A.D. (ed.). Fluvial Sedimentology. *Canadian Society of Petroleum Geologists Special Paper* 23: 153 – 186.

Matchen, D. L., Allen, J. L., Peck, R. L., and Mercier, D. 2011. Bedrock geologic map of the Bluestone National Scenic River: Flat Top and Pipestem Quadrangles, West Virginia: *West Virginia Geological and Economic Survey Open File Report OF-1101*, scale 1:24000.

Matchen, D. L., Kuehn, S.C., and Chandler, G. 2013. Preliminary Evaluation of an Unusual Limestone-Pebble Conglomerate from the upper Hinton (Mississippian) Formation of Southern West Virginia, U.S.A. *In*: Proceedings GSA Annual Meeting and Exposition, Denver, Colorado, 2013, Volume 42, Geological Society of America.

Maynard, J.P., Eriksson, K.A., and Law, R.D. 2006. The upper Mississippian Bluefield Formation in the Central Appalachian basin: A hierarchical sequence-stratigraphic record of a greenhouse to icehouse transition. *Sedimentary Geology* 192: 99-122.

McCreary, A. F., and Matchen, D. L. 2014. Evaluating an unusual limestone-pebble conglomerate in the upper Hinton Formation near Eads Mill, West Virginia. *Geological Society of America Abstracts with Program*, v. 46, Blacksburg, Virginia.

Miall, A.D. 1996. *The Geology of Fluvial Deposits: Sedimentary Facies, Basin Analysis, and Petroleum Geology.* Berlin Heidelberg: Springer-Verlag.

Miller, D. J., and Eriksson, K. A. 2000. Sequence stratigraphy of Upper Mississippian strata in the central Appalachians: A record of glacioeustasy and tectonoeustasy in a foreland basin setting. *AAPG Bulletin* 84(2): 210-233.

Mitchum, R. M., Jr. 1977. Seismic stratigraphy and global changes in sea level. Part 1: Glossary of terms used in seismic stratigraphy. *American Association of Petroleum Geologists* 26: 205 – 212.

North American Commission on Stratigraphic Nomenclature. 1983. North American Stratigraphic Code. *American Association of Petroleum Geologists Bulletin* 67: 841-875.

Owen, A., Nichols, G.J., Hartley, A.J., Weissmann, G.S., and Scuderi, L.A. 2015. Quantification of a distributive fluvial system: The Salt Wash DFS of the Morrison Formation, SW U.S.A. *Journal of Sedimentary Research* 85: 544 – 561.

Peck, R. L., Matchen, D. L., and Hunt, P. J. 2013. Bedrock geologic map of the New River Gorge National River: Hinton and Talcott Quadrangles, West Virginia: *West Virginia Geological and Economic Survey Open File Report OF-1301*, scale 1:24000.

Pinnix, J.A. 1993. Sedimentology of the Princeton Sandstone (upper Mississippian) in southeastern West Virgina [Master's thesis]: East Carolina University, 133 p.

Plink-Bjorklund, P., Wang, J., Belobraydic, M., McDowell, B., Don, J., Jaikla, C., and Shi, G. 2014. Distributive fluvial systems, fluvial megafans, terminal fans – stratigrapher's nightmare. *In*: Search and Discovery Article #50978. *AAPG Annual Convention and Exhibition*, Houston, Texas.

Posamentier, H.W., and James, D.P. 1993. An overview of sequence-stratigraphic concepts: uses and abuses. *In:* Posamentier, H.W. *et al.*, ed. *Sequence Stratigraphy and Facies Associations:* Special Publication of the International Association of Sedimentologists 18: 3 – 18.

Prothero, D. R., and Schwab, F. 2014. *Sedimentary Geology: An Introduction to Sedimentary Rocks and Stratigraphy*, New York: W. H. Freeman and Company.

Reading, H.G. (ed.). 1986. *Sedimentary Environments and Facies*. Oxford: Blackwell Scientific Publications

Reger, D. B. 1926. Mercer, Monroe, and Summers Counties: *West Virginia Geological Survey County Reports*, 963.

Sambrook Smith, G.H., Best, J.L., Ashworth, P.J., Fielding, C.R., Goodbred, S.L., and Prokocki, E.W. 2010. Fluvial form in modern continental sedimentary basins: Distributive fluvial systems: Comment: *Geology Forum*, p. e230.

Sloss, L.L. 1964. Tectonic cycles of the North American craton. *Kansas Geological Survey Bulletin* 169(2): 449 – 460.

Smith, D.G., and Smith, N.D. 1980. Sedimentation in anastomosed river systems: Examples from alluvial valleys near Banff, Alberta. *Journal of Sedimentary Petrology* 50: 157 – 164.

Vance, T. 2007. Marine Paleoecology of the Eads Mill Member, Hinton Formation, Upper Mississippian, West Virginia and Virginia [Master's thesis] Morgantown, West Virginia University.

Van Wagoner, J.C., Posamentier, H.W., Mitchum, R.M., Jr., Vail, P.R., Sarg, J.F., Loutit, T.S., and Hardenbol, J. 1988. An Overview of the Fundamentals of Sequence Stratigraphy and Key Definitions. *SEPM Special Publications* 42: 39 – 46.

Weber, N., Chaumillon, E., Tesson, M., and Garlan, T. 2004. Architecture and morphology of the outer segment of a mixed tide and wave-dominated-incised valley, revealed by HR seismic reflection profiling: The paleo-Charente River, France: *Marine Geology* 207: 17 – 38.

Weissmann, G.S., Hartley, A.J., Nichols, G.J., Scuderi, L.A., Olson, M., Buehler, H., and Banteah, R. 2010. Fluvial form in modern continental sedimentary basins: Distributive fluvial systems: *Geology* 38(1): 39 – 42.

Weissmann, G.S., Hartley, A.J., Nichols, G.J., Scuderi, L.A., Davidson, S.K., and Owen, A. 2011. Predicted progradational signatures of distributive fluvial systems (dfs), American Geophysical Union 2011 fall meeting, San Francisco, California